Research Square

Preprints are preliminary reports that have not undergone peer review.
They should not be considered conclusive, used to inform clinical practice,
or referenced by the media as validated information.

STG-GraphRAG: from Fully Automated Construction of Long-term Flood Spatio-Temporal Knowledge Graphs to Geography's First and Third Law-Constrained GraphRAG for Closed-loop Decision Support

Heng Tang
Zhejiang Merit Interactive Research Institute Co., Ltd
Yi Fang
Zhejiang Merit Interactive Research Institute Co., Ltd
Xiaoping Rui
ruixpsz@163.com

Hohai University
Mengru Gao
Hohai University
Yiheng Xie
Hohai University
Ninglei Ouyang
Hohai University

Research Article

Keywords: spatio-temporal constrained GraphRAG, long time-series flood knowledge graph, FloodBot, geographical laws, flood disaster decision support

Posted Date: November 18th, 2026

DOI: https://doi.org/10.21203/rs.3.rs-11547141/v1

License: This work is licensed under a Creative Commons Attribution 4.0 International License.
Read Full License

Additional Declarations: No competing interests reported.

STG-GraphRAG: from Fully Automated Construction of Long-term Flood Spatio-Temporal Knowledge Graphs to Geography's First and Third Law-Constrained GraphRAG for Closed-loop Decision Support

Heng Tang [a], Yi Fang [a], Xiaoping Rui [b, &], Mengru Gao [b], Yiheng Xie [b] and Ninglei Ouyang [b]

[a] Zhejiang Merit Interactive Research Institute Co., Ltd., Hangzhou, China; [b] School of Earth Sciences and Engineering, Hohai University, Nanjing, China

KEYWORDS

spatio-temporal constrained GraphRAG; long time-series flood knowledge graph; FloodBot; geographical laws; flood disaster decision support

ABSTRACT

To address dynamic perception lag and multi-source integration challenges in flood emergency response, this study proposes STG-GraphRAG, a closed-loop framework integrating automated long-time-series flood knowledge graph construction with geography-constrained retrieval-augmented generation. Using flood-related social media, images, and meteorological data from July 2024, we construct 31 daily snapshots of a heterogeneous flood knowledge graph. For each query, keyword matching and semantic embeddings identify candidate nodes, which are then filtered by spatial and temporal constraints. Geography-aware community expansion uses spatial proximity and attribute similarity to form an evidence subgraph for answer generation. Comparison of location mentions in social-media records and official documents showed different coverage across administrative levels; Hekou Town appeared in the social-media records on July 29 and in the compared official documents on July 31. This method enhances context relevance to 0.9818 and compresses the subgraph scale by 68.5%. By integrating spatio-temporal summarization and risk assessment modules, the system derives an internal risk-priority category from hotspot, emotion, and flood-event indicators. In the constructed benchmark, the system achieves an answer relevance of 0.7705, a faithfulness of 0.9687, and a human score of 4.4146 (out of 5). On the pooled FloodBot benchmark, STG-GraphRAG showed higher observed answer-relevance and human-score means than INITIAL. The link of this project: https://github.com/muhan-yy/STG-GraphRAG.

CONTACT Xiaoping Rui ✉ ruixpsz@163.com

1. Introduction

The scientific rigor and timeliness of emergency decision-making for flood disasters are directly critical to the safety of life and property. In recent years, artificial intelligence technologies (such as knowledge graphs, large language models, and retrieval-augmented generation) have provided new solution pathways for flood disaster auxiliary decision-making (Xue *et al.* 2022). Nevertheless, when addressing the dynamic evolution of flood disasters and the demands of high-risk decision-making, existing technical systems still expose deep theoretical defects that urgently require breakthroughs (Karimanzira *et al.* 2025; Liang *et al.* 2025; Hu *et al.* 2025; Ouyang *et al.* 2025).

Among these technologies, knowledge graphs have become a core tool for data organization in the flood disaster domain due to their advantage in structurally representing location entities, events, and relationships (Lu *et al.* 2023; Peng *et al.* 2023). For instance, Mao (2024) proposed a method for constructing urban waterlogging emergency knowledge graphs based on spatio-temporal processes, integrating

geographical, statistical, and social media data, and defining five core elements: time, events, attributes, geographical objects, and emergency activities. However, such research is plagued by the static data trap: knowledge graphs are primarily constructed based on historical data, lacking dynamic update capabilities and unable to capture the real-time evolution characteristics of flood disasters; secondly, the retrieval mechanism supports only single-attribute matching, lacking spatial distance and time window constraints, making it difficult to locate real-time risks in specific basins (Hofmeister *et al.* 2024). For example, the flood emergency knowledge graph constructed by Wang focuses on static entity relationships (Wang *et al.* 2025). Although it achieved associative queries for disaster events, it did not consider the spatial clustering characteristics of location entities, leading to redundancy in retrieval results, and did not involve dynamic attribute nodes such as sentiment indices, resulting in a single dimension of decision support. Furthermore, addressing the issue of insufficient dynamics, Chen (2025) proposed a self-improving retrieval-augmented generation framework that automatically constructs knowledge graphs from climate news and reduces semantic redundancy through an iterative optimization mechanism. However, this framework was not designed for the spatio-temporal characteristics of flood disaster scenarios and cannot handle the spatial dependency relationships of location entities and temporal evolution patterns; meanwhile, the scale of dataset for this graph is limited, and nodes contain only core elements such as disaster driving factors and influencing factors, lacking attribute information for auxiliary decision-making such as meteorological data and sentiment indices, which limits the comprehensiveness of decision support (Jiao *et al.* 2025; Ni *et al.* 2025).

Retrieval-Augmented Generation (RAG) technology, serving as a key bridge connecting large language models with external knowledge sources, has demonstrated significant potential in the field of disaster monitoring (Peng *et al.* 2025; Ruan *et al.* 2026). Its basic architecture comprises three core components: indexing, retrieval, and response generation, aiming to enrich the context of LLM by retrieving relevant information from external databases, thereby significantly improving the accuracy, relevance, and timeliness of answers while effectively suppressing the model's 'hallucination' phenomenon (Shi *et al.* 2025; Soontontam *et al.* 2025; Zhu *et al.* 2025; Liang *et al.* 2025). In the application scenario of disaster risk management, characterized by high risk and time-critical requirements, RAG has been proven to be an effective paradigm, capable of significantly improving the quality, specificity, and usability of LLM outputs by integrating external data such as news articles and event reports (Edge *et al.* 2024; Yao *et al.* 2025). For example, Bhatti (2024) proposed an early flood warning system based on LLM and RAG, utilizing text data from social media platforms to extract information such as flood warnings, evacuation orders, and casualties.

Studies employing RAG for flood disaster monitoring adopt data sources that over-rely on single platforms, lacking integration of multi-source data such as remote sensing and meteorological observations, which easily induces information bias. Moreover, the retrieval process does not incorporate spatio-temporal constraints, making it unable to filter information for specific basins or time periods, thereby difficult to capture high-dimensional relationships and support fine-grained decision-making. The GraphRAG framework enhances the global query capability and high-dimensional relationship extraction capability of long text corpora through knowledge graph construction, community detection, and hierarchical summarization (Edge *et al.* 2024). This framework provides a generic paradigm for combining RAG with knowledge graphs, but it is not adapted to the spatio-temporal characteristics of flood disaster scenarios. Specifically, the retrieval process lacks spatial range filtering (such as basin or administrative boundary constraints) and time window limitations, making it unable to accurately extract flood disaster information within specific spatio-temporal ranges. Furthermore, subgraph construction employs general community detection algorithms, failing to consider the spatial characteristics of location entities, which leads to retrieval results that cannot retain the spatial propagation characteristics of flood disasters. Han (2024) explicitly stated in a review that existing RAG technologies lack specialized design in spatio-temporal data processing, suffer from insufficient multi-dimensional similarity fusion, and exhibit poor explainability. This issue is

particularly prominent in flood disaster decision-making: decision-makers find it difficult to verify the data sources and reasoning logic of suggestions generated by LLM (Yao *et al.* 2025; Wu *et al.* 2025; Yao *et al.* 2025). Therefore, the spatio-temporal adaptability and multi-source fusion capability of RAG technology in disaster decision-making urgently require reconstruction.

To enhance the spatio-temporal processing capability of RAG, some scholars have conducted research on spatiotemporal-aware RAG. For instance, GeoGraphRAG is one of the pioneering works in this direction, successfully applying graph structures to automated geospatial modeling tasks for the first time (Liang *et al.* 2025). The core of this framework is an external knowledge base named S-GMKG, which contains functional modules and input-output data entities extracted from thousands of real geographical processing scripts, connected through massive relationships. Although GeoGraphRAG demonstrates innovative value, when directly applied to the special and stringent scenario of flood disaster emergency decision-making, it still exposes several key applicability challenges: it mainly relies on offline or semi-offline construction, resulting in long knowledge update cycles. The retrieval mechanism relies on global semantic similarity matching, making it difficult to efficiently handle multi-dimensional, fine-grained joint constraint queries. The output consists mainly of retrieved original nodes or subgraphs, lacking active multi-dimensional high-level insight analysis. Graph traversal efficiency on large-scale graphs is low, and explainability remains merely at the level of 'source origin,' making it difficult to clarify the specific composition of the decision basis.

Existing research applying technologies such as RAG to flood disaster auxiliary decision-making mainly focuses on risk assessment and information query (Chen *et al.* 2025). For example, although Bhatti's early flood warning system can generate warning information, decision support remains limited to location identification and casualty statistics, failing to achieve comprehensive calculation of multi-dimensional risk indicators, and lacking spatio-temporal summarization and anomaly detection modules, making it difficult to identify flood disaster propagation patterns and hotspot anomaly areas (Bhatti 2024). Furthermore, the insufficient explainability prevalent in such research results manifests as three major problems: information discontinuity, black-box decision-making, and ambiguous responsibility. The answers generated by LLM lack explicit connections with the original knowledge graph content. Decision-makers find it difficult to verify reliability, and when problems occur, cannot trace the root causes (Yu *et al.* 2025). This limitation may lead to serious consequences in flood disaster emergency decision-making, especially in critical stages such as evacuation decision-making and resource allocation in high-risk areas, where the verifiability of decision suggestions is crucial (Wen *et al.* 2025).

To summarize, although existing research has made progress in flood disaster knowledge graph construction, LLM, and RAG applications, there are still four key defects: 1) Knowledge graphs lack the capability for daily dynamic updates, unable to adapt to the real-time evolution characteristics of flood disasters. 2) RAG retrieval does not integrate spatio-temporal constraints and multi-dimensional similarity, making it difficult to accurately locate key emergency information. 3) Subgraph construction does not consider geographical constraints and the spatial clustering characteristics of geographic communities, leading to retrieval redundancy and low efficiency. 4) Decision support lacks spatio-temporal summarization, anomaly detection functions, and explainability design, unable to meet the comprehensiveness and reliability requirements of emergency decision-making.

To this end, this study proposes a closed-loop architecture for flood disaster auxiliary decision-making based on the fully automated construction of long-time-series flood disaster spatio-temporal knowledge graphs and retrieval-augmented generation integrating geographical law constraints (STG-GraphRAG). This framework automatically constructs a nationwide flood disaster heterogeneous dynamic graph updated daily, capturing the spatio-temporal evolution of entities and relationships. Then a constraint strategy integrating multi-dimensional node retrieval and spatio-temporal filtering mechanisms has been designed to improve

retrieval accuracy; combines the First Law of Geography, the Third Law of Geography, and network community detection algorithms to implement a Geographic Community Awareness Adaptive Subgraph Construction (GCAASC) method. And we develop a spatio-temporal summarization module integrating spatial analysis, time trends, propagation pattern recognition, and anomaly detection, and enhances decision explainability by explicitly annotating information sources and reasoning basis. This work provides a theoretically complete and verifiable technical paradigm for flood disaster emergency decision-making, significantly advancing the modernization process of disaster prevention, mitigation, and relief capabilities.

2. Methods

This study focuses on addressing the scientific challenge of long-term sequential dynamic decision support under multi-source heterogeneous data. By integrating multi-source heterogeneous data to construct a long-term sequential flood knowledge graph, and combining large language models with spatio-temporally constrained RAG (Retrieval Augmented Generation) technology to form an interpretable decision engine, this research achieves closed-loop support from disaster perception to emergency action. The effectiveness of the proposed method is validated using flood events from typical periods (such as July 2024, when China was in a high-incidence period for flood disasters), promoting a systematic transition from static knowledge bases to real-time decision support, and providing scientific, high-precision technical support for flood monitoring and response to emergency management departments.

2.1 Study Area and Research Data

This study takes China as the research area with flood disasters as the target scenario. As one of the countries most severely affected by flood disasters globally, the distribution and formation mechanisms of floods in China profoundly reflect the complex interactions between natural geographical conditions and human activities (Rentschler *et al.* 2022). Dominated by monsoon climate with uneven spatial and temporal distribution of precipitation, certain regions in China have become high-incidence areas for flood disasters due to the combined effects of climatic characteristics and topographical features, while the long-term formed drought-flood patterns show phased adjustments with climate change. These factors collectively constitute the fundamental conditions for flood disaster occurrence (Wang *et al.* 2022).

The spatio-temporal distribution of flood disasters in China exhibits significant regional differentiation characteristics. Basin-scale floods are the main manifestation in the central and eastern plain regions, where some river basins have experienced large-scale flood events multiple times in history due to the imbalance between river channel flood discharge capacity and flood inflow volume. In large cities of the central and eastern regions, urban waterlogging problems are particularly prominent due to dense population and infrastructure limitations, with relatively high frequency of waterlogging occurrence. Southwestern mountainous areas and some arid regions are mainly characterized by sudden flash floods, reflecting the differences in flood disaster types across different regions and the regional shortcomings in monitoring and early warning systems.

Climate change has produced significant impacts on the evolution of flood disaster risk. Changes in the intensity and frequency of extreme climate events may trigger restructuring of drought-flood patterns. Coupled with underlying surface changes brought by urbanization processes, this makes the impacts caused by floods of the same magnitude show an intensifying trend.

From the perspective of data support, the overall understanding of flood disasters is based on integrated analysis of multi-source observation and social perception data, including meteorological and hydrological

data, geospatial data, social media data, etc. These data provide fundamental support for analyzing the environment of flood disaster generation, evolution pathways, and impact scope (Yuan *et al.* 2022).

(1) Meteorological Observation Data

Meteorological data are the core physical variables driving flood disaster evolution. This study adopts ERA5 and other datasets as the primary meteorological data sources, among which the key data include: 1) Total Precipitation: as the direct trigger of flood disasters, this parameter is used to identify heavy precipitation events and their spatial distribution; 2) 2m Temperature: assists in analyzing snowmelt floods or severe convective weather accompanied by high temperatures; 3) 10m Wind Speed and 10m Wind Direction: used to evaluate the impacts of typhoons or cyclonic storms on coastal and inland regions; 4) Weather Type: includes categories such as convective precipitation and stratiform cloud precipitation, which helps discriminate the disaster-causing mechanisms of flood disasters.

(2) Social Media Text Data

Social perception data can compensate for the blind spots of traditional meteorological and hydrological monitoring in terms of spatio-temporal coverage, and can particularly reflect real-time disaster feedback and emotional changes from grassroots populations. This study collected publicly available text data published on major domestic social media platforms (primarily Weibo) during the period from July 1 to July 31, 2024. The data is stored in JSON format, with each record containing the following core fields: 1) Author ID (anonymized): used for deduplication and user behavior analysis; 2) Comment Content: the main text body, containing descriptions of flood disaster events, help-seeking information, opinion comments, etc.; 3) Geographic Location: positioning information attached when the user posted (accurate to POI or village/town level); 4) Timestamp: publication time accurate to seconds; 5) Image Links: if the text includes images, the URL is recorded for subsequent visual analysis.

(3) Disaster Image Data

This study screened entries containing images from the aforementioned Weibo texts to construct a disaster image dataset. Each image underwent the following processing workflow: 1) Image Classification: the SLIP-Flood model (Tang *et al.* 2025) was adopted for preliminary screening to remove images unrelated to flood disasters (such as advertisements, landscape pictures), retaining valid images containing water accumulation, house collapse, rescue scenarios, and other content; 2) Water Depth Estimation: based on the BEW-YOLOv8 model (Liu *et al.* 2024), semantic segmentation and depth estimation were performed on flood disaster scenes in the images, outputting specific water depth values (such as ‘water accumulation depth approximately 0.8 meters’). Since multiple images may exist for the same location, estimation results are stored in set form (Formula 5), preserving their uncertainty for subsequent comprehensive analysis.

The reshaping effect of human activities on flood disaster risk has become increasingly prominent. Land use changes during urbanization processes and resource development in specific regions have altered hydrological cycle processes, increasing the possibility of flood disaster occurrence in some areas. Meanwhile, some regions have improved flood control conditions through systematic engineering construction, reducing waterlogging risks. The complexity of this ‘natural-social’ dual-drive mechanism is an important component of the overall characteristics of flood disasters in China, and also determines the multi-dimensional attributes of flood disaster problems (Xu *et al.* 2023).

2.2. Research Framework

STG-GraphRAG integrates flood-related social-media text, disaster images, and meteorological data into daily heterogeneous graph snapshots and retrieves query-specific evidence for answer generation (**Fig1**). The framework has four layers: spatio-temporal alignment of input records; extraction of entities, attributes, and relations for graph construction; graph-level spatio-temporal analysis; and query-conditioned retrieval,

summarization, and answer generation. Sections 2.3 – 2.7 specify the graph representation and the operations used in the decision-support layer.

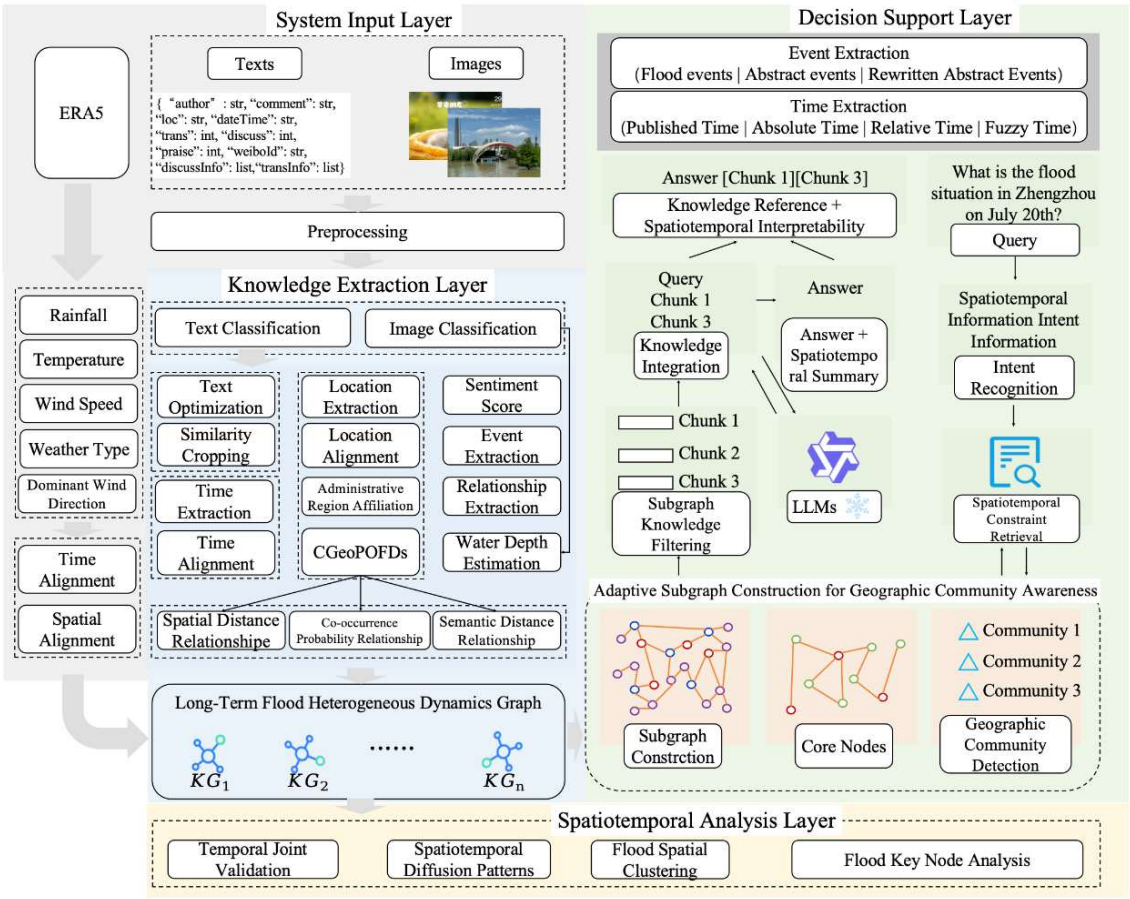


Fig1. STG-GraphRAG architecture.

(1) System Input Layer

This layer includes meteorological data such as ERA5 (rainfall, temperature, wind speed, weather type, dominant wind direction, etc.) and multi-modal social sensing data (structured text and disaster images). Among them, text data records metadata such as author (desensitized), comment content, geographical location, and timestamp in JSON format, while image data achieves disaster scene representation through visual feature extraction. In the preprocessing stage, data preliminary screening is achieved through text classification and image classification modules (Tang *et al.* 2025), and time alignment and space alignment mechanisms are introduced to map multi-source data to a unified spatio-temporal coordinate system, ensuring spatio-temporal consistency for subsequent analysis.

(2) Knowledge Extraction Layer

In this layer, the system processes text semantic information through modules such as text optimization, similarity clipping, and time extraction, combines location extraction, administrative division attribution, and flood geographic public opinion center modules to achieve geographical element parsing, and simultaneously employs sentiment scoring (Tang *et al.* 2022), event extraction, relation extraction, and water depth estimation modules to quantify disaster severity and social impact. Among them, the water depth estimation module converts visual information into quantifiable disaster indicators (Liu *et al.* 2024). The location extraction module identifies CGeoPOFDs, providing basic support for geographic perception enhancement (Tang *et al.* 2024). These features jointly constitute the node attributes and relational edges of

the heterogeneous graph, including three core associations: spatial distance relationships, co-occurrence probability relationships, and semantic distance relationships.

The system's core Long-term Temporal Flood Heterogeneous Dynamic Graph *(*KG_1, KG_2, …, KG_n*)* is constructed based on the above features. Each snapshot KG_1 in the graph represents a disaster element network within a specific time window. Nodes cover heterogeneous types such as meteorological entities, geographical regions, and disaster events, while edge relationships fuse physical associations (such as spatial proximity), semantic perception, and social perception associations (such as public opinion co-occurrence). An example of the specific Long-term Temporal Heterogeneous Dynamic Graph is shown in **Fig2**.

(3) Spatio-temporal Analysis Layer

After the graph construction, it enters the spatio-temporal analysis phase. The temporal joint verification module is used to verify the temporal correlation between the graph information and the official documents of the Ministry of Water Resources, thereby proving the rationality of the graph constructed in this work. Then, the spatio-temporal diffusion law model is utilized to reveal disaster propagation characteristics, and high-risk areas and hub nodes are identified through flood spatial clustering and key node analysis.

(4) Decision Support Layer

Given a user query, the system identifies its requested date, geographic scope, and decision intent. It first retrieves candidate graph nodes by keyword matching (Equation 7) and ranks them using Qwen3-Embedding-4B similarity (Equation 8). Administrative-area or basin constraints and the time index then restrict the candidate set (Section 2.4). The resulting seed nodes are expanded into a geographically informed subgraph (Section 2.5), from which the system derives spatial extent, temporal patterns, anomaly indicators, and a heuristic risk score (Section 2.6). The generator then composes an answer from this evidence; Section 3.4 reports Qwen3-8B as the default inference model. Finally, the citation check in Section 2.7 verifies the presence and relevance of cited graph identifiers. Each stage passes its output to the next, so an answer can be traced back to the retrieved graph evidence.

2.3. Flood Spatio-temporal Knowledge Graph Construction Theory

The core idea of heterogeneous graph modeling lies in allowing the graph to contain multiple types of nodes and edges, thereby more truthfully reflecting the complex interactions between different entities in the real world. In flood disaster scenarios, involving various heterogeneous information such as geographical locations, meteorological elements, disaster events, and social emotions, it is difficult to fully depict these multiple elements and their dynamic associations if a homogeneous graph is adopted. Therefore, this study introduces the heterogeneous graph modeling idea, abstracting entities of different granularities into heterogeneous nodes, and defining multiple relationship types based on their internal connections to construct a flood knowledge graph capable of fusing multi-source data and capturing spatio-temporal evolution.

To construct a real flood disaster knowledge base, this study constructs a Long-term Temporal Flood Heterogeneous Dynamic Graph (LTHDG) to model the spatio-temporal evolution process of China flood events in July 2024. Specifically, this study takes location entities as core nodes, and meteorological data, flood events, administrative divisions, sentiment indices, water depth estimation, etc., as attribute nodes, forming a star topology structure through multiple relationships such as spatial proximity and semantic co-occurrence, thereby achieving the organic integration of multi-modal information. This heterogeneous graph

structure not only retains the inherent attributes of each entity but also provides a rich semantic foundation for subsequent spatio-temporal analysis and decision support.

The graph is based on a daily unit (a total of 31 time snapshots, corresponding to July 1st to 31st). Each snapshot is a heterogeneous graph, with core nodes being geographical location entities (such as cities, towns, etc.). Relationships between nodes fuse three dimensions of space, semantics, and text co-occurrence, while node attributes integrate multi-source heterogeneous data such as meteorology, flood events, administrative divisions, social perception (emotion), and physical state (water depth). The graph aims to capture the dynamic propagation patterns, regional correlations, and social impacts of flood disasters to provide data-driven decision support. This section elaborates on the graph design from two perspectives: the conceptual layer and the ontological layer.

2.3.1. Flood Graph Conceptual Layer

The core idea of LTHDG is to regard flood disasters as a spatio-temporal-semantic coupled system: location entities are the system 'anchor points', their relationship networks represent the spatial diffusion of disasters, semantic associations (such as mention patterns in media reports), and text co-occurrence (such as joint occurrence in social media), while attribute nodes inject multi-modal data (meteorology, administrative divisions, emotions, etc.), forming a 'Location-Environment-Human Behavior' closed-loop feedback.

The 'dynamicity' of the graph is reflected in two levels: 1) Time granularity requires daily snapshots to capture the gradual changes in the flood disaster state; 2) Structural evolution requires nodes, relationships, and attributes to be dynamically added or deleted with the development of the disaster situation (such as the emergence of new inundated areas or sentiment index mutations).

(1) Node Types

The graph contains two types of nodes: (i) core nodes (location entities, denoted as $\mathscr{L}$), representing location entities extracted from Weibo text; and (ii) attribute nodes (auxiliary entities), including meteorological information ($\mathscr{M}$), flood events ($\mathscr{F}$), administrative divisions (A), sentiment index ($\mathscr{E}$), and water depth estimation (D). Each location entity can connect to multiple attribute nodes, forming a star topology (location as the core, attributes as radiating branches).

(2) Relationship Types

1) Distance

We calculate the great-circle distance between location entities from their WGS-84 coordinates using the Haversine formula. Distances are expressed in kilometres.

$$\text{distance}(l_i,l_j)=2R*\arcsin\sqrt{\sin\left(\frac{\phi_j-\phi_i}{2}\right)^2+\cos(\phi_i)\cos(\phi_j)\sin\left(\frac{\lambda_j-\lambda_i}{2}\right)^2} \quad (1)$$

where $l_i,l_j \in L$ are location entities; ϕ_i and λ_i denote the WGS-84 latitude and longitude of l_i, respectively, with analogous notation for l_j. All angular coordinates are converted to radians before calculation, and $R=6371$ km is the mean Earth radius. Thus, distance(l_i,l_j) is measured in kilometres.

2) Semantic

Based on the path hop count of the text dependency tree, it measures the strength of the association between positions in the semantic space. Given a text corpus U, for each text $t \in U$, if positions l_i and l_j are reachable in the dependency tree of t, then the semantic distance is the average path hop count; otherwise, it is infinite. The daily aggregation formula is:

$$\text{semantic}(l_i,l_j)=\frac{1}{|U_d|}\sum_{t \square U_d} \text{hop_average}(l_i,l_j,t) \tag{2}$$

where U_d represents the text set on day t, and hop_average(·) returns the average number of hops in the dependency tree.

3) Intersection

This represents the probability that two entities simultaneously exist in a single Weibo post, reflecting perceived social connections. The calculation formula is as follows:

$$\text{intersection}(l_i,l_j)=\frac{|\{t \in U_d : l_i \in t \wedge l_j \in t\}|}{|U_d|} \tag{3}$$

where the numerator represents the number of texts that contain both l_i and l_j, and the denominator is the total number of texts for the day.

4) Flood Event Entity Relationships

Table 1. Description of entity relationship types in flood disaster events.

Relationship Type	Description (Subject-Object)	Example
Occurred In	A flood event occurred at a certain location	(Heavy rain and flood, occurred in, Zhengzhou City)
Occurrence Time	A flood event corresponds to a certain time	(Flooding, occurrence time, 2024-07-05)
Impact	A flood event affected a certain entity	(Heavy rain and flood, impact, Metro Line 5)
Measures Taken	A certain rescue measure was implemented at the location/event	(Xinxiang City, measures taken, sandbag reinforcement of river embankments)
Losses Caused	A flood event caused a certain loss	(Flooding, losses caused, 10 houses collapsed)
Affected Population	A flood event is associated with a certain affected population	(Evacuation action, affected population, 200 citizens)
Adjacent Relationship	There is a spatial relationship between locations	(Zhengzhou City, adjacent relationship, Xinxiang City)
Chronological Order	There is a chronological order in time	(2024-07-05, chronological order, 2024-07-06)
Triggered	One flood event directly caused another flood event	(Heavy rainfall, triggered, torrential rain and flooding)
Organize and Implement	A certain entity (government, agency) leads and implements flood-related measures	(Xinxiang Municipal Government, organize and implement, sandbag reinforcement of river embankments)

Relationship Type	Description (Subject-Object)	Example
Issue warning	A certain entity (meteorological and emergency response departments) issues early warning information to specific areas regarding flood risks	(Henan Provincial Meteorological Bureau, issue warning, red alert for torrential rain)
Providing Relief	A certain entity (government or non-profit organization) provides relief services such as living assistance and medical care to disaster victims.	(Xinxiang Civil Affairs Bureau, Providing Relief, the affected people)

The above three types of relationships represent the edge types between location entities in the knowledge graph. To highlight the relationship types between entities in different flood events, this study uses prompting engineering to extract flood events and various entity relationship types from short texts on Weibo. Detailed prompts are provided in Prompt 2 of Appendix A. Related explanations are shown in the table 1.

(3) Attribute Aggregation Mechanism

1) Sentiment Index

The sentiment index E_l at position l is the average sentiment score of the associated Weibo text:

$$E_l^{(d)}=\frac{1}{n_l^{(d)}}\sum_{k=1}^{n_l^{(d)}} e_k^{(d)} \tag{4}$$

where $n_l^{(d)}$ is the number of associated texts on day d, and $e_k^{(d)}$ is the sentiment score of a single text.

2) Water Depth Estimation

The water depth estimation D_l at location l is the set of estimation results from all associated images (preserving uncertainty, not taking an average):

$$D_l^{(d)}=\{D_{l,1}^{(d)},D_{l,2}^{(d)},\ldots,D_{l,m}^{(d)}\} \tag{5}$$

where $D_{l,k}^{(d)}$ represents the water depth estimation result of the *k-th* image.

3) Other attributes (meteorology, administrative divisions, flood events) are directly related to the original data.

(4) Dynamic Evolution Mechanism

The graph models long-term temporal characteristics through time slices. Let the graph $G^{(d)}=(V^{(d)},E^{(d)},A^{(d)})$ be the graph snapshot on day d ($d\in\{1,2,\ldots,31\}$), where: $V^{(d)}=L^{(d)}\cup M^{(d)}\cup F^{(d)}\cup A^{(d)}\cup E^{(d)}\cup D^{(d)}$ is the node set. $E^{(d)}$ is the relation set, which contains three types of edges: distance, semantic and intersection. $A^{(d)}$ is the attribute mapping function, which binds the attribute nodes to the positions.

2.3.2. Flood Map Ontology Layer

This section abstracts the concept layer into a machine-scaled ontology (Xue *et al.* 2022; Zhong *et al.* 2023; Yang *et al.* 2022). The core of the ontology layer is the location-centered ontology, whose class hierarchy, data attributes, and object attribute constraints are shown in Table 2 and Table 3 (Peng *et al.* 2023).

Table 2. Class hierarchy description.

Top Class			Subclass		
Class Name	Description	Data Attributes	Class Name	Description	Data Attributes
Location	Core class	hasLatitude hasLongituate hasName	\	\	\
Attribute	Abstract parent class	\	MeteorologicalData	Meteorological data class	hasWindSpeed (float) hasRainfall (float)
			FloodEvent	Flood events	hasEventType
			AdministrativeDivision	Administrative divisions	Province City District
			SentimentIndex	Sentiment index class	hasSentimentValue
			WaterDepthEstimation	Water depth estimation	HasDepthValue
Relation	Abstract relationship class	\	SpatialRelation	Spatial distance class	hasDistanceValue (float)
			SematicRelation	Semantic distance class	hasHopCount (float)
			IntersectionRelation	Co-occurrence distance class	hasProbability (float)
TemporalContext	Time sequence node	hasDate	\	\	\
DataSource	Record raw data	hasSource	\	\	\

Table 3. Formal description of attributes and relations.

Property type	Attribute name	Description
Object data (Define connections between nodes)	hasAttribute	Location→Attribute （1:N）
	hasSpatialRelationWith	Location × Location → SpatialRelation （Symmetry properties）
	hasSemanticRelationWith	Location × Location → SemanticRelation （Symmetry properties）
	hasCooccurrenceWith	Location × Location → CooccurrenceRelation （Symmetry properties）
	belongsTo	Location × AdministrativeDivision （Administrative ownership）
Data Attributes	hasSentimentValue	For SentimentIndex only, updated daily

Property type	Attribute name	Description
(Define text values)	hasDepthSet	WaterDepthEstimation implements a collection using rdf:List

To facilitate downstream tasks, we transform the three location relationships defined in Equations (1) – (3) into dimensionless contributions and combine them into a weighted edge for each daily snapshot.

$$gwf(l_i,l_j) = \alpha * s_d(l_i,l_j) + \beta * s_s(l_i,l_j) + \gamma * s_i(l_i,l_j)$$

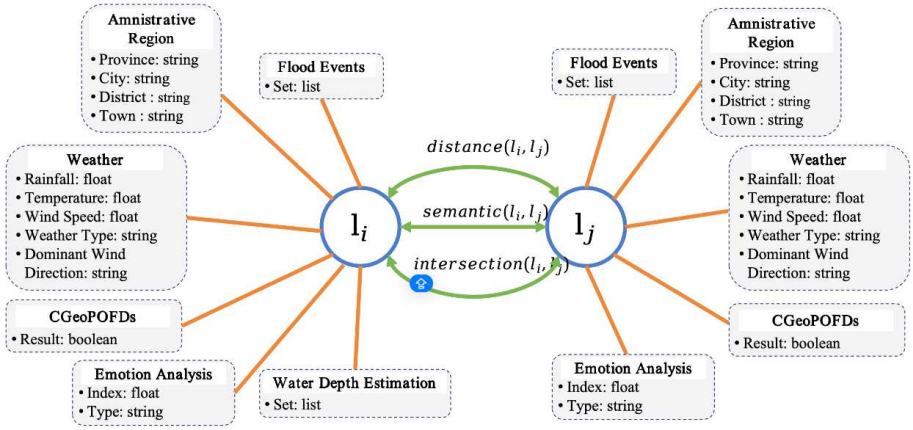
$$s_d = \begin{cases} \max(1 - distance(l_i,l_j)/100,\ 10^{-5}), & 0 < distance(l_i,l_j) < 100\text{km} \\ 0, & \text{otherwise} \end{cases}$$

$$s_s = \begin{cases} \max(1 - semantic(l_i,l_j)/3,\ 10^{-5}), & 0 < semantic(l_i,l_j) \le 3 \\ 0, & \text{otherwise} \end{cases} \quad (6)$$

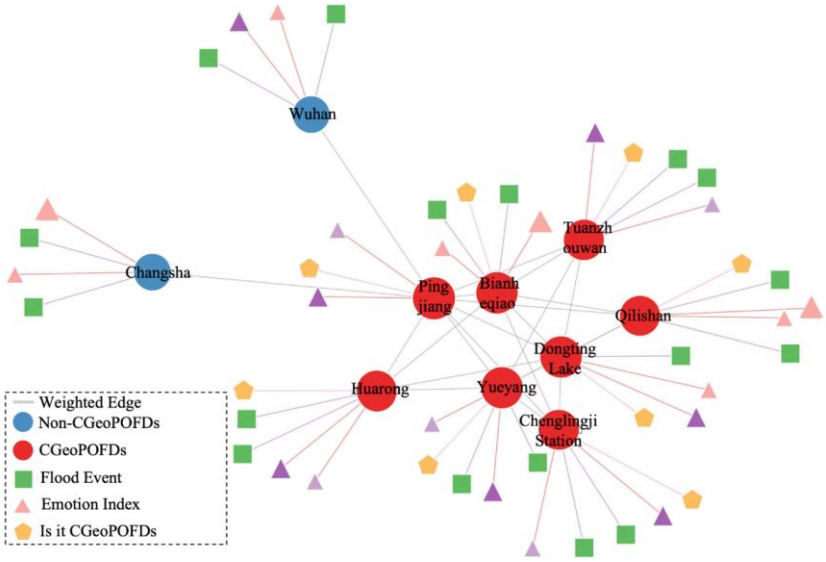
$$s_i = \begin{cases} intersection(l_i,l_j), & intersection(l_i,l_j) > 0.4 \\ 0, & \text{otherwise} \end{cases}$$

where, α, β and γ are the corresponding weight values, which are determined by experimental results (see **Fig10**).

Fig1 is a schematic diagram of the spatio-temporal heterogeneous flood graph constructed in this study. Since the purpose of this study is to realize the application of automated flood decision-making based on LTHDG, the final knowledge graph is stored in binary form.



(a) Schematic diagram of the graph nodes



(b) Detailed graph information (partial nodes, taking the weighted edge GWF as an example)

Fig2. Example of spatio-temporal heterogeneity graph of flood disaster (single time node).

2.4. Spatio-temporally Constrained Flood Knowledge Retrieval

Spatio-temporally constrained flood knowledge retrieval is the core module of this system. By integrating multi-dimensional retrieval strategies and spatio-temporal filtering mechanisms, it achieves accurate positioning of the flood knowledge graph. This module parses the spatio-temporal constraints from user queries, then executes a multi-stage retrieval strategy to generate a set of candidate nodes highly relevant to the query.

2.4.1. Multidimensional Node Retrieval

Node retrieval has two stages: keyword-based candidate screening followed by embedding-based ranking of the surviving nodes. The first stage controls the search space; the second ranks candidates by semantic similarity to the query. Let the graph $G^{(d)}=(V^{(d)},E^{(d)},A^{(d)})$. For a given query q, the coarse-grained retrieval is defined as follows:

$$V_{keyword}=\{v\in V^{(d)} \mid \exists k\in K_q, k\subseteq desc(v)\} \tag{7}$$

where K_q is the set of keywords extracted from query q, and $desc(v)$ represents the text description of node v. In the coarse ranking stage, named entity recognition technology is used to extract positional keywords.

In the fine ranking stage, the semantic similarity between the query and the node description text is calculated, and the Qwen3-Embedding-4B model is used to generate embedding vectors (Zhang *et al.* 2025):

$$e_q=Embedding(q),\ e_v=Embedding(desc_v) \tag{8}$$

$$sim_{sem(q,v)} = cos(e_q, e_v) = \frac{e_q \cdot e_v}{||e_q|| \cdot ||e_v||}$$

where e_q represents the embedding vector of the query, e_v represents the embedding vector of the node description text, $Embedding(\cdot)$ represents the embedding vector generation model, $sim_{sem(q,v)}$ represents the similarity between the query and the node description text, and $cos(\cdot,\cdot)$ represents the cosine similarity function.

Finally, the k nodes with the highest similarity are selected as the candidate set V_{sem}. This system uses a sliding window strategy to process graph nodes, with a window size of w, which significantly reduces the processing requirements for large-scale graphs.

2.4.2. Spatio-temporal Filtering Mechanism

This system parses the spatio-temporal constraints $C_{st}=(C_s, C_t)$ from the query, where C_s is the spatial constraint and C_t is the temporal constraint. Spatial constraints include two types: 1) Administrative division constraints. Let the set of administrative divisions mentioned in the query be $A_q=\{a_1,a_2,\ldots,a_m\}$, then the pre-constructed administrative division index I_{admin} filters the node $V_{space}=\cup_{a\in A_q} I_{admin}[a]$; 2) Hydrological basin constraints. If the query involves a specific basin (such as 'Yangtze River Basin', 'Huai River Basin', etc.), then the basin index I_{basin} filters the node $V_{basin}=I_{basin}[basin\ name]$. Temporal constraints mainly handle time points. Let the query time constraint be t_q, and the map time index be I_{time}, then: $V_{time}=I_{time}[t_q]$.

After keyword and embedding retrieval, the system applies the parsed spatial constraint, if any, to the candidate nodes and then applies the temporal constraint. Matches for multiple administrative locations are combined by union; when an index lookup produces matches, those nodes are intersected with the current candidate set.

2.5. Adaptive Flood Subgraph Construction Based on Geographic Community Awareness

This module introduces the first law of geography (Tobler *et al.* 1970) and the third law of geography (Zhu *et al.* 2018) into subgraph construction, integrates geographic community structure with adaptive search strategy, and solves the problem of information redundancy or missing information caused by traditional fixed-hop-number subgraph construction methods. The procedure detects geographic communities, estimates community cohesion, constructs an initial query-centred subgraph by adaptive BFS (Section 2.5.4), and then evaluates similarity-ranked cross-community candidates using the connectivity criteria in Section 2.5.3.

2.5.1. Geographic Community Detection

STG-GraphRAG uses the Louvain algorithm to optimize the modularity Q for detecting geographic communities (Blondel *et al.* 2008):

$$Q = \frac{1}{2m}\sum_{i,j}\left[A_{ij} - \frac{k_i k_j}{2m}\right]\delta(c_i, c_j) \tag{9}$$

where A_{ij} is the edge weight between nodes i and j in the undirected graph supplied to Louvain (zero if no edge exists), $k_i = \sum_j A_{ij}$ is the weighted degree of node i, $m = \frac{1}{2}\sum_{ij} A_{ij}$ is the total undirected edge weight, c_i is the community of node i, and δ is the Kronecker delta function (Blondel *et al.* 2008).

When the Louvain algorithm fails, STG-GraphRAG reverts to DBSCAN-based geographic clustering (Ester *et al.* 1996): $DBSCAN(P, \epsilon, minPts)$, where P is the set of node coordinates, $\epsilon = 0.5°$, *and* $minPts = 3$. This fallback uses raw longitude – latitude coordinates. The $0.5°$ radius is separate from the kilometre-valued distance in Equation (1).

2.5.2. Calculation of Community Cohesion

The first law of geography emphasizes 'the closer, the more relevant.' To apply this law to construct adaptive subgraphs, this study developed the indicator 'community cohesion':

$$Cohesion(C_k) = 0.6 * \frac{1}{1 + \frac{\overline{d_{geo}}}{100}} + 0.4 * \frac{E_{internal}}{max(|V(C_k)| * (|V(C_k)| - 1)/2, 1)} \tag{10}$$

where $\overline{d_{geo}}$ represents the average geographical distance (km) within the community, and $E_{internal}$represents the number of edges within the community. The first term measures geographical density, and the second term measures topological connectivity. $V(C_k)$ denotes the set of nodes belonging to community C_k, and $E_{internal}$ denotes the number of edges whose two endpoints are both in C_k.

2.5.3. Calculation of Location Node Similarity

The third law of geography emphasizes 'geographical similarity,' meaning that the more similar the geographical environments, the more similar the characteristics of geographical targets. To apply this law to construct adaptive subgraphs, this study constructs an index called 'location node similarity,' which is jointly determined by spatial location, attribute features, and social perception. The initial subgraph G_{sub} is constructed by the adaptive BFS procedure specified in Section 2.5.4. The similarity and connectivity rules below consider additional nodes from other communities after this initial subgraph has been formed.

The comprehensive similarity between node u and node v, $Sim_{geo}(u, v)$, is defined as the weighted sum of multidimensional features:

$$Sim_{geo}(u, v) = \sum_{k \in F} w_k \cdot Sim_k(u, v) \tag{11}$$

where F ={space, weather, flood, emotion} is the feature set, and w_k is the corresponding weight. And $w_{Sim_{space}(u,v)} = 0.25$, $w_{Sim_{weather}(u,v)} = 0.35$, $w_{Sim_{flood}(u,v)} = 0.30$, $w_{Sim_{emotion}(u,v)} = 0.10$. $Sim_{space}(u, v)$ represents spatial similarity (based on administrative division matching and geographical distance decay), $Sim_{weather}(u, v)$ represents meteorological similarity (based on rainfall differences), $Sim_{flood}(u, v)$ represents disaster similarity (based on flood event frequency), and $Sim_{emotion}(u, v)$ represents emotional similarity (based on sentiment index). The similarity of each sub-item is calculated as follows:

$$
\begin{aligned}
&Sim_{space}(u, v)=\lambda_1 \cdot I_{admin}(u, v)+\lambda_2 \cdot \max(0, 1-\frac{d_{haversine}(u, v)}{D_{max}}) \\
&Sim_{weather}(u, v)=1-min(\frac{|Rain_u-Rain_v|}{R_{normalization}},1) \\
&Sim_{flood}(u, v)=1-min(\frac{|Count_u-Count_v|}{C_{normalization}},1) \\
&Sim_{emotion}(u, v)=1-|Emo_u-Emo_v|
\end{aligned}
\tag{12}
$$

where λ_1 (default 0.7) and λ_2 (default 0.3) represent weights, $I_{admin}(u, v)$ equals 1 when the two nodes have the same province and city, 0.5 when they share a province but belong to different cities, and 0 when their provinces differ, $d_{haversine}(u, v)$ represents the distance calculated using the Haversine formula, D_{max} is the maximum effective distance threshold (default 200km), $Rain_*$ represents the rainfall corresponding to the location node, $R_{normalization}$ represents the normalized value of rainfall difference (default 50), $Count_*$ represents the number of flood events corresponding to the location node, $C_{normalization}$ represents the normalized value of the difference in the number of flood events (default 10), and Emo_{u} and Emo_{v} are node-level emotion indices on a 0 – 1 scale.

To overcome the limitations of local communities, STG-GraphRAG filters a candidate set from nodes that are in different geographical communities but have high similarity to the seed node V_{seed}. For each seed node (i.e., Retrieved Nodes hereinafter referred to as V_{seed}), s ∈ V_{seed}, the candidate node set C_s is defined as:

$$
C_s=Top\text{-}5\{v \in V \backslash V_{sub} | Community(v) \neq Community(s)\}_{ranked\ by\ Sim_{geo}(s,v)} \tag{13}
$$

where Community(·) represents the community where the node is located, $V\backslash V_{sub}$ denotes the subset of V excluding V_{sub}. All subsequent occurrences of the backslash operator '\' follow this same convention.

Each seed retains at most five cross-community candidates. Duplicate candidates from different seeds are merged and ranked by their highest similarity to any seed; the resulting set of at most 50 distinct candidates is denoted C_{all}. This cross-community limit is separate from the node-retrieval limit in Section 2.4.1.

After obtaining candidate nodes, to ensure that the enhanced subgraph satisfies both geographical similarity and topological connectivity, this study proposes two node selection and addition strategies.

(1) Direct Topological Connectivity

This strategy requires that candidate node v must have an edge connection with at least one node in the existing subgraph $G_{sub}=(V_{sub},E_{sub})$, where G_{sub} refers to the subgraph constructed using the 'community cohesion' index and dynamic hop count, i.e., 'Retrieved Nodes', 'Nodes Covered by One Hop', and 'Nodes Covered by Two Hops' in **Fig3**. The intermediate node set V_{direct} and edge set E_{direct} are represented as follows:

$$V_{direct}=V_{sub}\cup\{v\in C_{all}|\exists u\in V_{sub},(u,v)\in E_{original}\}$$
$$E_{direct}=E_{sub}\cup\{(u,v)\in E_{original}|u\in V_{sub},v\in V_{direct}\setminus V_{sub}\} \quad (14)$$

where $E_{original}$ is the edge set of the full daily graph, E_{sub} contains edges already in G_{sub}. The direct-connectivity stage adds a candidate only when it has an edge to the initial subgraph. Let $C_{remaining} = C_{all} \setminus V_{direct}$; only these remaining candidates enter the path-reliability stage.

(2) Path Reliability Constraint

Unlike direct connectivity, this strategy considers candidates linked to G_{sub} by simple paths of two or three edges. The reliability weight W(P) of path P is defined as the product of the weights of all edges on the path, which is used as a multiplicative path-strength score:

$$W(P)=\prod_{e\in P} w(e) \quad (15)$$

For a candidate node v, calculate the optimal path reliability $R(v,G_{sub})$ between it and any node in the subgraph G_{sub}:

$$R(v,G_{sub})=\max_{u\in V_{sub}}\left(\max_{\substack{P:u\to v\\ 2\le|P|\le 3}}\prod_{e\in P} w(e)\right) \quad (16)$$

Let $P^*(v)$ be a path attaining the maximum in Equation (16), with fewer edges preferred when scores tie. If no eligible path exists, $R(v,G_{sub})=0$. For the remaining candidates, a positive reliability score must also meet the threshold τ to qualify for addition to the enhanced subgraph.

$$C_{path} = \{v \in C_{remaining}: R(v, G_{sub}) > 0, R(v, G_{sub}) \geq \tau\}, \quad (17)$$

$V_{enhanced}=V_{direct}\cup \bigcup_{v\in C_{path}} V(P^*(v))$,

$$E_{enhanced}=E_{direct}\cup \bigcup_{v\in C_{path}} E(P^*(v))$$

where

t

he threshold τ is the 25th percentile of positive $R(v, G_{sub})$ values among the remaining candidates for the current query. If non

However, because this strategy requires Dijkstra's algorithm to calculate the shortest path between a candidate node and all nodes in G_{sub} each time a candidate node is evaluated, its time complexity is $O(L*Q*(X+Zlog_Z))$, where L represents the number of candidate nodes, Q represents the number of nodes in the subgraph G_{sub}, X represents the number of edges in the current overall graph, and Z represents the number of nodes in the current overall graph. Therefore, this strategy has a high time consumption. This strategy currently has room for improvement and is not suitable for real-time decision-making in flood disaster management.

2.5.4. Adaptive BFS Expansion

Assuming the query geographic scope level is $g_q\in\{local, regional, national\}$ (determined through keyword matching), and the base maximum hop count is h_{base}, then the maximum hop count for node v is:

$$h_{max}(v)=\left\lfloor \min(h_{base}*\left(1+Cohesion\left(Community(v)\right)\right), h_{limit}(g_q))\right\rfloor \quad (18)$$

where $h_{limit}(local)=20$, $h_{limit}(regional)=40$, *and* $h_{limit}(national)=\infty$. The floor operator converts the calculated limit to an integer number of BFS hops. For a node whose community has no cohesion score, the base hop count is used before applying the geographical-scope limit. The cross-community edge weight threshold is $\theta_{cross}=\begin{cases}0.3 & if \text{ Same community}\\ 0.5 & if \text{ Different community}\end{cases}$. The edge weight is calculated as $\omega_{edge}(u,v)=(\prod_{r\in R}(\omega_r+\epsilon))^{1/|R|}$, where R represents the set of edge relationship types (Distance, Semantic, and Intersection). In the GWF graph, these three relationship weights are fused into a single stored GWF edge weight before BFS traversal; therefore, the traversal uses one stored edge weight and $|R|=1$ here. Since this study uses the GWF edge type for inference, ω_r is the corresponding type weight, $\epsilon=0.001$ is the smoothing constant, and $h_{base}=10$.

Fig3 schematically contrasts fixed-hop expansion with geographically constrained subgraph selection. Blue nodes are query-retrieved seeds; the two lighter green shades denote nodes reached within one and two hops, respectively; and dark-green nodes represent nodes selected using geographic similarity. Orange nodes are excluded from the resulting subgraph. The three-hop setting in this illustration is separate from the experimental base hop count of 10. The figure illustrates differences in node selection and does not

imply that Equation (18) reduces the base hop count.

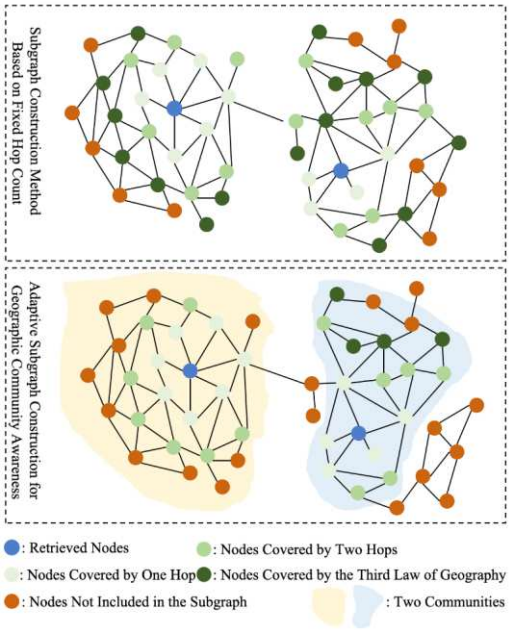


Fig3. Schematic comparison of fixed-hop expansion and geography-aware subgraph selection.

2.6. Spatio-temporal Summary Module for Flood Submaps

The spatio-temporal summary module provides context for subsequent generation by performing structured analysis of the characteristics of flood submaps. This module includes four core components: spatial scope analysis, time trend analysis, spatio-temporal anomaly monitoring, and risk assessment.

2.6.1. Spatial Scope Analysis

After STG-GraphRAG acquires a subgraph, it calculates the subgraph's spatial boundary. Let the node coordinate set be $P=\{(lon_i,lat_i)\}_{i=1}^{n}$, then the bounding box is $B=(min(lon),\min(lat),\max(lon),\max(lat))$. The coverage area is approximated using the Haversine formula: $A=d_{width}*d_{height}$, where d_{width} is the east-west distance and d_{height} is the north-south distance. The geographic center point is calculated as follows:

$$C_{center}=(\frac{min(lon)+max(lon)}{2},\frac{min(lat)+max(lat)}{2}) \tag{19}$$

where lon represents longitude, lat represents latitude, $max(\cdot)$ represents the maximum value, and $min(\cdot)$ represents the minimum value.

2.6.2. Time Trend Analysis

Assuming the event time set in the subgraph is $T=\{t_1,t_2,\ldots,t_m\}$, this system counts the number of events in each time period:

$$N_{morning}=\sum_{t\in T} I(6{:}00\le t\le 12{:}00)$$

$$N_{afternoon}=\sum_{t\in T} I(12{:}01\le t\le 18{:}00)$$

$$N_{evening}=\sum_{t\in T} I(18{:}01\le t\le 23{:}59) \tag{20}$$

$$N_{night}=\sum_{t\in T} I(00{:}00\le t\le 05{:}59)$$

where $I(\cdot)$is the indicator function.

2.6.3. Spatio-temporal Anomaly Monitoring

STG-GraphRAG performs two types of spatio-temporal anomaly detection on the retrieved subgraphs: 1) Hotspot anomaly detection. Assuming the proportion of hotspot nodes (CGeoPOFDs) in the subgraph is $r_{hot}=\frac{|V_{hot}|}{|V|}$, where $|V_{hot}|$ represents the number of hotspot nodes, anomalies are identified when $r_{hot}>0.7$ or $r_{hot}=0$ and the total number of nodes $|V|>5$. 2) Sentiment anomaly detection. The sentiment index $z_v=\frac{e_v-\mu_e}{\sigma_e}$ is calculated, where μ_e and σ_e represent the average sentiment value and standard deviation of the subgraph, respectively, and e_v represents the sentiment index of each text. When $|z_v|>1$, it is marked as an anomalous region.

2.6.4. Risk Assessment

STG-GraphRAG calculates multidimensional risk indicators for the retrieved subgraphs:

$$f_1=\frac{|V_{hot}|}{|V|}$$

$$f_2=1-\frac{1}{|V|}\sum_{v\in V} e_v$$

$$f_3=\frac{1}{|V|}\sum_{v\in V}|E_v| \tag{21}$$

$$\tilde{f}_3=min\left(\frac{f_3}{95th_{percentile}(f_3)},\ 1\right)$$

$$R=0.4*f_1+0.3*f_2+0.3*\tilde{f}_3$$

$$L_R=\begin{cases} \text{High Risk} & \text{if } R>0.7 \\ \text{Medium Risk} & \text{if } 0.4<R\leq 0.7 \\ \text{Low Risk} & \text{if } R\leq 0.4 \end{cases}$$

where f_1 represents hotspot density, f_2 represents emotional risk, f_3 represents event density, $\widetilde{f_3}$ is the result of f_3 normalization, R represents comprehensive risk score, E_v denotes the set of flood-event entities associated with node v in the retrieved subgraph, and $|E_v|$ is the number of those event entities, and L_R is the risk level determination result. $95th_{percentile(f_3)}$ is the 95th percentile of node-level event counts within the retrieved subgraph.

Equation (21) is applied only when the retrieved subgraph is nonempty and the 95th percentile of its node-level flood-event counts is greater than zero. Otherwise, the event-density term is undefined, and no risk score or risk level is reported. A subgraph with no recorded flood events is therefore not automatically classified as low risk.

2.7. Enhanced Spatio-temporal Interpretability of Flood Disaster Decision-Making

STG-GraphRAG employs a spatio-temporal interpretability module to address three core issues: information gaps, black-box decision-making, and ambiguity of responsibility. It enhances system transparency through citation verification and geographic visualization. The core component of this module is the citation verification mechanism.

This system generates unique identifiers for entities in the heterogeneous dynamic graph of flood disasters:

$$\begin{aligned} ID_{node}(v)&=hash(v, prov(v), lat(v), lon(v), date) \\ ID_{event}(e)&=hash(sub(e), rel(e), obj(e), date) \\ ID_{analysis}(a)&=hash(type(a), content(a)[:50], date) \end{aligned} \tag{22}$$

where $prov(v)$ represents the province of node v, $lat(v)$ represents the latitude of the node, $lon(v)$ represents the longitude of the node, $date$ represents the date, e represents the event triple, $sub(e)$ represents the subject in the event triple, $rel(e)$ represents the relation in the event triple, $obj(e)$ represents the object in the event triple, a represents the analysis result, $type(a)$ represents the type of the analysis result, and $content(a)$ represents the content of the analysis result.

Suppose the response generated by the LLM is r, where the set of citation identifiers is $T=\{i_1,i_2,\ldots,i_k\}$, and the validation function is $valid(i)=I(i\in G)\wedge I(relevance(r,i)>\theta_{rel})$, where $relevance(r,i)$ is calculated through keyword matching or semantic similarity, and $\theta_{rel}=0.3$ is the threshold. The citation coverage evaluation metric is $C_{coverage}=\frac{|\{i\epsilon T \mid valid(i)=1\}|}{|T|}$.

3. Experiments and Results

3.1. Text Optimization Module Evaluation

This section conducts semantic consistency validation experiments for the text optimization module in the STG-GraphRAG system (the Prompt for text optimization is provided in Appendix A). As a core component of the feature extraction layer, this module aims to enhance the readability of social media text while preserving original semantic information, thereby supporting subsequent spatiotemporal-constrained retrieval and decision generation. The experiments employ the Qwen3-Embedding-4B model (Zhang *et al.* 2025) to compute vector representations of texts before and after optimization, and calculate cosine similarity to verify whether the module maintains semantic consistency while improving readability.

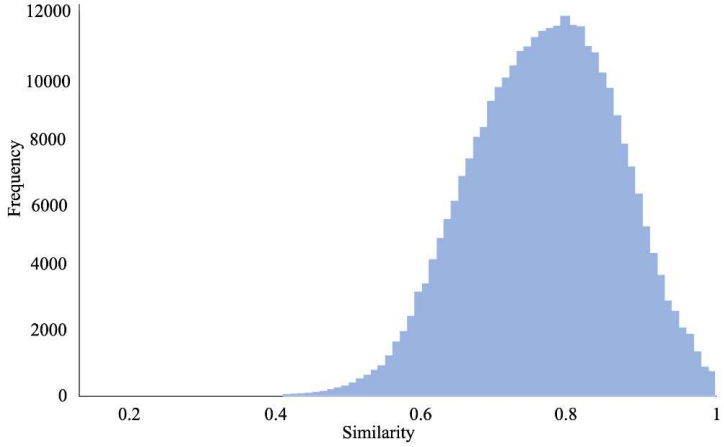


Fig4. Text optimization evaluation.

The experimental results are shown in **Fig4**, where the similarity distribution exhibits a clear right-skewed normal distribution characteristic. Statistical data show that 93.7% of samples have similarity exceeding 0.7, and 99.7% of samples have similarity exceeding 0.5, with the peak located in the range around 0.82, indicating that the text optimization process maintains a high degree of fidelity to the original semantics.

Approximately 0.3% of samples have similarity below 0.5, and these data primarily originate from original texts containing abundant internet slang or specialized meteorological terminology. Analysis indicates that when the original text contains severe grammatical errors or semantic ambiguity, the text optimization module performs substantial semantic reconstruction to meet subsequent processing requirements. Although this may lead to semantic deviation in a small portion of samples, considering that these original texts themselves have extremely poor readability, moderate semantic reconstruction actually improves information usability.

The experimental results also demonstrate that the collaborative work between the text optimization module and Qwen3-Embedding-4B achieves a balance between semantic fidelity and readability enhancement (Zhang *et al.* 2025). The central tendency of the similarity distribution (with a standard deviation of only 0.10) reflects the stable performance of this module, providing high-quality input data for downstream tasks.

3.2. Spatio-temporal Analysis of Long-Term Temporal Graph

3.2.1. Temporal Joint Validation

(1) Administrative Division Granularity Analysis

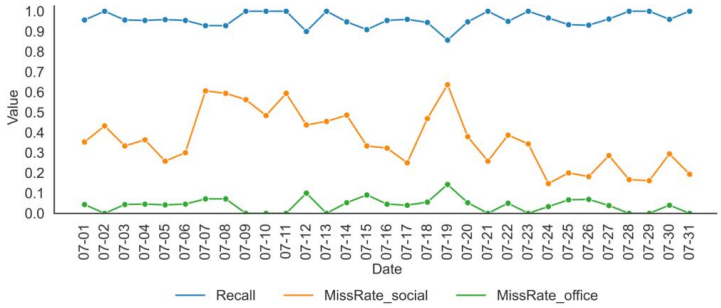
To verify the rationality of the long-term temporal flood heterogeneous dynamic graph constructed in this work, this study designs a temporal joint validation experiment to evaluate the temporal consistency between location entities in the knowledge graph constructed from social media and location entities in official documents from the Ministry of Water Resources. This experiment targets four administrative division granularities: provincial, municipal, district, and town/village levels, and employs three core metrics for evaluation: 1) Recall: the proportion of location entities in official documents that appear in the knowledge graph; 2) MissRate_social: the proportion of location entities in the knowledge graph that do not appear in official documents; 3) MissRate_office: the proportion of location entities in official documents that do not appear in the knowledge graph. The experiment covers the complete cycle from July 1 to 31, 2024, with independent validation evaluations conducted daily (as shown in **Fig5**). The day-by-day comparisons of location-entity mentions at different administrative levels are presented in **Fig11** in Appendix C.

Fig5 displays the temporal changes of the three evaluation metrics under different administrative division granularities. In the provincial-level evaluation (Fig5 subplot a), the Recall metric remains in the range of 0.86 to 1.0, and the MissRate_office metric fluctuates between 0 and 0.17, indicating that social media data and official documents have high consistency at the provincial level. MissRate_social remains between 0.15 and 0.65, suggesting that social media data has a certain supplementary effect on official documents at the provincial level.

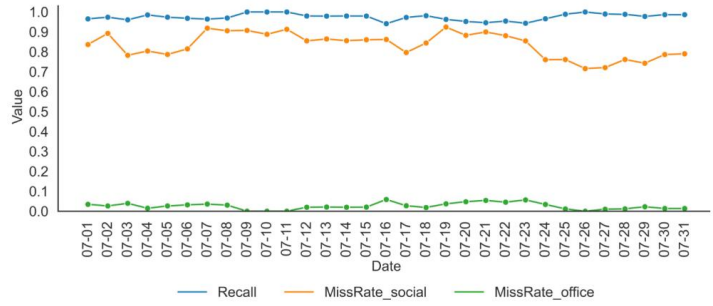
The municipal-level evaluation (**Fig5** subplot b) presents a similar trend to the provincial level but with increased magnitude. Notably, the overall MissRate_social metric is larger compared to the provincial level, indicating that social media data has a stronger supplementary effect on official documents at the municipal level than at the provincial level.

The district-level evaluation (**Fig5** subplot c) shows an overall decline in the Recall metric compared to (a) and (b), while MissRate_office shows an overall increase. This indicates that at the district level, the recall capability of social media data for official documents appropriately declines. However, MissRate_social still remains in a relatively high range, indicating that the supplementary capability of social media data for official documents remains strong.

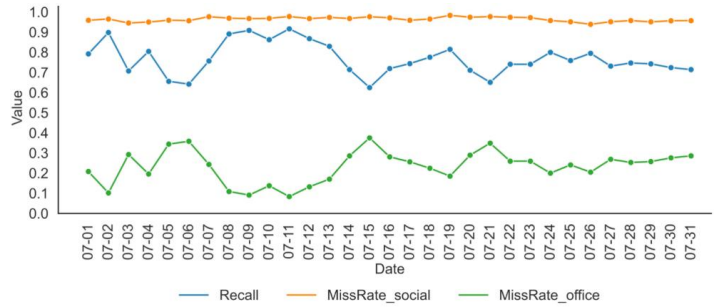
The town/village-level evaluation results (**Fig5** subplot d) reveal the most significant data deviation: Recall further declines overall, and MissRate_office further increases overall, meaning that at the town/village level, the recall capability of social media data for official documents further decreases. However, at this point, MissRate_social still remains at a relatively high level, and comprehensively analyzing (a), (b), and (c) reveals that as the administrative division hierarchy becomes more refined, MissRate_social shows an overall upward trend. This indicates that official documents rarely record town/village-level disaster information, while social media contains abundant grassroots information, validating the necessity of constructing a dynamic knowledge graph to supplement official data, and also confirming that traditional methods struggle to capture fine-grained disaster evolution.



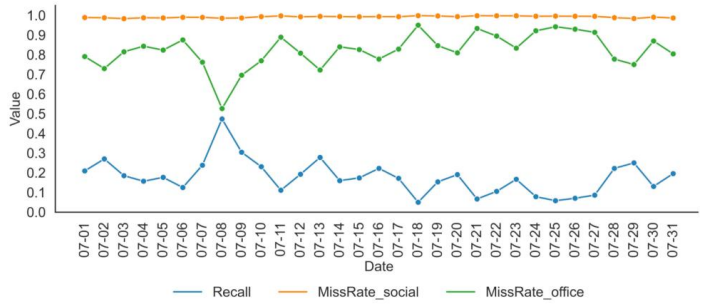
(a) Provincial level



(b) City level



(c) District level



(d) Township level

Fig5. Granularity analysis of administrative divisions at different levels.

(2) Location Entity Co-occurrence Analysis

To further analyze the differences in administrative division granularity, this study statistics the overlap situation of daily top-k location entities between social media and official documents (see Appendix C). This distribution pattern further visually confirms the bias in coverage of different administrative division granularities between social media platforms and official platforms. Official documents tend to record higher-level administrative divisions (provincial, municipal), while social media covers disaster information at different fine granularities (provincial, municipal, district, town/village). The high MissRate_office and low Recall at the town/village level (**Fig5** subplot (d)) are not defects in knowledge graph construction, but

rather reflect the complementary characteristics of multi-source data: social media captures grassroots disaster information not covered by official sources, which is precisely the core value of LTHDG design (compensating for the deficiencies of official platforms through daily dynamically updated social media platforms).

(3) Timeliness Comparison: The Hekou Town Example

At the town/village level, the two sources differed in when they mentioned Hekou Town. In the social-media records, Hekou Town ranked fourth among location mentions on July 29, third on July 30, and ninth on July 31. It first appeared in the compared official documents on July 31. This case shows a two-day difference in the timing of location mentions in the observed sources; it does not establish that the graph predicted a future flood event.

Across administrative levels, the comparison shows that social-media records and official documents contain partly different location mentions. The Hekou Town case illustrates an earlier social-media mention in this dataset, while the available comparison does not establish general predictive performance. The graph can therefore be considered a complementary information source whose individual disaster reports require independent verification.

3.2.2. Spatio-temporal Diffusion Patterns

(1) Temporal Characteristics of Administrative Division Mention Frequency

As shown in **Fig6**, the daily mention frequency of administrative divisions at different levels exhibits distinct phased characteristics. Multiple peaks exist within July, among which July 23rd to 28th constitutes the highest peak platform, with city-level entities having the highest mention count (daily average exceeding 6000 times), followed by province-level entities. Notably, a global peak appears on July 26th, which highly coincides with the timing of flood disaster events across the country on that day, verifying the sensitive response characteristics of social media data to sudden flood disasters. The mention frequency fluctuations of province-level (prov), city-level (city), and district-level (district) entities are relatively large, indicating that macro-level disaster discussions are more susceptible to short-term event fluctuations, exhibiting strong temporal volatility. In contrast, the mention frequency of town-level (town) entities is overall lower, indicating that micro-level disaster discussions are less frequent.

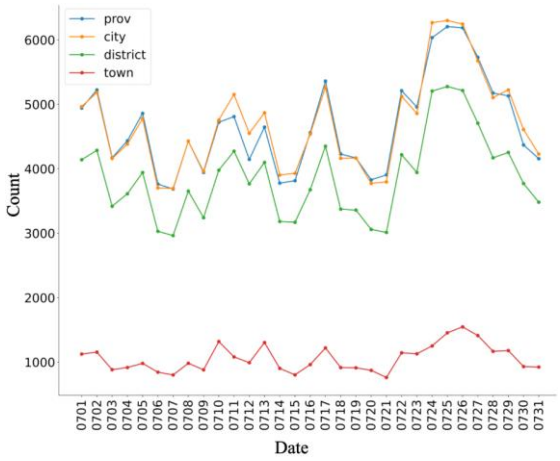


Fig6. Daily frequency of mentions of administrative divisions at different levels.

（2）Evolution Patterns of Administrative Division Diversity

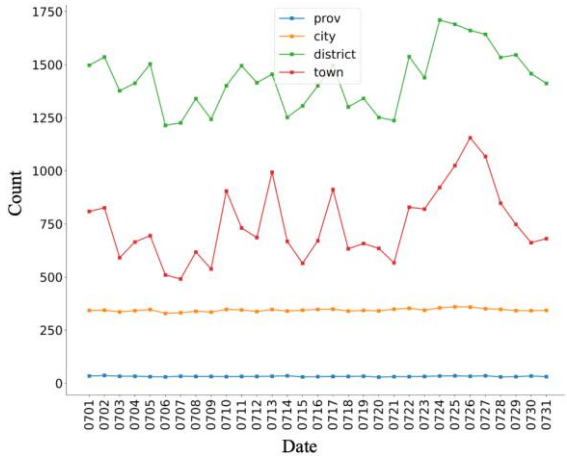


Fig7. Number of duplicate categories for different levels of administrative divisions each day.

Fig7 displays the daily number of deduplicated categories of administrative divisions at different levels. The data indicate that the mention frequency of district-level (district) location entities is overall higher than that of town-level (town), a phenomenon that does not match the actual total numbers of administrative divisions at these two levels, namely, the actual number of town-level divisions nationwide is far greater than that of district-level divisions. This abnormal phenomenon indicates that during flood disasters, netizens' attention to district levels is greater than to towns.

（3）Dynamic Monitoring of Newly Added Administrative Division Entities

Fig8 reveals the daily characteristics of newly added quantities of administrative divisions at different levels. From the overall trend, it can be observed that town-level entities exhibit the greatest volatility, followed by district-level, city-level, and province-level. This indicates that during flood disasters, the set of districts, cities, and provinces that netizens focus on is relatively fixed, and as time progresses, it is difficult for new location entities to emerge. At the town level, the set of locations that netizens focus on continues to change, meaning that social media platforms are more sensitive to flood disaster events at the town level.

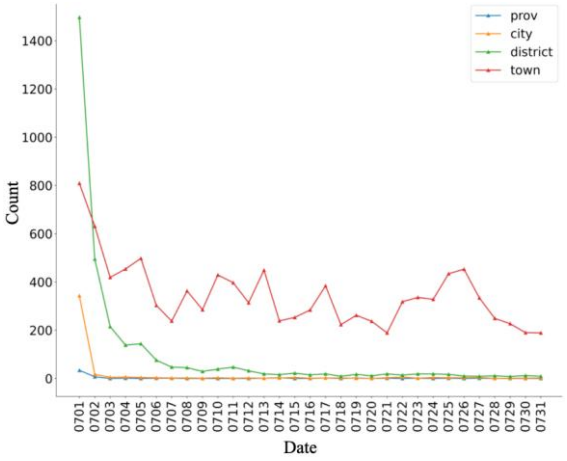


Fig8. Daily number of newly added administrative divisions.

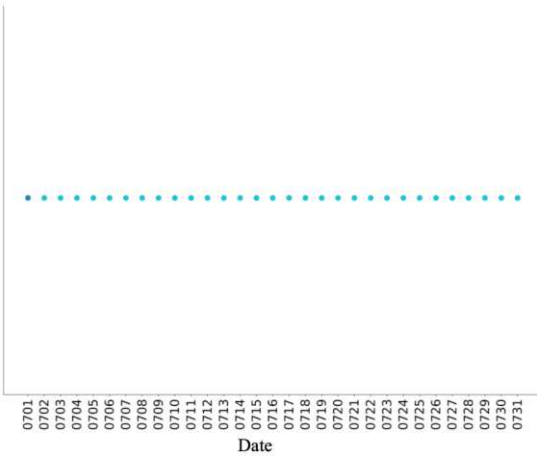


Fig9. The administrative division level that changes most drastically every day (dark blue: district, light blue: town).

Fig9 displays the distribution of administrative division levels with the most drastic daily changes. It can be observed that throughout the entire July period, the administrative division level with the highest change frequency is town-level (town), with only July 1st being district-level (district). This further proves the phenomenon mentioned above. Through analysis of the original Weibo text, it was found that this phenomenon is consistent with the actual situation of disaster information sinking to lower levels.

3.2.3. Flood Disaster Spatial Clustering

To mine the spatio-temporal characteristics of flood disaster geographical public opinion centers in LTHDG, this study conducts spatio-temporal analysis on all CGeoPOFDs at different administrative division levels (district level, city level, province level) on a daily basis (detailed result figures see **Fig12** in Appendix D).

According to the analysis results at the district level, it can be observed that CGeoPOFDs exhibit a dispersed but non-random distribution pattern. The Yangtze River corridor region and the South China Sea coastal region constitute two main aggregation belts, indicating that coastal/riverine flood disaster public opinion is constrained by the orientation of water system boundary lines.

When the scale is elevated to the city level, the spatial aggregation effect is significantly strengthened. The aggregation pattern in the Yangtze River basin undergoes a structural transformation: from the full-line distribution at the district level, it contracts into ‘lake-centered’ discrete hotspot clusters, with areas surrounding Poyang Lake and Dongting Lake being the main aggregation zones. The number of hotspots at the city level decreases, proving that scale aggregation effectively reduces information redundancy.

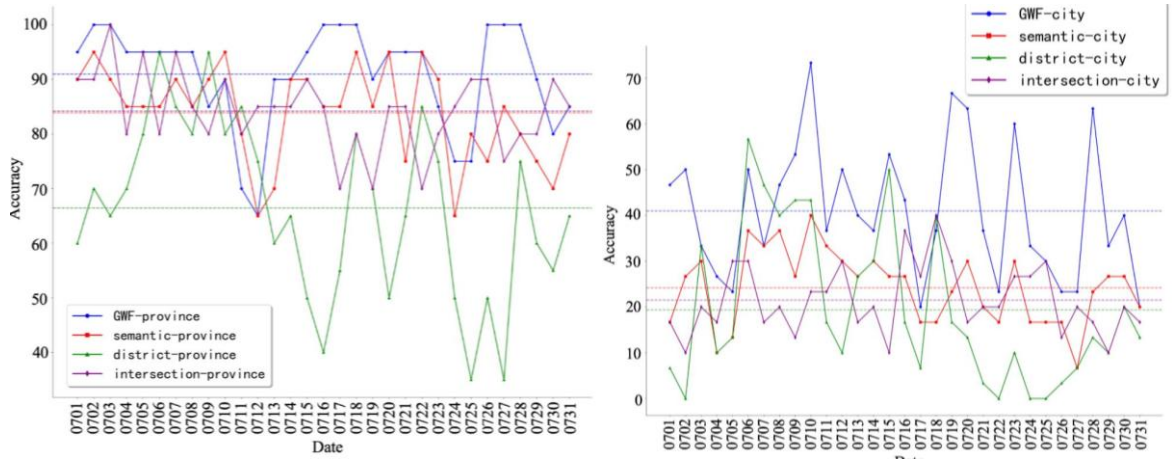
Provincial-scale analysis presents a macroscopically stable pattern, forming a five-pole structure with Sichuan Province, Hunan Province, Shaanxi Province, Henan Province, and Guangdong Province as cores. These provinces maintained hotspot status for extended periods during the 31-day observation period, indicating that the provincial scale possesses strong temporal stability, while also verifying that public opinion transmission exhibits obvious regional dependency characteristics.

3.2.4. Flood Disaster Key Node Analysis

To verify the effectiveness of key node identification in the flood disaster spatio-temporal heterogeneous graph, this study conducted key node analysis on the long-temporal-sequence graph. The evaluation adopts the Precision metric, defined as the proportion of key nodes identified by the system that

exist in the official documents of the Ministry of Water Resources. The experiment compares four types of graph structures: retaining only semantic distance edges (semantic), retaining only spatial distance edges (distance), retaining only co-occurrence probability edges (intersection), and weighted edges fusing all three types of edges (GWF).

Each subgraph in **Fig10** includes four types of line charts, with each type's line name format in the legend being 'relationship type-administrative division level', for example, 'semantic-city' indicates information using semantic distance relationship (semantic) at the city level.



(a) Provincial Level (b) City Level

Fig10. Analysis of key nodes in flood disasters at different administrative levels.

Subgraph (a) of **Fig10** displays the precision variation trend of province-level key node identification. Among single-relationship graphs, semantic and intersection perform similarly (average precision rates of 83.87% and 84.19%, respectively), while the distance method has the lowest performance (average precision 66.45%), indicating that relying solely on geographical distance is insufficient for accurately identifying provincial-level flood disaster key nodes. The GWF method maintains stable high performance throughout the entire July period, with an average precision rate reaching 90.97%, significantly superior to single-relationship graphs. This verifies this method's sensitive capture capability for key nodes during disaster peak periods and confirms the necessity of multi-dimensional relationship fusion.

Subgraph (b) of **Fig10** displays the city-level key node identification results. Compared with the province-level results, city-level precision was generally lower. The GWF graph achieved an average precision of 40.97%, higher than the three single-relation graphs in this analysis (semantic: 24.19%; distance: 19.35%; intersection: 21.51%). The city-level results exhibit obvious volatility, with precision peaks appearing on July 21st and July 22nd (58.7%). This phenomenon indicates that when disasters concentrate and erupt, the consistency between social media data and official documents significantly improves.

When constructing GWF, this study constructs corresponding weights based on the precision values of the three types of edges in the two administrative division levels. For example, based on the province-level precision results, the weights of the three types of edges can be determined as: semantic : distance : intersection = 0.36 : 0.28 : 0.36, this weight ratio is approximately the same as the ratio of precision rates of the three types of edges. By analogy, the weights at the city level are derived as: semantic : distance : intersection = 0.37 : 0.30 : 0.33. Finally, the average value is taken to obtain the weight values for constructing GWF, namely semantic : distance : intersection = 0.365 : 0.29 : 0.345. The coefficients were selected from the same July source-overlap comparison shown in **Fig10**. Therefore, **Fig10** is an in-sample description of the selected weighting scheme and is not an independent test of out-of-sample key-node precision.

The experimental results reveal two important phenomena: 1) Province-level precision is significantly higher than city-level, this difference mainly originates from the differences in data granularity of social media platforms and coverage scope of official documents. The Ministry of Water Resources official documents focus more on large-scale disaster overviews, while small-scale precise detail coverage is insufficient. 2) The GWF method is significantly superior to single-relationship graphs at both levels, verifying the necessity of conducting downstream tasks based on weighted graphs.

The low precision at the city level is mainly influenced by three aspects: 1) Social media data exhibits uneven urban coverage, with first-tier and provincial capital cities having more data volume than ordinary prefecture-level cities; 2) Official documents have delays in recording small-scale disasters (as mentioned earlier), resulting in insufficient real-time performance; 3) High spatial heterogeneity of disasters within cities, making it difficult for a single node to accurately represent the situation.

3.3. STG-GraphRAG System Testing

3.3.1. Benchmark Dataset

To systematically evaluate the performance of STG-GraphRAG in flood disaster assisted decision-making scenarios, this study constructed a comprehensive Benchmark dataset (FloodBot), covering 155 typical decision-making scenarios during China's flood disaster period in July 2024. This dataset covers core decision-making links including flood disaster monitoring, risk assessment, and resource scheduling. Detailed information about this dataset is presented in Table 4. Appendix B provides a test example of STG-GraphRAG. This section will elaborate on the construction principles, structural characteristics, and evaluation value of this dataset.

The Benchmark dataset design follows three core principles: spatio-temporal precision, decision orientation, and scenario diversity. Spatio-temporal precision requires each query to explicitly specify spatio-temporal scope. Decision orientation ensures query content meets actual emergency decision-making needs, such as risk area identification and resource scheduling priority determination; scenario diversity covers the full flood disaster cycle (warning, occurrence, diffusion, recession) and multi-scale spatial scope (provincial regions, intra-urban areas).

Table 4. FloodBot description.

Feature Dimension	Category	Quantity	Proportion	Example
Temporal Distribution	Early July	30	19.4%	The flood correlation between Jiang'an District and Jianghan District in Wuhan City on July 8.
	Mid-July	60	38.7%	Comparison of flood disaster hotspots in the Yangtze River Basin and the Yellow River Basin on July 17.
	Late July	65	41.9%	The areas surrounding Poyang Lake in Jiangxi Province that require the most urgent rescue on July 28.
Space Scale	National-level	40	25.8%	Flood disaster situation in the middle and upper reaches of the Yangtze River Basin on July 15.

Feature Dimension	Category	Quantity	Proportion	Example
Query Type	Provincial-level Region	60	38.7%	What are the distribution characteristics of flood-prone areas in Guangdong Province on July 20?
	City-level	55	35.5%	The flood disaster caused by heavy rainfall in Zhengzhou City on July 20.
	Regional Status Inquiry	40	25.8%	The most severely affected areas of Nanjing City by floods on July 20.
	Hotspot Recognition	35	22.6%	What are the flood-prone areas in Wuhan City, Hubei Province on July 15?
	Risk Assessment	30	19.4%	Risk level assessment of flood disasters in various regions of Hunan Province on July 20.
	Association Analysis	25	16.1%	What is the correlation between the flood situations between Guangzhou and Shenzhen on July 22?
	Forecast and Early Warning	25	16.1%	Based on the flood disaster situation in Jiujiang City on July 18, identify high-risk areas for the next 24 hours.
Decision Dimension	Spatial Decision	70	45.2%	The geographical scope of the flood impact in Jiangxi Province on July 20 was analyzed.
	Time Decision	35	22.6%	What was the overall sentiment of Beijing's internet users on July 20?
	Multidimensional Decision Making	50	32.2%	Which areas in Jiangxi Province experienced fewer flood events but showed abnormally low emotional indices on July 16?
Difficulty Level	Basic Level	75	48.4%	Only flood events occurring on July 20 and located in Wuhan City are displayed.
	Advanced Level	55	35.5%	Identify the propagation pattern of the flood disaster in the Yangtze River Basin on July 15.
	Expert Level	25	16.1%	The clustering pattern of urban flooding hotspots in Wuhan on July 20 was analyzed.

The temporal dimension of the dataset covers July 1st to 31st, and the spatial dimension spans the Yangtze River Basin, Huai River Basin, Yellow River Basin, and Pearl River Basin, involving 12 key flood control provinces including Hubei, Henan, Guangdong, Jiangxi, Hunan, and Sichuan. Query types are divided into five categories: regional status queries, hotspot identification, risk assessment, correlation analysis, and prediction warning. These queries are classified by difficulty level: basic level requires only single data source support; advanced level requires multi-source data fusion; expert level requires spatio-temporal reasoning and prediction capabilities.

3.3.2. Evaluation Metrics

To comprehensively evaluate the effectiveness of each module in the STG-GraphRAG system, this

study designed five core evaluation metrics, conducting quantitative analysis from three dimensions: knowledge retrieval quality, generated content accuracy, and decision practicality. All evaluations are based on the Benchmark dataset constructed in this study. Considering the randomness existing in large language models, this study conducted 3 rounds of testing for each test case, and the final metrics are the average values of the 3 rounds of test results.

Average Node Count characterizes the subgraph scale constructed by the system for each query. This metric reflects the system's information filtering efficiency. Smaller values indicate the system can more precisely locate key knowledge and avoid information overload. The core objective of the GCAASC module is to reduce redundant nodes through the geographic community awareness mechanism; this metric directly validates the design objective of this module.

Context Relevance measures location-entity matching between the retrieved subgraph and the query using a Precision@k-style measure. Since STG-GraphRAG conducts flood disaster knowledge retrieval based on temporal entities and location entities, wherein temporal entities are used for knowledge graph retrieval and location entities are used for subgraph search within the knowledge graph, this study uses the precision of subgraph location entities compared to user query location entities as the context relevance measurement metric. Due to the context length limitation of large language model inputs, this study performs 'sorting + Top-k' pruning operations on nodes within the knowledge graph during subgraph construction (this study retained Top 500 location nodes for further screening by subsequent modules such as spatio-temporal constraint retrieval). This metric ranges in [0,1], with larger values indicating retrieval results better align with query intent. According to the spatio-temporal constraint retrieval module designed in this study, this metric validates whether the spatio-temporal filtering mechanism effectively improves retrieval precision.

Answer Relevance evaluates the matching degree between the system's final output and user queries, calculated as $AnswerRel(query,answer)=cosine(emb(query), emb(answer))$, where $query$ represents user query, $answer$ represents system output, and $emb(\cdot)$ denotes 2560-dimensional vectors generated using Qwen3-Embedding-4B (Zhang *et al.* 2025). This metric directly reflects whether the system understands user needs. The spatio-temporal interpretability enhancement module aims to improve the relevance between generated content and queries, and this metric validates the achievement degree of this objective.

Faithfulness measures the consistency between system-generated content and retrieved knowledge, defined as $Faithfulness(answer,context)$, i.e., the proportion of facts in the answer that can be verified by retrieved knowledge. The $Faithfulness(\cdot)$ function indicates the model released by Laurer (2024). This metric is crucial for disaster decision-making, as erroneous information may lead to serious consequences. This metric validates whether STG-GraphRAG effectively suppresses the hallucination problem of large language models.

Human raters assessed the answers to the 155 FloodBot questions for usefulness and granularity using the 1–5 rubric in Table 5. For each answer, the two ratings from each rater were combined as "0.3 * usefulness + 0.7 * granularity", and the five composite ratings were averaged. The system-level human score is the mean of the answer-level scores included in that system's three-run evaluation. This measure describes rater-perceived usefulness and specificity; it does not directly measure factual correctness or source support.

The rubric in Table 5 assigns usefulness and granularity scores from 1 to 5. For an answer rated by five people, let U_r and G_r denote the usefulness and granularity scores assigned by rater r. The answer-level human score is $H=(1/human_sum)\sum_{r=1}^{5}(0.3*U_r+0.7*G_r)$. The human_sum denotes the count of human. The system-level score is the mean of the answer-level scores for the responses included in that system's evaluation.

Table 5. Human rating rubric.

Scoring Criteria	Value	Points assignment instructions
Usefulness	5	At least 90% of the content is useful information, highly focused on decision-making.
	4	70% to 89% is useful, with a small amount of irrelevant content.
	3	50-69% of the information is useful, roughly balanced with useless information.
	2	10-49% useful, most is noise.
	1	Less than 10% useful; contains misleading content.
Granularity	5	90% or more of the useful information is fine-grained.
	4	70-89% fine granularity, with a small amount of generalization
	3	40 – 69% of the useful information is fine-grained, with the remainder presented at a coarser level.
	2	10-39% fine granularity, mainly for general description.
	1	Less than 10% is considered fine-grained, lacking specific operational details.

3.3.3. Evaluation Results

Table 6. Ablation experiment results.

		Model type				
		STG-GraphRAG	no_GEORETRIVAL	no_GCAASC	no_SUMMARY	INITIAL
Evaluation indicators	Average Node Count	463	512	1469	462	\
	Context Relevance	0.9818	0.9093	0.9991	0.9818	\
	Answer Relevance	0.7705	0.705	0.6733	0.7091	0.5391
	Faithfulness	0.9687	0.9588	0.9588	0.9683	\
	Human score	4.4146	4.2206	4.4231	4.428	3.5126

Note: 'no_GEORETRIVAL' indicates removal of the 'spatio-temporal Constraint Retrieval Module', 'no_GCAASC' indicates removal of the 'GCAASC Module', 'no_SUMMARY' indicates removal of the 'Spatio-temporal Summary Module', and 'INITIAL' indicates 'no modules used'. The basic maximum hop count for constructing subgraphs in this study is set to 10. Human score is the pooled mean of the five-rater usefulness and granularity ratings described in Section 3.3.2; it is not a measure of independently verified factual accuracy.

Table 6 summarizes the results across all 155 FloodBot questions, which cover the four river basins and 12 provinces described in Section 3.3.1. The Hekou Town example in Section 3.2.1 separately illustrates

a township-level difference in the timing of location mentions between social-media records and the official documents examined; it is not the sole system evaluation.

(1) Impact of Modules on Knowledge Retrieval Efficiency

As shown in Table 6, the absence of the GCAASC module leads to a surge in average node count to 1469, representing a 217.3% increase compared to our system STG-GraphRAG (463). This phenomenon validates the effectiveness of the geographic community-aware adaptive subgraph construction method proposed in this study. GCAASC effectively identifies spatially aggregated entities, substantially reducing subgraph scale. After removing this module, the traditional breadth-first search based subgraph construction method generates a large number of spatially discrete nodes, significantly increasing information processing costs. In comparison, the absence of the GEORETRIVAL module increases node count by only 10.6%, indicating that the spatio-temporal constraint retrieval module has limited impact on knowledge retrieval scope control, but significant impact on knowledge quality. Notably, SUMMARY module removal has minimal impact on node scale, which aligns with the design expectation of this study: the spatio-temporal summary module primarily optimizes knowledge representation rather than retrieval scope, and its core functionality manifests in subsequent generation stages.

(2) Impact of Modules on Context Quality

The context relevance metric reveals the differentiated contributions of modules. Removal of the GEORETRIVAL module leads to a 0.0725 decrease in relevance, with particularly evident performance in spatio-temporally sensitive queries. This result confirms that the spatio-temporal filtering mechanism of the spatio-temporal constraint retrieval module designed in this study, particularly hydrological basin constraints and temporal indexing, is crucial for capturing disaster dynamics. Removal of the GCAASC module causes a slight 0.0173 increase in relevance. In-depth analysis reveals that overly strict subgraph construction methods filter out weakly connected but relevant nodes, thereby losing some correlation information. This indicates that the GCAASC module requires further optimization to balance geographic aggregation and information completeness. SUMMARY module removal does not change relevance (0.9818), proving that spatio-temporal summary does not affect knowledge retrieval quality; its value is embodied in the knowledge transformation stage.

(3) Impact of Modules on Generated Content Quality

The answer relevance metric indicates that all modules contribute to final output quality, but to varying degrees. The complete model STG-GraphRAG achieves 0.7705, significantly superior to the initial model (0.5391). The GCAASC module contributes the most. Its removal causes a 0.0972 decrease in relevance, which validates the necessity of the community detection method considering geographic features proposed in this study for maintaining the spatial propagation characteristics of disaster situations. Removal of GEORETRIVAL and SUMMARY modules causes relevance decreases of 0.0655 and 0.0614, respectively. The former primarily affects spatio-temporal accuracy, while the latter weakens multi-dimensional risk assessment, such as missing risk level determination, making outputs lack decision anchors. The faithfulness metric remains at high levels across all variants (greater than 0.95), proving that the prompt engineering designed in this study enables the large language model (Qwen) to possess strong basic fact-following capabilities.

(4) Comprehensive Impact of Modules on Decision Practicality

Human evaluation reveals more complex module interactions from the perspective of decision practicality. The complete model scores 4.4146, approaching the 5-point upper limit. Removal of the GEORETRIVAL module causes an absolute decrease of 0.1940 in the human score, primarily due to increased spatio-temporally inaccurate information, such as using geographic knowledge unrelated to user Query. This validates the importance of the spatio-temporal constraint retrieval module for decision reliability.

Surprisingly, removal of SUMMARY and GCAASC modules instead causes slight score increases (4.4280 and 4.4231, respectively). Analysis from the granularity perspective reveals that the macro-level knowledge generated by the spatio-temporal summary module reduces the proportion of fine-grained flood disaster knowledge, thereby reducing comprehension efficiency for non-professional decision-makers. Removal of the GCAASC module introduces more subgraph nodes, thereby increasing the proportion of flood disaster knowledge, ultimately improving human scores. However, according to other metrics, the GCAASC removal operation also introduces some noise. Therefore, the human score metric growth amplitude is relatively small.

The initial model scores the lowest (3.5126), which aligns with the inherent defects of general large language models and the limitations of general large language models when addressing flood disaster scenarios, namely that general large language models have lower knowledge distribution timeliness and lack more fine-grained information. Compared to the complete model, STG-GraphRAG can extract fine-grained information from real-time flood disaster knowledge graphs, thereby improving the system's capability to capture real-time, fine-grained flood disaster information.

3.4. System Cost and Performance Evaluation

Table 7 summarizes the reported mean runtime and token-use statistics for the main stages of the FloodBot evaluation. To quantitatively evaluate the speed and cost of applying this system in actual flood disaster scenarios, this study, based on the Benchmark, assesses average time consumption and Token cost (Since this system uses the online Qwen3-8B model for inference by default, the Token cost of calling the API needs to be considered. Of course, locally deployed Qwen3-8B models can also be chosen, in which case hardware providing at least 24GB video memory is required for inference). Corresponding monetary costs are also listed when calculating Token costs. From the statistical results, it can be observed that time consumption is primarily concentrated in the 'Generate Answer' module, accounting for 90.25%. Therefore, if further promoting the application of STG-GraphRAG in real-time flood disaster decision-making scenarios is needed in the future, speed optimization efforts can be focused on the 'Generate Answer' module. From the statistical results, it can be observed that an average decision requires a monetary cost of 0.019 yuan, which is acceptable compared to the actual decision support strength produced by the system.

Table 7. Speed and cost statistics.

Module Name	Module Introduction	Average Time Loss	Token Cost
Date Extraction	Extract date from Query	0.3958s	\
Subgraph Construction	Construct a subgraph based on the spatio-temporal information and related methods in the query.	4.0692s	\
Context Building	Construct a context based on the query and subgraph for use as input to the downstream LLM.	0.0004s	\
Generate Answer	The LLM function is used to generate the answer; an online API is used here.	41.3316s	Input Tokens: 25708(0.013RMB) Output Tokens: 1509(0.003RMB) Reasoning Tokens: 503(0.003RMB)
Reference Verification	Check whether cited graph identifiers exist and are relevant to the generated content.	0.0003s	\
ALL	\	45.7973s	27720(0.019RMB)

4. Discussion

The STG-GraphRAG system proposed in this study provides a breakthrough solution for flood disaster auxiliary decision-making by integrating spatio-temporal heterogeneous graphs with geographic awareness enhanced generation technology. The experimental results not only verify the technical advantages of the system but also reveal the underlying laws of flood disaster knowledge representation and decision support. This section will deeply explore the theoretical significance, methodological innovations, and practical value of the research findings, elucidating their application potential in the field of flood disaster management.

4.1. Theoretical Breakthrough in Spatio-temporal Dynamic Knowledge Representation

The long-term sequential flood heterogeneous dynamic graph constructed in this study achieves a paradigm shift from static knowledge representation to a dynamic spatio-temporal knowledge network. Temporal joint validation experiments reveal a key phenomenon: social media data and official documents exhibit complementary spatio-temporal distribution characteristics. The province-level Recall metrics remain in the range of 0.86 to 1.0, while the village/town-level Recall decreases significantly, yet the coverage of social media on village/town-level disaster conditions remains high. This finding challenges the traditional single authoritative data dependency mode of disaster information acquisition and proves the important value of dynamic knowledge graphs in capturing fine-grained disaster evolution. The Hekou Town example illustrates both the value and the limit of comparing reporting times across sources: a social-media location mention preceded its appearance in the official documents examined here by two days. Such a difference may support earlier situational awareness, but it does not measure flood forecasting accuracy or show that social-media reports are more reliable than official information. These sources should be used as complementary inputs subject to verification.

4.2. Cognitive Adaptation Mechanism of Spatio-temporal Constraint Retrieval

The experimental results of the spatio-temporal constraint retrieval module (removing this module reduced context relevance from 0.9818 to 0.9093) reveal the cognitive specificity of disaster decision-making. Traditional RAG systems rely on global semantic matching, whereas flood disaster decision-making requires strict spatio-temporal boundary constraints. The multi-dimensional retrieval strategy designed in this study, by integrating keyword matching, semantic embedding, and spatio-temporal filtering, achieves a paradigm shift from ‘semantic relevance’ to ‘spatio-temporal precision.’ Deep analysis indicates that this mechanism is effective because it simulates the cognitive process of human experts in disaster analysis: first locating the spatio-temporal scope, then focusing on key entities, and finally evaluating associative relationships. This finding offers theoretical implications for the application of RAG technology in high-risk decision fields: in life-critical scenarios, retrieval mechanisms must exceed semantic similarity and integrate domain-specific constraints to ensure the spatio-temporal precision of decisions.

4.3. Scientific Value of Geographic Community Awareness Mechanism

The GCAASC module achieves a breakthrough in the cognitive modeling of spatial relationships by integrating First and third Laws of Geography into the subgraph construction process. Experimental data shows that this module reduced the average number of nodes from 1469 to 463, with a reduction rate of 68.5%, while maintaining context relevance at a high level of 0.9818. This effectiveness stems not only from technical optimization but also reflects the intrinsic spatial laws of flood propagation: disaster information

spreads non-uniformly in geographic space, following the principle of 'spatial proximity priority.' The 'Dynamic Monitoring Results of Newly Added Administrative Division Entities' further verify this law. This difference reveals the core role of scale effects in disaster cognition: macro-scale disaster conditions present stable patterns and clear associations, while micro-scale conditions are interfered with by multiple factors such as intra-urban heterogeneity and uneven data coverage. The GCAASC module dynamically adjusts the search scope through community cohesion metrics, which is essentially an adaptive modeling of disaster spatial heterogeneity, representing a new paradigm of the fusion of Geographic Information Science and Graph Neural Networks. This mechanism solves the fundamental defect of traditional RAG systems in disaster scenarios (ignoring the spatial dependency of location entities, causing retrieval results to lose the spatial continuity of disaster propagation).

4.4. Decision Gain Mechanism of Multi-Source Data Complementarity

This study verifies the gain mechanism of multi-source data fusion for disaster decision-making through systematic experiments. Benchmark evaluation shows that the complete STG-GraphRAG system is significantly superior to the initial model in two key metrics: answer relevance and human score. This gap mainly stems from the system's collaborative utilization capability of real-time heterogeneous data. In particular, the introduction of dynamic attribute nodes such as emotion indices and water depth estimation enables the system to capture the closed-loop feedback of 'Location-Environment-Human Behavior,' which is unachievable by single data sources. Spatio-temporal diffusion law analysis reveals an important phenomenon. The mention frequency and diversity evolution of administrative divisions at different levels show obvious differentiation. Village/town-level entities exhibit the highest volatility, while province-level entities are relatively stable. This phenomenon confirms the scale dependency of flood disaster information propagation (grassroots disaster conditions change rapidly but attract short-term attention, while macro disaster conditions change slowly but have lasting impacts). STG-GraphRAG integrates these dimensions through multi-dimensional risk assessment indicators, achieving the transformation from data to decision. This mechanism not only improves decision quality but also reconstructs the disaster cognitive framework: disasters are not merely physical processes but complex coupled systems of social sensing, spatial relationships, and temporal evolution.

5. Conclusions

This study proposes a flood disaster auxiliary decision-making system based on spatio-temporal heterogeneous graphs and geographic awareness enhanced generation (STG-GraphRAG). By constructing a daily updated national-scale flood heterogeneous dynamic graph, designing a multi-dimensional node retrieval and spatio-temporal filtering mechanism, achieving an adaptive subgraph construction method for geographic community awareness, and developing a spatio-temporal summary module integrating spatial analysis, time trends, propagation pattern recognition, and anomaly detection, the system significantly improves the scientificity and timeliness of flood disaster auxiliary decision-making. Experimental validation indicates that the STG-GraphRAG system has achieved the following breakthroughs in multiple dimensions:

(1) In terms of graph construction, temporal joint validation confirms that the long-term sequential flood heterogeneous dynamic graph constructed by the system is highly complementary to official documents. At the village/town level, some location mentions in social-media records were absent from or earlier than those in the compared official documents.

(2) In terms of key module efficiency, the adaptive subgraph construction method for geographic community awareness reduces the average number of nodes from 1469 to 463, with a reduction rate of 68.5%, while maintaining context relevance at a high level of 0.9818. The spatio-temporal constraint retrieval module raises context relevance from 0.9093 to 0.9818 (an absolute increase of 0.0725), effectively solving the problem of traditional RAG systems lacking spatio-temporal precision in disaster scenarios. The spatio-temporal summary module significantly enhances the decision value of generated content through a multi-dimensional risk assessment mechanism.

(3) In terms of overall system performance, STG-GraphRAG achieves an answer relevance of 0.7705 on the Benchmark dataset, maintains faithfulness at 0.9687, and obtains a human score of 4.4146 (out of a full score of 5), significantly superior to the initial model, proving the practical value of the system in flood disaster auxiliary decision-making.

Although this study has achieved a series of innovative results in flood disaster graph construction and intelligent reasoning, certain limitations still exist in terms of data coverage, spatio-temporal granularity, and model generalization. Future research can proceed from the following aspects:

(1) Depth Expansion of Multi-Source Heterogeneous Data Fusion. The current system mainly relies on social media text and images, resulting in uneven coverage in capturing disaster conditions in rural areas with low social media usage. Future work will integrate multi-source heterogeneous information such as satellite remote sensing, IoT sensors, weather radar, and structured data from emergency departments to build a more comprehensive dynamic sensing network. Meanwhile, knowledge distillation technology will be introduced to transfer knowledge from professional domain large models (e.g., weather prediction large models) to enhance the understanding capability of professional flood disaster knowledge, thereby constructing a more comprehensive and accurate flood disaster knowledge representation system.

(2) Construction of spatio-temporal Granularity Dynamic Optimization Mechanism. The existing system updates the graph on a daily basis, which is insufficient in responding to extreme flood events that evolve rapidly at the hour level. In the future, an incremental update and priority scheduling mechanism will be designed to achieve hour-level dynamic refreshing for key areas. Meanwhile, incremental learning technology of Graph Neural Networks will be introduced to avoid the computational burden caused by full graph reconstruction, thereby achieving rapid response to sudden flood disasters and improving the system's adaptability to extreme events.

Funding
This research received no external funding.

Competing Interests
The authors have no competing interests.

Author contributions
Conceptualization, Heng Tang, Yi Fang and Xiaoping Rui; methodology, Heng Tang and Yi Fang; software, Heng Tang; validation, Heng Tang, Yi Fang, Mengru Gao, Yiheng Xie and Ninglei Ouyang; formal analysis, Heng Tang and Mengru Gao; investigation, Heng Tang and Yi Fang; resources, Yiheng Xie and Ninglei Ouyang; data curation, Heng Tang and Yi Fang; writing—original draft preparation, Heng Tang and Yi Fang; writing—review & editing, Xiaoping Rui, Mengru Gao, Yiheng Xie and Ninglei Ouyang; visualization, Heng Tang and Yi Fang; supervision, Xiaoping Rui; project administration, Xiaoping Rui; funding acquisition, Xiaoping Rui. All authors have read and agreed to the published version of the manuscript.

Notes on contributors

Heng Tang is a PhD candidate at the School of Earth Sciences and Engineering, Hohai University. He holds a doctoral degree. His research direction is the construction and reasoning of flood knowledge graphs based on multimodal data.

Fang Yi is the Founder and CEO of Merit Interactive Co., Ltd., a data intelligence company. He is a Doctor of Engineering (D.Eng.) candidate at the School of Engineering, Zhejiang University, and serves as an Industry Professor at Zhejiang University of Finance and Economics. His research focuses on data intelligence and artificial intelligence, with expertise in leveraging big data to address interdisciplinary challenges in areas such as public health, public transportation, public safety, and precision marketing.

Xiaoping Rui is a professor at the School of Earth Sciences and Engineering of Hohai University. He holds a doctoral degree. His research interests include the theory and application of remote sensing geographic information systems.

Mengru Gao is a master student at the School of Earth Sciences and Engineering, Hohai University. Her research direction is the construction and reasoning of flood disaster graphs based on social sensing data.

Yiheng Xie is a PhD candidate at the School of Earth Sciences and Engineering, Hohai University. His research direction is scene recognition and detection based on remote sensing

Ninglei OuYang is a PhD candidate at the School of Earth Sciences and Engineering, Hohai University. His research interests include carbon cycle and ecological monitoring.

Code Availability

https://github.com/muhan-yy/STG-GraphRAG

References

Blondel, V.D., Guillaume, J.L., Lambiotte, R. & Lefebvre E. 2008. Fast unfolding of communities in large networks. *Journal of statistical mechanics: theory and experiment* 10: P10008.

Bhatti, M. 2024. Using large language models for early flood analysis: A case study. *Lappeenranta University of Technology*.

Chen, X., & Hao, H. 2025. A Self-Improving, RAG-Enhanced Framework for Automatic Knowledge Graph Construction from Climate Event News. *Proceedings of the International ISCRAM Conference*. Halifax, Nova Scotia, Canada.

Ester, M., Kriegel, H.P., Sander, J., & Xu, X.W. 1996. A density-based algorithm for discovering clusters in large spatial databases with noise. *proceedings of the kdd* 96(34): 226-231.

Edge, D., Trinh, H., Cheng, N., Bradley, Joshua., Chao, A., Mody, A., Truitt, S., Metropolitansky, D., Ness, R.O. & Larson, J. 2024. From local to global: A graph rag approach to query-focused summarization. *arXiv preprint arXiv:240416130*.

Hofmeister, M., Brownbridge, G., Hillman, M., Mosbach, S., Akroyd, J., Lee, K.F. & Kraft, M. 2024. Cross-domain flood risk assessment for smart cities using dynamic knowledge graphs. *Sustainable Cities and Society* 101: 105113.

Han, H., Wang, Y., Shomer, H., Guo, K., Ding, J.Y. & Lei, Y.J., Halappanaver, M., Rossi, R.A., Mukherjee, S., Tang, X.F., He, Q., Hua, Z.G., Long, B., Zhao, Tong., Shah, N., Javari, A., Xia, Y.L. & Tang, J.

L. 2024. Retrieval-augmented generation with graphs (graphrag). *arXiv preprint arXiv:250100309*.

Hu, R.J., Yue, Z.H., Zhou, Y.Z. & Zhou, H.J. 2025. Research on the Representation and Construction Tech nique of Event Causality Graph Based on Large Language Models. *Proceedings of the 4th Internation al Conference on Computer, Artificial Intelligence and Control Engineering.* Heifei, China 672-679.

Jiao, J.F., Park, J., Xu, Y.M., Sussman, K. & Atkinson, L. 2025. SafeMate: A Modular RAG-Based Agent for Context-Aware Emergency Guidance. *arXiv preprint arXiv:250502306*.

Karimanzira, D., Rauschenbach, T., Hellmund, T. & Ritzau, L. 2025. Improved Flood Management and Ri sk Communication Through Large Language Models. *Algorithms* 18(11): 713.

Lu, F., Zhu, Y.Q. & Zhang, X.Y. 2023. Research progress and prospects of spatiotemporal knowledge grap hs. *Journal of Geoinformation Science* 25(6): 1091-1105.

Laurer, M., Atteveldt, W.V., Casas, A. & Welbers, K. 2024. Less annotating, more classifying: Addressing the data scarcity issue of supervised machine learning with deep transfer learning and bert-nli. *Politic al Analysis* 32(1): 84-100.

Liu, B., Li, Y.B., Feng, X.K. & Lian, P.G. 2024. BEW-YOLOv8: A deep learning model for multi-scene a nd multi-scale flood depth estimation. *Journal of Hydrology* 645: 132139.

Liang, J.Y., Hou S.Y., Zhao, A.Q., Xu, Q.Y., Xiang, L.G., Li, R. & Wu, H.Y. 2025. Design and application of a semantic-driven geospatial modeling knowledge graph based on large language models. *Geo-spa tial Information Science* 1-20.

Liang, J.Y., Hou, S.Y., Jiao, H.Y., Qing, Y.X., Zhao, A.Q., Shen, Z.X., Xiang, L.G. & Wu, H.Y. 2025. Ge oGraphRAG: A graph-based retrieval-augmented generation approach for empowering large language models in automated geospatial modeling. *International Journal of Applied Earth Observation and G eoinformation* 142: 104712.

Mao, W., Shen, J., Su, Q., Liu, S.H., Pirasteh, S. & Ishii, K. 2024. A Method for Constructing an Urban W aterlogging Emergency Knowledge Graph Based on spatiotemporal Processes. *ISPRS International Jo urnal of Geo-Information* 13(10): 349.

Ni, H., Liu, F., Ma, X.Y., Su, L.X., Wang, S.Q., Yin, D.W., Xiong, H. & Liu, H. 2025. TP-RAG: Benchma rking Retrieval-Augmented Large Language Model Agents for spatiotemporal-Aware Travel Plannin g. *Proceedings of the 2025 Conference on Empirical Methods in Natural Language Processing*. Suzh ou, China 12403-12429.

Ouyang, L., Li, H. & Liu, J., 2025. Enhancing engineering risk analysis with knowledge graph-driven retrie val-augmented generation. *32st EG-ICE International Workshop on Intelligent Computing in Enginee ring.* Glasgow, United Kingdom 1-3.

Peng, F.L., Qiao, Y.K. & Yang, C. 2023. Building a knowledge graph for operational hazard management of utility tunnels. *Expert Systems with Applications* 223: 119901.

Peng, Z.M., Kuai, X., Ke, Sh.S., Dong, X.H. & Guo, R.Z. 2025. Enhancing geodatabases operability: adva nced human-computer interaction through RAG and Multi-Agent Systems. *Big Earth Data* 9(2): 217-242.

Peng, C.Y., Xia, F., Naseriparse, M. & Osborne, F. 2023. Knowledge graphs: Opportunities and challenge s. *Artificial intelligence review* 56(11): 13071-13102.

Rentschler, J., Salhab, M. & Jafino, B.A. 2022. Flood exposure and poverty in 188 countries. *Nature comm unications* 13(1): 3527.

Ruan, W.L., Dang, X.L., Zhou, Z.Y., Lyu, S. & Liang, Y.X. 2026. A Retrieval Augmented Spatio-Tempor al Framework for Traffic Prediction. *Proceedings of the AAAI Conference on Artificial Intelligence* 40 (46): 39163-39172.

Shi, J.M., Zhou, S.Z., Jin, B.W., Hu, W., Tian, R.C., Wang, S.W., Narasimhan, G. & Ham, J.W. 2025. Hyp ercube-RAG: Hypercube-Based Retrieval-Augmented Generation for In-domain Scientific Question-

Answering. *arXiv preprint arXiv:250519288*.

Soontontam, G., Dindam, T., Kheaksong, A., Srisomboon, K. & Sanguansat, P. 2025. Enhancing Thai Rice Query Assistance through a Knowledge-Driven Approach Using GraphRAG. *International Scientific Journal Of Engineering And Technology (ISJET)* 9(1): 19-30.

Tobler, W.R. 1970. A computer movie simulating urban growth in the Detroit region. Economic geography 46(sup1): 234-240.

Tang, H., Xu, H.W., Rui, X.P., Heng, X.B. & Song, Y. 2022. The identification and analysis of the centers of geographical public opinions in flood disasters based on improved naïve Bayes network. *Internatio nal journal of environmental research and public health* 19(17): 10809.

Tang, H., Rui, X.P., Xu, H.W. & Xie, Y.H. 2024. Identifying the centers of geographical public opinions in flood disasters based on improved conditional random field and focus theory. *International Journal o f Disaster Risk Reduction* 110: 104612.

Tang, H., Rui, X.P., Li, J.R., Ouyang, N.L., Xie, Y.H., Liu, X.D. & Bi, Y.M. 2025. SLIP-flood: Soft-combi nation of Swin Transformer and Lightweight Language-Image Pre-training for Flood Images Classific ation. *International Journal of Applied Earth Observation and Geoinformation* 139: 104543.

Wang, Y.H., Li, C.L., Liu, M., Cui, Q., Wang, H., Lv, J.S., Li, B.L., Xiong, Z.P. & Hu, Y.M. 2022. Spatial characteristics and driving factors of urban flooding in Chinese megacities. *Journal of Hydrology* 613: 128464.

Wu, M.F., Luo, S.Q., Xu, H. & Sun, W.X. 2025. Optimizing Emergency Decision-Making for Natural Disa ster Using Light Retrieval Augmented Generation. *Proceedings of the 2025 8th International Confere nce on Advanced Algorithms and Control Engineering (ICAACE), IEEE.* Shanghai, China 2237-2241.

Wang, G., Liu, Y., Liu, S.K., Zhang, L. & Yang, L.Q. 2025. REMFLOW: RAG-enhanced multi-factor rain fall flooding warning in sponge airports via large language model. *International Journal of Machine L earning and Cybernetics* 1-21.

Wen, C.C., Lin, Y.T., Qu, X.K., Li, N., Liao, Y., Li, X. & Lin, H. 2025. RS-RAG: Bridging Remote Sensin g Imagery and Comprehensive Knowledge with a Multi-Modal Dataset and Retrieval-Augmented Ge neration Model. *arXiv preprint arXiv:250404988*.

Xue, B. & Zou, L. 2022. Knowledge graph quality management: A comprehensive survey. *IEEE Transacti ons on Knowledge and Data Engineering* 35(5): 4969-4988.

Xu, Z.L., Xiao, T.S., He, W.C., Wang, Y. & Jiang, Z. 2023. Spatial knowledge-infused hierarchical learnin g: An application in flood mapping on earth imagery. *Proceedings of the 31st ACM International Con ference on Advances in Geographic Information Systems.* Hamburg, Germany 1-10.

Yuan, F.X., Xu, Y.C., Li, Q.C. & Mostafavi, A. 2022. Spatio-temporal graph convolutional networks for ro ad network inundation status prediction during urban flooding. *Computers, Environment and Urban S ystems* 97: 101870.

Yang, Y.H., Huang, Chao., Xia, L.H. & Li, C.L. 2022. Knowledge graph contrastive learning for recomme ndation. *Proceedings of the 45th international ACM SIGIR conference on research and development i n information retrieval.* Madrid, Spain 1434-1443.

Yao, L.W., Ren, F., Du, K.X. & Du, Q.Y. 2025. From knowledge graph construction to retrieval-augmente d generation: a framework for comprehensive earthquake emergency support. *Geo-spatial Informatio n Science* 1-21.

Yao, L., Ren, F. & Du, Q. 2025. R2D-EQ: a two-stage workflow for risk reasoning and decision-making in earthquake emergency scenarios. *Expert Systems with Applications* 130178.

Yu, R.L., Luo, S.Y., Ghosh, R., Li, L.Y., Xie, Y.Q. & Jia, X.W. 2025. Rag for geoscience: What we expec t, gaps and opportunities. *arXiv preprint arXiv:250811246*.

Yang, A., Li, A.F., Yang, B.S., Zhang, B.C., Hui, B.Y., Zheng, B., Yu, B.W., Gao, C., Huang, C.G., Lv, C.

X., Zheng, C.J., Liu, D.Y.H., Zhou, F., Huang, F., Hu, F., Ge, H., Wei, H.R., Lin, H., Tang, J.L., Yang, J., Tu, J.H., Zhang, J.W., Yang, J.X., Yang, J.X., Zhou, J., Zhou, J.R., Lin, J.Y., Dang, K., Bao, K.Q., Yang, K.X., Yu, L., Deng, L.H., Li, M., Xue, M.F., Li, M.Z., Zhang, P., Wang, P., Zhu, Q., Men, R., Gao, R.Z., Liu, S.X., Luo, S., Li, T.H., Tang, T.Y., Yin, W.B., Ren, X.Z., Wang, X.Y., Zhang, X.Y., Ren, X.C., Fan, Y., Su, Y., Zhang, Y.C., Zhang, Y.E., Wan, Y., Liu, Y.Q., Wang, Z.K., Cui, Z.Y., Zhang, Z.R., Zhou, Z.P. & Qiu, Z.H. 2025. Qwen3 technical report. *arXiv preprint arXiv:250509388*.

Zhu, A.X., Lu, G.N., Qin, C.Z. & Zhou, C.H. 2018. Spatial prediction based on Third Law of Geography. *Annals of GIS* 24(4): 225-240.

Zhong, L.F., Wu, J., Li, Q., Peng, H. & Wu, X.D. 2023. A comprehensive survey on automatic knowledge graph construction. *ACM Computing Surveys* 56(4): 1-62.

Zhu, Z.L., Huang, T.C., Wang, K., Ye, J.D., Cheng, X.H. & Luo, S.Q. 2025. Graph-based Approaches and Functionalities in Retrieval-Augmented Generation: A Comprehensive Survey. *ACM Computing Surveys* 58(10): 1-38.

Zhang, Y.Z., Li, M.X., Long, D.K., Zhang, X., Lin, H., Yang, B.S., Xie, P.J., Yang, An., Liu, D.Y.H., Lin, J.Y., Huang, F. & Zhou, J.R. 2025. Qwen3 Embedding: Advancing Text Embedding and Reranking Through Foundation Models. *arXiv preprint arXiv:250605176*.

Appendices

Appendix A. The prompts for core functionality.

Prompt 1: Text Cleaning and Optimization for Weibo Flood Disasters [Since this project primarily focuses on processing Chinese text, some of the Chinese examples within the prompts have not been translated into English. This is a necessary measure, as translating them into English would introduce noise into the prompts. Subsequent prompts have been handled in the same manner.]

Task and Role Description: You are a disaster information processing expert responsible for cleaning raw Weibo text to provide high-quality data input for building a flood disaster knowledge graph. You will precisely optimize the input Weibo text, improving readability while strictly preserving the original semantics.

Core Principles (Must be followed):

1. Zero Semantic Alteration

1) Retain all key facts: time, location, disaster details (e.g., water level/casualty figures), requests for assistance, organization names, and other original data points.

2) Do not add/speculate on information not mentioned (e.g., do not supplement unstated numbers of affected people).

3) If there are contradictions in the original text (e.g., ‘no casualties’ and ‘1 person missing’), retain the contradictory statements but mark them as [[Contradictory in the original text]).

2. Readability Enhancement Rules

1) Noise Removal:

 Remove duplicate characters (e.g., ‘救命啊啊啊’ → ‘救命’), meaningless symbols (‘～～～’ → ‘~’), and emoticons.

 Remove Weibo-specific noise: @usernames, super topic tags #XXX# (but retain keywords within the tags, e.g., #河南暴雨# → ‘河南暴雨’).

2) Spoken Language to Written Language Conversion:

 Correct non-standard expressions (‘俺村淹了’ → ‘我们村被淹’), but retain key dialect terms (e.g., ‘圩堤’ should not be changed to ‘堤坝’).

 Reorganize fragmented sentences (‘水！进屋了 快帮’ → ‘汛已进屋内，急急助内’).

3) Structural Optimization:

 Merge scattered short sentences (‘雨重。路断了。回来去.’ → ‘暴雨导致道路断，居民不能返家’).

 Add logical segments to long texts (each segment ≤ 3 sentences), using blank lines to separate different event subjects.

3. Safety Red Lines

1) Sensitive Information De-identification: Replace mobile phone numbers/ID cards/detailed addresses with ‘[De-identified]’, but retain the administrative region (e.g., ‘XX Township XX Village’).

2) Prioritize Requests for Assistance: Retain keywords indicating urgent needs (‘lack of food’, ‘someone is injured’), and do not simplify to generalized descriptions.

4. Processing Flow (Step-by-Step Execution):

1) Noise Layer: Remove emoticons, duplicate punctuation, @ mentions, and URL links.

2) Semantic Layer: Verify the completeness of key facts (5W1H elements). If missing, retain vague descriptions from the original text (e.g., ‘a certain place’ without guessing the specific location).

3) Expression Layer:

 Convert colloquial/internet slang into written language (‘extremely terrible’ → ‘critical situation’),

 Correct obvious typos (‘bad news’ → ‘flood situation’), but retain the original text if in doubt.

4) Output Verification: Compare sentence by sentence before and after optimization to ensure no new/deleted facts are added.

Output Format (Output only the cleaning result, no explanation/title/extra content):

[Optimized Text]

Example:

Input: Yesterday there was hail and heavy rain. The river embankment cracked. Old Wang said it was at least 2 meters wide. I don't know if that's true.

Output: Yesterday there was hail and heavy rain in the area, and a crack appeared in the river embankment. According to Lao Wang, the crack is about 2 meters wide, but this information has not yet been verified.

Prompt 2: Entity Relationship Extraction

Task and Role Description: As an information extraction expert in the field of flood disaster relief, you are tasked with completing the ‘Entity Identification Supplement’ and ‘Entity Relationship Triple Extraction’ tasks from the following target text. All entity relationship triples must be output in the specified JSON format, strictly adhering to the following: 1. Based solely on text content, without fabricating information; 2. Covering both ‘relationships of already extracted entities’ and ‘relationships of newly added entities’; 3. Ensuring correct JSON syntax (correct double quotes, commas, and array structure), with no non-JSON redundant content.

- Core Definitions (To be strictly followed)

1. Entity Types: Includes time entities (e.g., ‘2024-07-05’), location entities (e.g., ‘Zhengzhou City’, ‘Hanjiang River Wuhan Section’), flood event entities (e.g., ‘rainstorm floods’, ‘urban flooding’), infrastructure (e.g., ‘Metro Line 5’), rescue measures (e.g., ‘sandbag reinforcement of river embankments’), affected population (e.g., ‘200 citizens’), damage situation (e.g., ‘10 houses collapsed’), and affected population (e.g., ‘200 citizens’).

2. Entity-Relationship Triples: The core structure is ‘(Subject Entity, Relation Type, Object Entity)’. ‘Entity Type’ and ‘Text Evidence’ need to be added to support validation. A single triple contains the following fields:

- subject: Subject entity (the initiator of the relationship in the text)
- subject_type: Type of the subject entity (selected from the above entity types)
- relation: Relation type (refer to the ‘Relation Type Reference Table’ below; new types can be added to fit the text)
- object: Object entity (the receiver of the relationship in the text)
- object_type: Type of the object entity (selected from the above entity types)
- text_evidence: The original text fragment proving the existence of the relationship (directly copied, with double quotes)

3. Relationship Type Reference Table：

Relationship Type	Description (Subject->Object)	Example

Occurs at	Flood event occurs at a location	Rainstorm flood → Zhengzhou City
Occurrence time	Flood event corresponds to a time	Waterlogging → 2024-07-05 14:00
Affects	Flood event affects an entity	Rainstorm flood → Metro Line 5
Take measures	A rescue measure is implemented at a location/event	Xinxiang City → Sandbag reinforcement of river embankment
Cause losses	Flood event leads to a loss	Waterlogging → 10 collapsed houses
Involves people	Flood event involves affected people	Evacuation operation → 200 citizens
Adjacent relation	Spatial relation between locations	Zhengzhou City → Xinxiang City
Temporal order	Temporal sequence between times	2024-07-05 → 2024-07-06
Triggers	One flood event directly causes another flood event	Heavy rainfall → Rainstorm flood
Organized implementation	A subject (government, agency) leads flood-related measures	Xinxiang Municipal Government → Sandbag reinforcement of river embankment
Issue warning	A subject (meteorological, emergency department) issues warning for flood risk to a specific area	Henan Provincial Meteorological Bureau → Red rainstorm warning
Provide relief	A subject (government, charity) provides living, medical, and other relief services to affected people	Xinxiang Civil Affairs Bureau → Disaster-affected people

- Task Steps

1. Step One: Substantive Matching and Supplementation (Handled by Case)

- If an entity of a certain type is marked as ‘None’ in the [List of Entities Extracted for This Type] (indicating that the entity of this type has not been extracted): Directly extract the entity of this type from the [Target Text], mark the entity type, and then remove it from the check (no ‘Not Extracted’ judgment);

- If an entity of a certain type has specific content in the [List of Entities Generated]: Supplement the text with newly generated entities of this type;

- Supplement the text with ‘Other Related Entities’ (such as basic, rescue facilities and measures, etc.) not included in the [List of Copied Entities], highlighting the entity type and text copy (directly copy the text version). If none are found, mark ‘No New Related Entities’.

2. Second Step: Triple Extraction

- Based on all entities identified in Step 1 (including extracted entities and newly added entities), extract all entity relationships present in the text and generate triples;

- If an entity has no associated relationships (e.g., only mentioning ‘a certain community’ but not associated with any event/time), it does not need to be included in the triple list.

- If the same relationship is mentioned multiple times in the text, only one triple needs to be generated (text can be merged based on key fragments).

- If a new relationship is used outside the ‘Relation Type Reference Table,’ ‘new_relation_explain’ needs to be added to the output ‘supplementary_info’ to explain the definition of the new relationship (e.g., ‘Traffic Control: Location → Measures, Traffic control is implemented at a certain location due to flooding’).

- Output Format (Output JSON only; no other text)

{

‘entity_relation_triples’: [

{

‘subject’: ‘Subject Entity Content’,

‘subject_type’: ‘Subject Entity Type’,

‘relation’: ‘Entity Type’,

‘object’: ‘Object Entity Content’,

‘object_type’: ‘Object Entity Type’,

‘text_evidence’: ‘Original Excerpt Proving the Relationship’

},

{

‘subject’: ‘Subject Entity Content’,

‘subject_type’: ‘Subject Entity Type’,

‘relation’: ‘Entity Type’,

‘object’: ‘Object Entity Content’,

‘object_type’: ‘Object Entity Type’,

‘text_evidence’: ‘Original Excerpt Proving the Relationship’

}

],

‘supplementary_info’: {

‘unmentioned_entities’: [‘Extracted entities not mentioned in the text (fill with an empty array if none)’],

‘new_entities’: [

{

‘entity’: ‘Newly Added Entity Content’,

‘entity_type’: ‘Newly Added Entity Type’,

‘text_evidence’: ‘Source Basis for Newly Added Entities’

}

]

}

}

- Input Information

1. [List of Extracted Entities] (If no entity type has been extracted, enter ‘None’; if some entities have been extracted, enter the specific entities, separated by commas):

- Time Entities (If you find that some time entities do not appear in the text, it is assumed that all content in this text is related to the time entities here): [Enter the time entities extracted by the user here, such as ‘July 5, 2024’ or ‘Mid-July’]

- Location Entities: [Enter the location entities extracted by the user here, such as ‘Zhengzhou City’ or ‘Han River’]

- Flood Event Entities: [Enter the flood event entities extracted by the user here, such as ‘Rainstorm Flood’ or ‘Water Level Exceeds Warning Level’]

2. [Target Text]:

[Enter the Chinese flood text to be processed here, such as ‘On July 5, 2024, Zhengzhou City experienced heavy rainfall, triggering torrential floods and causing urban flooding. Some stations on Metro Line 5 were temporarily closed. On July 6, Xinxiang City also experienced flooding. The local government organized personnel to reinforce river embankments with sandbags and evacuated more than 200 affected residents.’]

Appendix B. Example of STG-GraphRAG.

User: Geographical distribution of flood events in Hubei Province on July 18, 2024.

STG-GraphRAG：

The floods in Hubei Province on July 18, 2024, exhibited significant spatial heterogeneity. The following is an analysis of their geographical distribution and impact:

[Geographical Distribution of Floods]

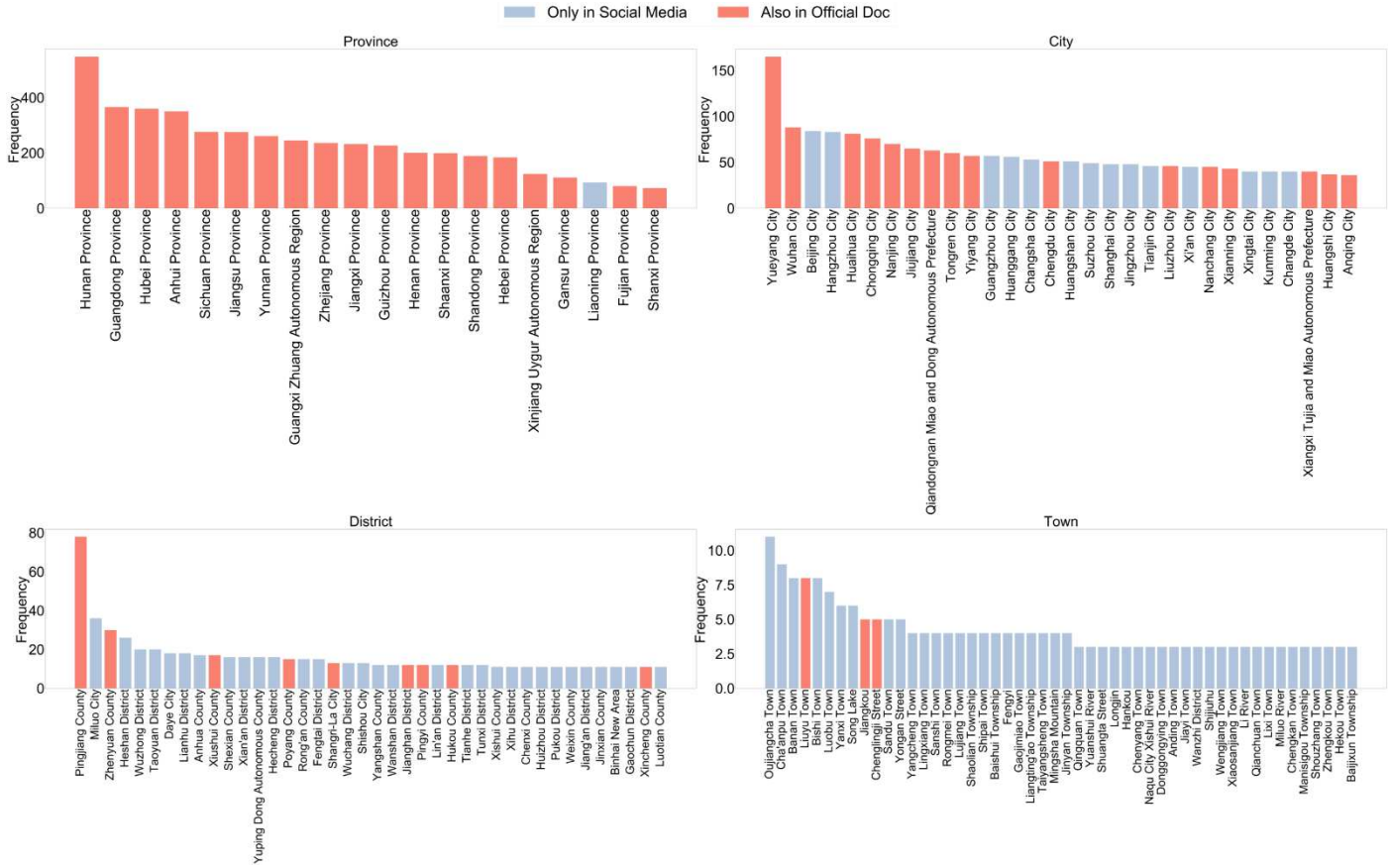
1. **Wuhan Metropolitan Area**: As a core hotspot, Wuhan (emotional index 0.85)[12] and surrounding areas (such as Nan'anzui and Lvjiang'an in Wuhan) experienced significant flooding[8,10,13]. This was mainly manifested in the ‘clear separation’ landscape caused by the rising water level of the Yangtze River in Wuhan[1-5, 11], and drowning incidents occurred[16].

This area was affected by heavy rainfall during the plum rain season[1,6,11]. Meteorological data showed a maximum temperature of 34℃ and a wind speed of 43.9 m/s.
2. **Hanjiang River Basin:** The water level in the Longgang Bridge area of the Hanjiang River (emotion index 0.18) rose significantly due to 21.4 mm of rainfall [2,18,20]. Zhuji Town (emotion index 0.15) and Raoliang Town (emotion index 0.15) in Xiangzhou District were under an orange rainstorm warning [14,15], leading to secondary disasters such as urban flooding and farmland waterlogging.
3. **Middle Reaches of the Yangtze River:** The water levels in the Yichang section (emotion index 0.50) and the Three Gorges Dam area (emotion index 0.50) exceeded warning levels, prompting the Three Gorges Reservoir to open nine floodgates [5,6]. The Jingjiang Dike (emotion index 0.52) [9] experienced increased pressure due to heavy rainfall and requires continuous monitoring. 4. **Abnormal Areas**: Huangzhou (emotion index 0.12) [7] and Sheqi County in Nanyang City showed obvious abnormalities. Although meteorological data did not show extreme rainfall, the emotion index was lower than that of the surrounding areas, which may indicate that the disaster was not fully reported.
[Multidimensional Impact Analysis]
Emotional Index: The emotional index in areas such as Wuhan and Yichang[17] is higher than the national average (0.53), reflecting better post-disaster recovery results; the emotional index in areas such as Huangzhou and Zhuji Town[7,19] is lower, and potential risks need to be monitored.
Meteorological Characteristics: Rainfall in the Hanjiang River Basin (21.4 mm) is significantly higher than that in the Yangtze River Mainstream (0.9 mm), forming a pattern of ‘flooding in the north and drought in the south,’ requiring attention to cross-basin scheduling.
Hydrological Correlation: The Three Gorges Reservoir discharge (emotional index 0.77) directly affects the water level of the Yangtze River in the Yichang section, forming a ‘reservoir-river section’ linkage effect.
[Risks and Recommendations]
1. **High-Risk Areas**: Landslide monitoring needs to be strengthened in areas such as Zhuji Town that are under rainstorm warnings[14,15], and Wuhan city should strengthen its emergency drainage capacity for urban flooding. 2. **Decision Recommendations**:
- Conduct disaster assessments in areas with abnormally low sentiment indices, such as Huangzhou and Nanyang, and improve the information reporting mechanism;
- Optimize the Three Gorges Reservoir scheduling plan to balance flood control needs between upstream and downstream areas;
- Establish a cross-regional joint prevention and control system in the Hanjiang River basin to prevent the spread of secondary disasters.
[Citation Basis]
1. [Citation: Node: N_Wuhan_Hubei_089ba5, Node: N_Wuhan Nan'anzui_Hubei_e2a718] - Flood events and meteorological data in Wuhan area
2. [Citation: Node: N_Hanjiang Longgang Bridge waters_Hubei_7d2ba9, Node: N_Zhuji Town_Hubei_acaa11] - Disaster data in the Hanjiang River Basin and Nanyang City
3. [Citation: Node: N_Yichang section_Hubei_b3adab, Node: N_Three Gorges Dam_Hubei_fa4851] - Monitoring point information of the middle reaches of the Yangtze River
4. [Citation: Analysis: HOT_ec226a, Analysis: EMO_02f775] - Hotspot areas and sentiment analysis conclusions
5. [Citation: Event: E_Three Gorges Reservoir_100846, Analysis: RSK_2a9315] - Recommendations for Three Gorges Reservoir scheduling and risk assessment
6. [Reference:Node:N_Three Gorges Dam_Hubei Province_fa4851] Three Gorges Dam (Xiling District, Yichang City, Hubei Province) - Hotspot Area: Yes, Sentiment Index: 0.50
7. [Reference:Node:N_Huangzhou_Hubei Province_88d85b] Huangzhou (Huangzhou District, Huanggang City, Hubei Province) - Hotspot Area: Yes, Sentiment Index: 0.12
8. [Reference:Event:E_Yangtze River Wuhan_19a047] Confluence of the Yangtze and Han Rivers, Adjacent Association, Wuhan South Bank (Location: Yangtze River Wuhan)
9. [Reference:Node:N_Jingjiang Embankment_Hubei Province_9bd2e5] Jingjiang Embankment (Gongan County, Jingzhou City, Hubei Province) - Hotspot Area: Yes, Sentiment Index: 0.52
10. [Reference:Node:N_Wuhan South Bank_Hubei Province_e2a718] Wuhan South Bank (Hanyang District, Wuhan City, Hubei Province) - Hotspot Area: Yes, the sentiment index is 0.77.
11. [Reference:Event:E_Yangtze River Wuhan_4bf6c7] Continuous heavy rainfall during the plum rain season has caused the water level of the Yangtze River in Wuhan to rise continuously. (Location: Yangtze River Wuhan)

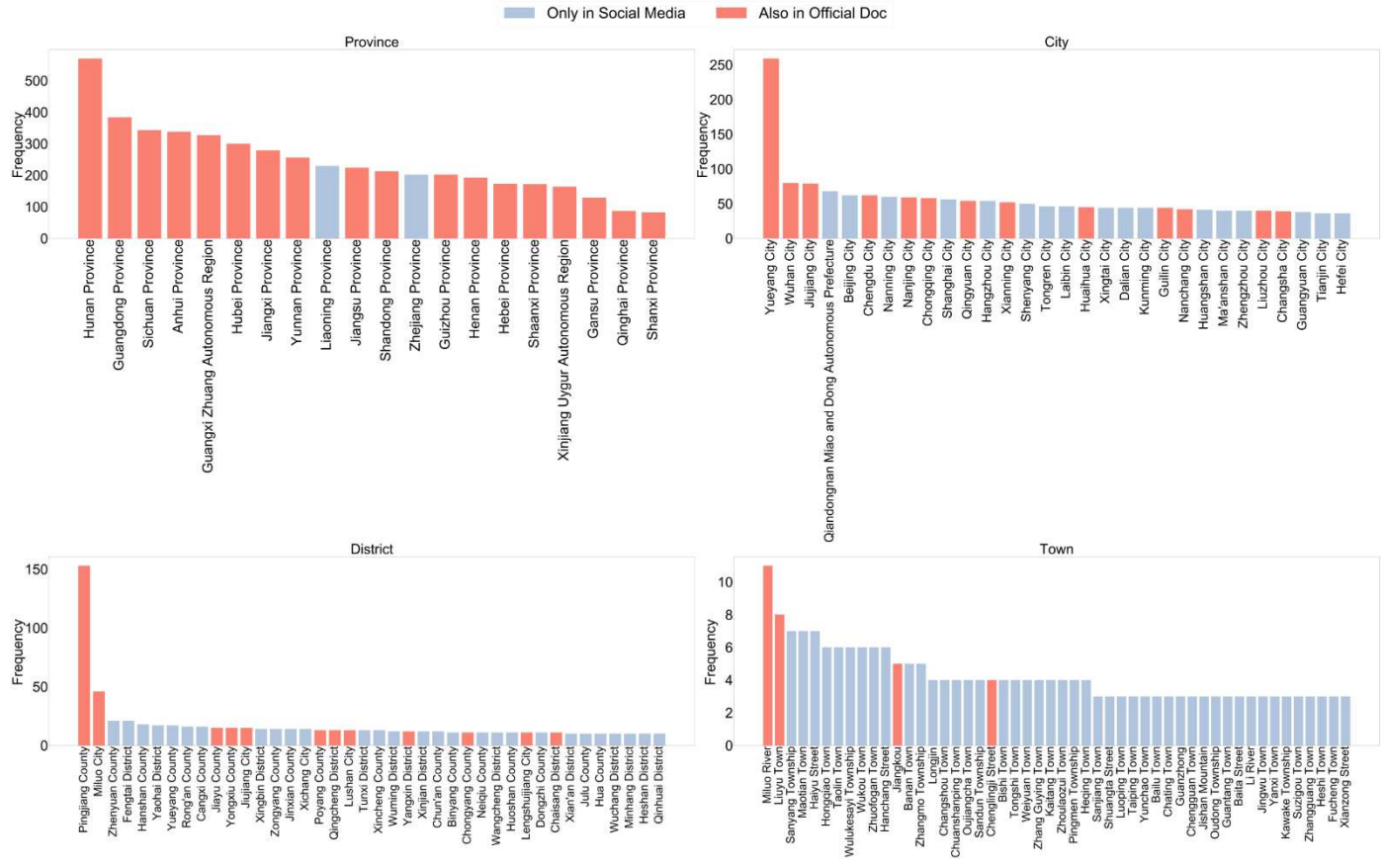
12. [Reference:Node:N_Wuhan_Hubei Province_089ba5] Wuhan (Wuhan City, Hubei Province) - Hotspot Area: Yes, Sentiment Index: 0.85
13. [Reference:Node:N_Lvjiang'an_Hubei Province_309816] Lvjiang'an (Jiang'an District, Wuhan City, Hubei Province) - Hotspot Area: Yes, Sentiment Index: 0.85
14. [Reference:Node:N_Zhuji Town_Hubei Province_acaa11] Zhuji Town (Xiangzhou District, Xiangyang City, Hubei Province) - Hotspot Area: Yes, Sentiment Index: 0.15
15. [Reference:Event:E_Zhuji Town_57d5d0] Orange rainstorm warning issued, affecting Taihe Town and surrounding towns. (Location: Zhuji Town)
16. [Reference: Event: E_Wuhan_1ce0c3] Drowning. A 17-year-old boy involved. (Location: Wuhan)
17. [Reference: Node: N_Yichang Section_Hubei Province_b3adab] Yichang Section (Yichang City, Hubei Province) - Hotspot Area: No, Sentiment Index: 0.50
18. [Reference: Node: N_Hanjiang Longgang Bridge Water Area_Hubei Province_7d2ba9] Hanjiang Longgang Bridge Water Area (Laohekou City, Xiangyang City, Hubei Province) - Hotspot Area: No, Sentiment Index: 0.18
19. [Reference: Event: E_Zhuji Town_ca3459] Sheqi County Meteorological Observatory issued a warning: Orange rainstorm warning. (Location: Zhuji Town)
20. [Reference: Event: E_Hanjiang Longgang Bridge Water Area_eb56d3] Significant water level rise occurred in the Hanjiang Longgang Bridge water area. (Location: (Hanjiang River Longgang Bridge waterway)
[Citation Evaluation]
☑ Valid Citations (20):
1. [Node: N_Wuhan_Hubei_089ba5, Node: N_Wuhan Nan'anzui_Hubei_e2a718] - Flood events and meteorological data in Wuhan area
2. [Node: N_Hanjiang Longgang Bridge Water Area_Hubei_7d2ba9, Node: N_Zhuji Town_Hubei_acaa11] - Disaster data in the Hanjiang River Basin and Nanyang City
3. [Node: N_Yichang Section_Hubei_b3adab, Node: N_Three Gorges Dam_Hubei_fa4851] - Monitoring point information of the middle reaches of the Yangtze River
4. [Analysis: HOT_ec226a, Analysis: EMO_02f775] - Hotspot areas and sentiment analysis conclusions
5. [Event: E_Three Gorges Reservoir_100846, Analysis: RSK_2a9315] - Recommendations for Three Gorges Reservoir scheduling and risk assessment
6. [Node: N_Three Gorges Dam_Hubei Province_fa4851] Three Gorges Dam (Xiling District, Yichang City, Hubei Province) - Hotspot Area: Yes, Sentiment Index: 0.50
7. [Node: N_Huangzhou_Hubei Province_88d85b] Huangzhou (Huangzhou District, Huanggang City, Hubei Province) - Hotspot Area: Yes, Sentiment Index: 0.12
8. [Event: E_Yangtze River Wuhan_19a047] Confluence of the Yangtze and Han Rivers, Adjacent Connection, Wuhan South Bank (Location: Yangtze River Wuhan)
9. [Node: N_Jingjiang Embankment_Hubei Province_9bd2e5] Jingjiang Embankment (Gongan County, Jingzhou City, Hubei Province) - Hotspot Area: Yes, Sentiment Index: 0.52
10. [Node: N_Wuhan South Bank_Hubei Province_e2a718] Wuhan South Bank (Hanyang District, Wuhan City, Hubei Province) - Hotspot Area: Yes, Sentiment Index: 0.77
11. [Event: E_Yangtze River Wuhan_4bf6c7] Continuous heavy rainfall during the plum rain season has caused the water level of the Yangtze River in Wuhan to rise continuously. (Location: Yangtze River Wuhan)
12. [Node: N_Wuhan_Hubei Province_089ba5] Wuhan (Wuhan City, Hubei Province - Hotspot Area: Yes, Sentiment Index: 0.85
13. [Node: N_Lvjiang'an_Hubei Province_309816] Lvjiang'an (Jiang'an District, Wuhan City, Hubei Province) - Hotspot Area: Yes, Sentiment Index: 0.85
14. [Node: N_Zhuji Town_Hubei Province_acaa11] Zhuji Town (Xiangzhou District, Xiangyang City, Hubei Province) - Hotspot Area: Yes, Sentiment Index: 0.15
15. [Event: E_Zhuji Town_57d5d0] Orange rainstorm warning issued, affecting Taihe Town and surrounding towns. (Location: Zhuji Town)
16. [Event: E_Wuhan_1ce0c3] Drowning. A 17-year-old boy involved. (Location: Wuhan)
17. [Node: N_Yichang Section_Hubei Province_b3adab] Yichang Section (Yichang City, Hubei Province - None) - Hotspot Area: No, Sentiment Index: 0.50
18. [Node: N_Hanjiang Longgang Bridge Water Area_Hubei Province_7d2ba9] Hanjiang Longgang Bridge Water Area (Laohekou City, Xiangyang City, Hubei Province) - Hotspot Area: No, Sentiment Index: 0.18

19. [Event: E_Zhuji Town_ca3459] Sheqi County Meteorological Observatory issued an orange rainstorm warning. (Location: Zhuji Town)
20. [Event: E_Hanjiang Longgang Bridge Water Area_eb56d3] Significant water level rise occurred in the Hanjiang Longgang Bridge water area. (Location: Hanjiang Longgang Bridge water area)
⚠ Invalid or low-relevance citations (0):
Citation quality assessment: High quality (100.0% valid citation rate)
Recommendation: Prioritize information with valid citations when making decisions, and be cautious about content with no citations or low-quality citations.

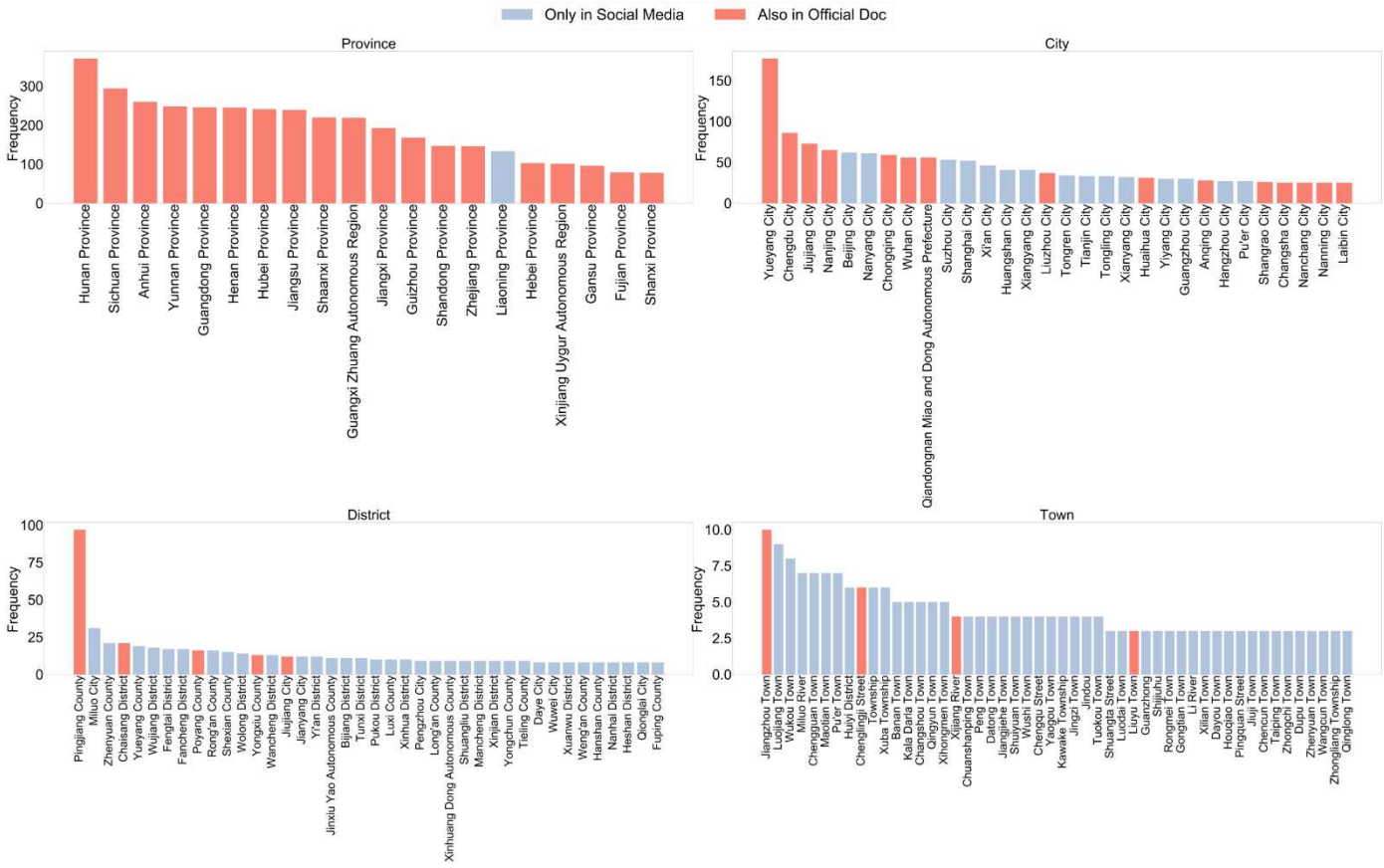
Appendix C. Daily statistics on location entities across different administrative division levels.



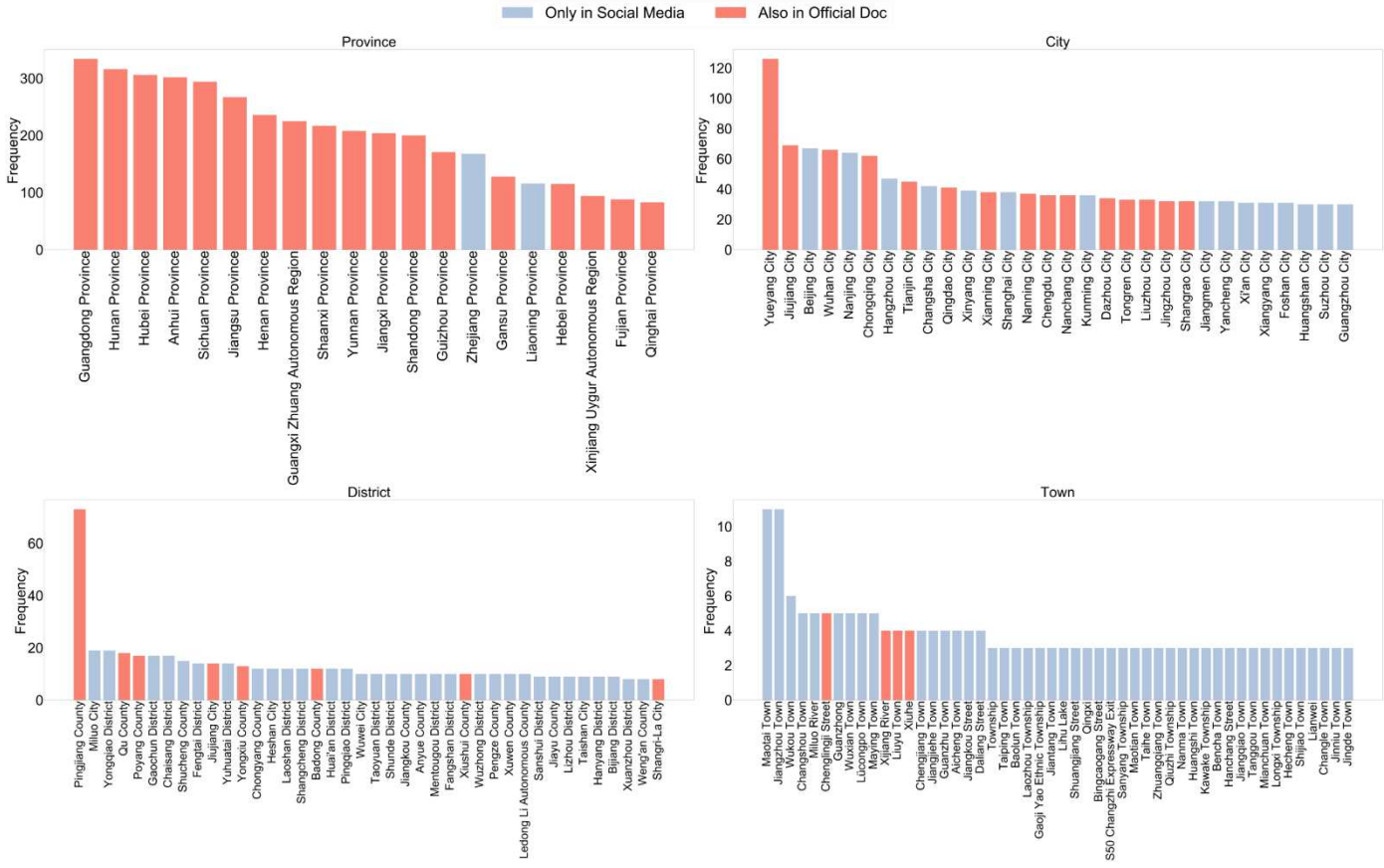
(July 1)



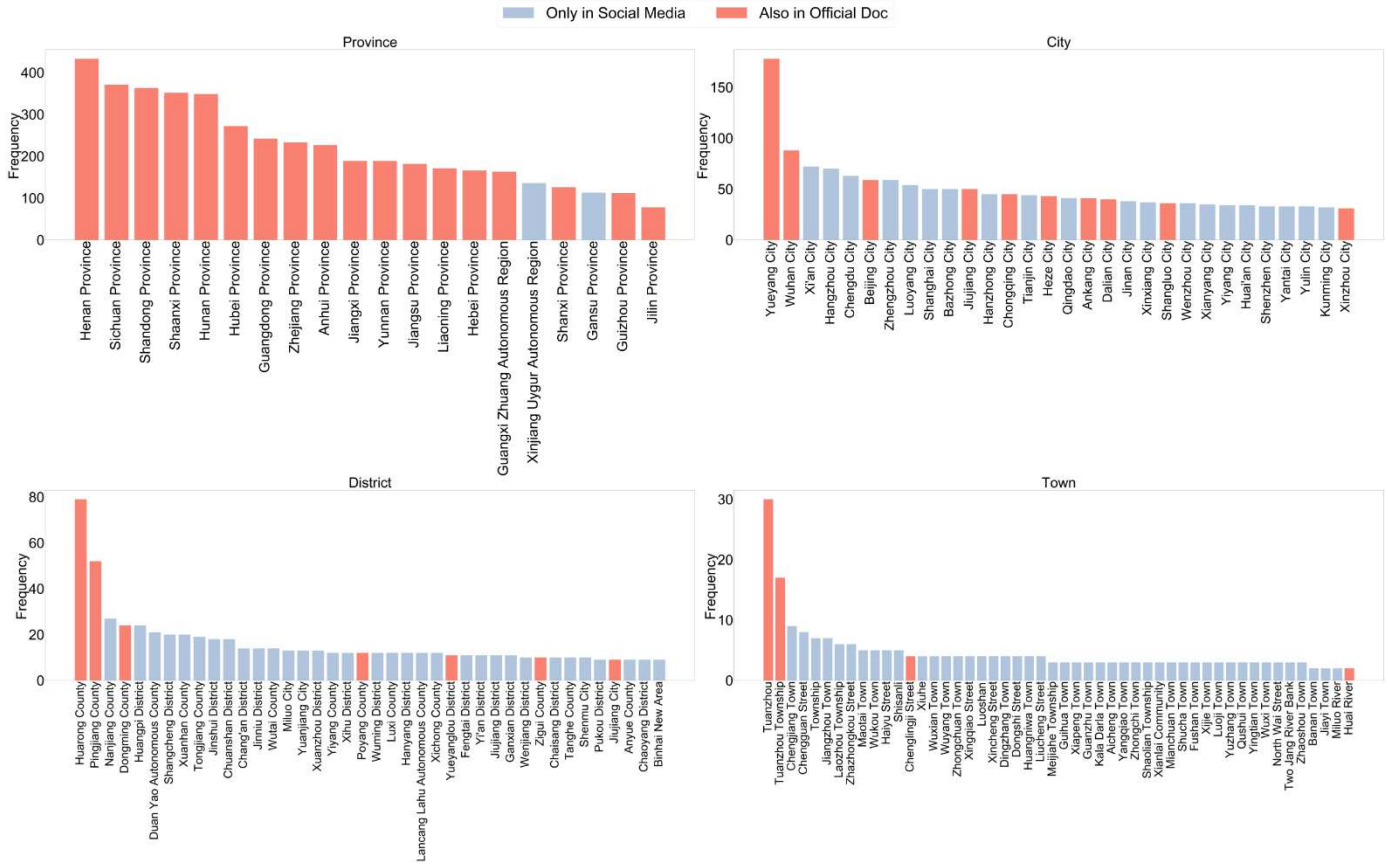
(July 2)


Only in Social Media
Also in Official Doc
Province
Frequency
Hunan Province
Sichuan Province
Anhui Province
Yunnan Province
Guangdong Province
Henan Province
Hubei Province
Jiangsu Province
Shaanxi Province
Guangxi Zhuang Autonomous Region
Jiangxi Province
Guizhou Province
Shandong Province
Zhejiang Province
Liaoning Province
Hebei Province
Xinjiang Uygur Autonomous Region
Gansu Province
Fujian Province
Shanxi Province
City
Yueyang City
Chengdu City
Jiujiang City
Nanjing City
Beijing City
Nanyang City
Chongqing City
Wuhan City
Qiandongnan Miao and Dong Autonomous Prefecture
Suzhou City
Shanghai City
Xi'an City
Huangshan City
Xiangyang City
Liuzhou City
Tongren City
Tianjin City
Tongling City
Xianyang City
Huaihua City
Yiyang City
Guangzhou City
Anqing City
Hangzhou City
Pu'er City
Shangrao City
Changsha City
Nanchang City
Nanning City
Laibin City
District
Pingjiang County
Miluo City
Zhenyuan County
Chaisang District
Yueyang County
Wujiang District
Fenglai District
Fanzheng District
Poyang County
Rongan County
Shexian County
Wolong District
Yongxiu County
Wancheng District
Jiujiang City
Jianyang City
Yi'an District
Jinxiu Yao Autonomous County
Bijiang District
Tunxi District
Pukou District
Luxi County
Xinhua District
Pengzhou City
Long'an County
Xinhuang Dong Autonomous County
Shuangliu District
Mancheng District
Xinjian District
Yongchun County
Tieling County
Daye City
Wuwei City
Xuanwu District
Wengan County
Hanshan County
Nanhai District
Heshan District
Qionglai City
Fuping County
Town
Jiangzhou Town
Luojiang Town
Wukou Town
Miluo River
Chengguan Town
Meiling Town
Puer Town
Huiyi District
Chenglingji Street
Township
Xuba Township
Banan Town
Kaili Town
Changzhou Town
Qingyun Town
Xihongmen Town
Xijiang River
Chuanshanjing Town
Feng Town
Datong Town
Jiangjiehe Town
Shuiyuan Town
Wushi Town
Chengqu Street
Yaogou Town
Kawakle Township
Jingzi Town
Jindou
Tuokou Town
Shuangta Street
Luodai Town
Liuyu Town
Guangzhong
Shijiuhu
Rongmei Town
Gonglian Town
Li River
Xilian Town
Dayou Town
Pingquan Street
Jiuji Town
Chencun Town
Taiping Town
Zhongchi Town
Dapu Town
Zhenyuan Town
Wangcun Town
Zhongjiang Township
Qinglong Town

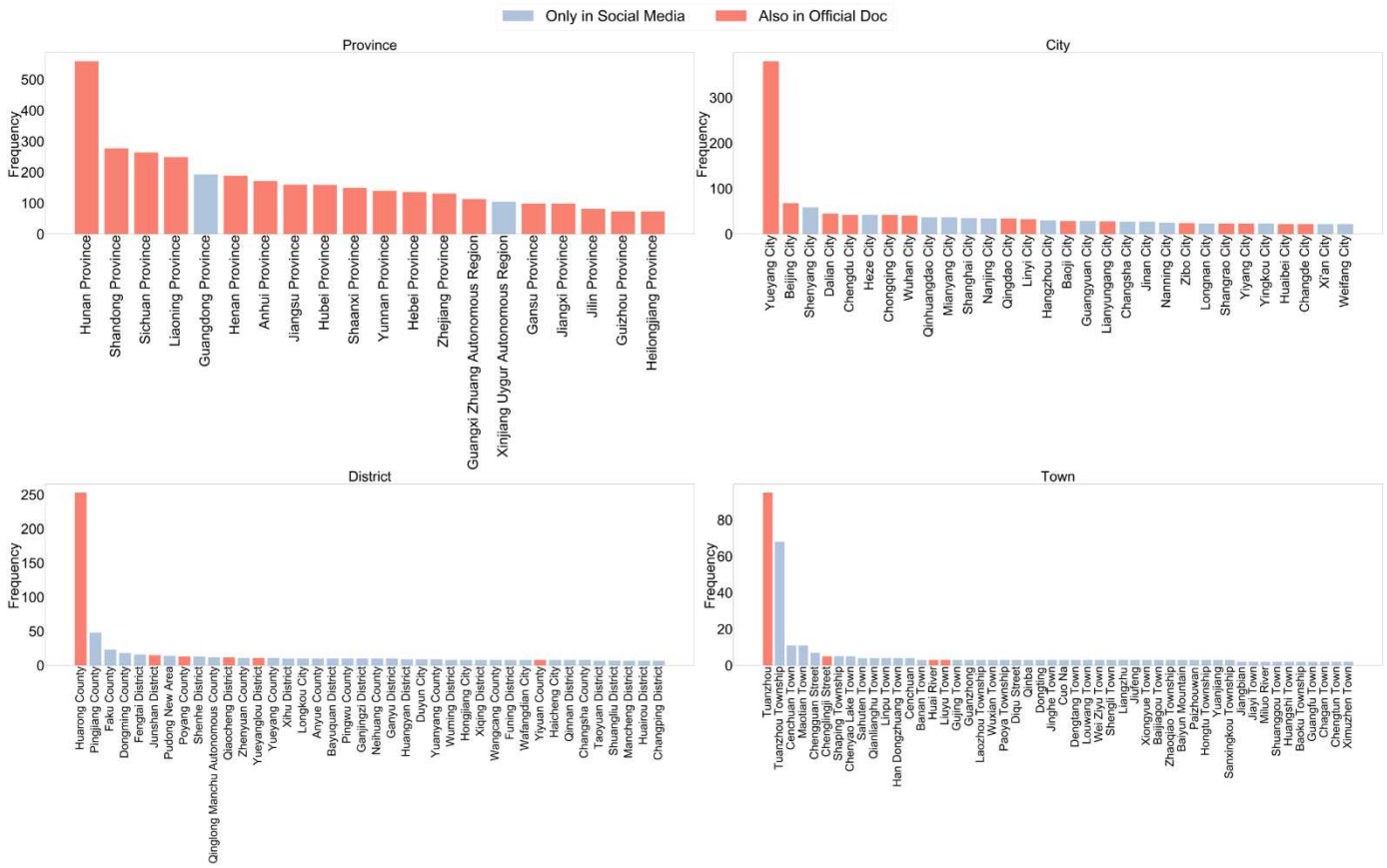
(July 3)


Only in Social Media
Also in Official Doc
Province
Frequency
Guangdong Province
Hunan Province
Hubei Province
Anhui Province
Sichuan Province
Jiangsu Province
Henan Province
Guangxi Zhuang Autonomous Region
Shaanxi Province
Yunnan Province
Jiangxi Province
Shandong Province
Guizhou Province
Zhejiang Province
Gansu Province
Liaoning Province
Hebei Province
Xinjiang Uygur Autonomous Region
Fujian Province
Qinghai Province
City
Yueyang City
Jiujiang City
Beijing City
Wuhan City
Nanjing City
Chongqing City
Hangzhou City
Tianjin City
Changsha City
Qingdao City
Xinyang City
Xianning City
Shanghai City
Nanning City
Chengdu City
Nanchang City
Kunming City
Dazhou City
Tongren City
Liuzhou City
Jingzhou City
Shangrao City
Jiangmen City
Yancheng City
Xi'an City
Xiangyang City
Foshan City
Huangshan City
Suzhou City
Guangzhou City
District
Pingjiang County
Miluo City
Yongqiao District
Qu County
Poyang County
Gaochun District
Chaisang District
Shucheng County
Fenglai District
Jiujiang City
Yuhuatai District
Yongxiu County
Heshan City
Chongyang County
Laoshan District
Shangcheng District
Badong County
Hua'an District
Pingqiao District
Wuwei City
Taoyuan District
Shunde District
Jiangkou County
Anyue County
Mentougou District
Fangshan District
Xiushui County
Wuzhong District
Pengze County
Xuwen County
Ledong Li Autonomous County
Sanshui District
Jiayu County
Lizhou District
Taishan City
Hanyang District
Bijiang District
Xuanzhou District
Weng'an County
Shangri-La City
Town
Maotai Town
Jiangzhou Town
Wukou Town
Changshou Town
Miluo River
Chengjiangli Street
Qiaozhou Town
Wuxian Town
Lücongpo Town
Mayang Town
Xijiang River
Liuyu Town
Xiaba Town
Chengjiang Town
Jiangjiehe Town
Guanzhu Town
Aicheng Town
Jiangkou Street
Dafang Street
Taiping Town
Baolun Town
Laozhou Township
Gaoji Yao Ethnic Township
Jiantang Town
Lhu Lake
Shuangjiang Street
Qingxi
Bingcaogang Street
S50 Changzhi Expressway Exit
Sanyang Township
Maotian Town
Zhuangjiang Town
Qiuzhi Township
Nanma Town
Huangshi Town
Kawakle Township
Baocha Town
Hanxing Street
Jiangdiao Town
Tanggou Town
Mianchuan Town
Longxi Township
Hecheng Town
Shijiao Town
Liuyuan Town
Changle Town
Jinniu Town
Jingde Town

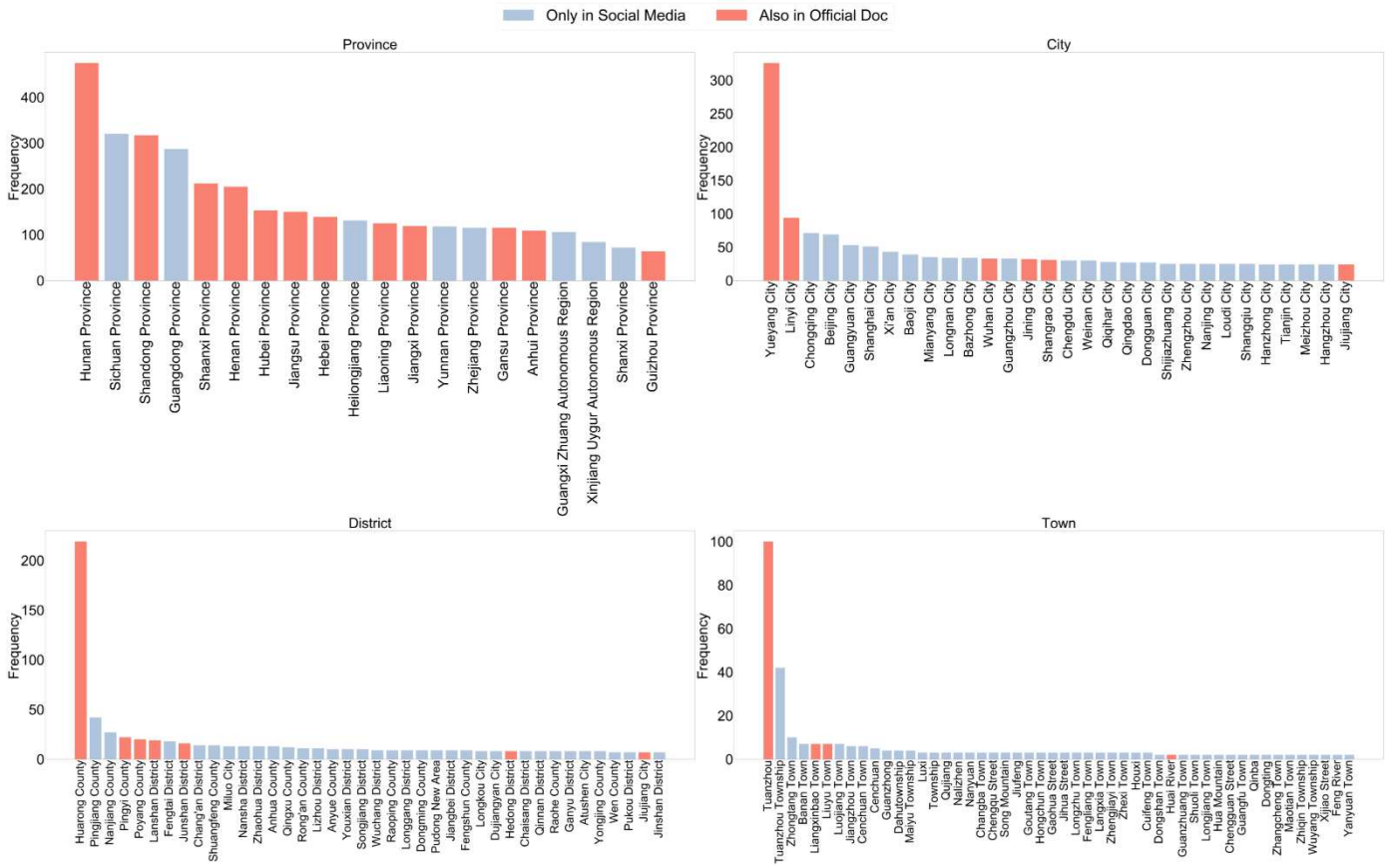
(July 4)


Only in Social Media
Also in Official Doc
Province
Frequency
Henan Province
Sichuan Province
Shandong Province
Shaanxi Province
Hunan Province
Hubei Province
Guangdong Province
Zhejiang Province
Anhui Province
Jiangxi Province
Yunnan Province
Jiangsu Province
Liaoning Province
Hebei Province
Guangxi Zhuang Autonomous Region
Xinjiang Uygur Autonomous Region
Shanxi Province
Gansu Province
Guizhou Province
Jilin Province
City
Yueyang City
Wuhan City
Xi'an City
Hangzhou City
Chengdu City
Beijing City
Zhengzhou City
Luoyang City
Shanghai City
Bazhong City
Jiujiang City
Hanzhong City
Chongqing City
Tianjin City
Heze City
Qingdao City
Ankang City
Dalian City
Jinan City
Xinxiang City
Shangluo City
Wenzhou City
Xianyang City
Yiyang City
Hua'an City
Shenzhen City
Yantai City
Yulin City
Kunming City
Xinzhou City
District
Huarong County
Pingjiang County
Nanjiang County
Dongming County
Huangpi District
Duan Yao Autonomous County
Shangcheng District
Xuanhan County
Tongliang County
Jinshui District
Chuanshan District
Chang'an District
Jinnu District
Wutai County
Miluo City
Yuanjiang City
Xuanzhou District
Yiyang County
Xihu District
Poyang County
Wuning District
Luxi County
Hanyang District
Lancang Lahu Autonomous County
Xichong County
Yueyanglou District
Fengtai District
Yi'an District
Jiujiang District
Ganxian District
Wenjiang District
Zigui County
Chaisang District
Tanghe County
Shenmu City
Pukou District
Jiujiang City
Anyue County
Chaoyang District
Binhai New Area
Town
Tuanzhou
Tuanzhou Township
Chengjiang Town
Chengguan Street
Township
Jiangzhou Township
Laozhou Township
Zhazhongkou Street
Wukou Town
Haiyu Street
Shuiyuan Street
Chenglingji Subdistrict
Xiuhe
Wuxian Town
Wuyang Town
Zhongzhuan Town
Xingjiao Street
Luogang Street
Xincheng Street
Dingzhang Town
Dongshi Street
Huangniwa Town
Liucheng Street
Meijiashi Township
Guta Town
Xiapeng Town
Guanzhu Town
Kala Daria Town
Aicheng Town
Yangdao Town
Zhuzhou Town
Shanlian Township
Xiantai Community
Mianchuan Town
Shucha Town
Fushan Town
Xiji Town
Luyi Town
Yuzhang Town
Qushui Town
Yingtian Town
Wuxi Town
North Yi'ai Street
Two Rivers Park Area
Zhaoshou Town
Banan Town
Jiayi Town
Miluo River
Huai River

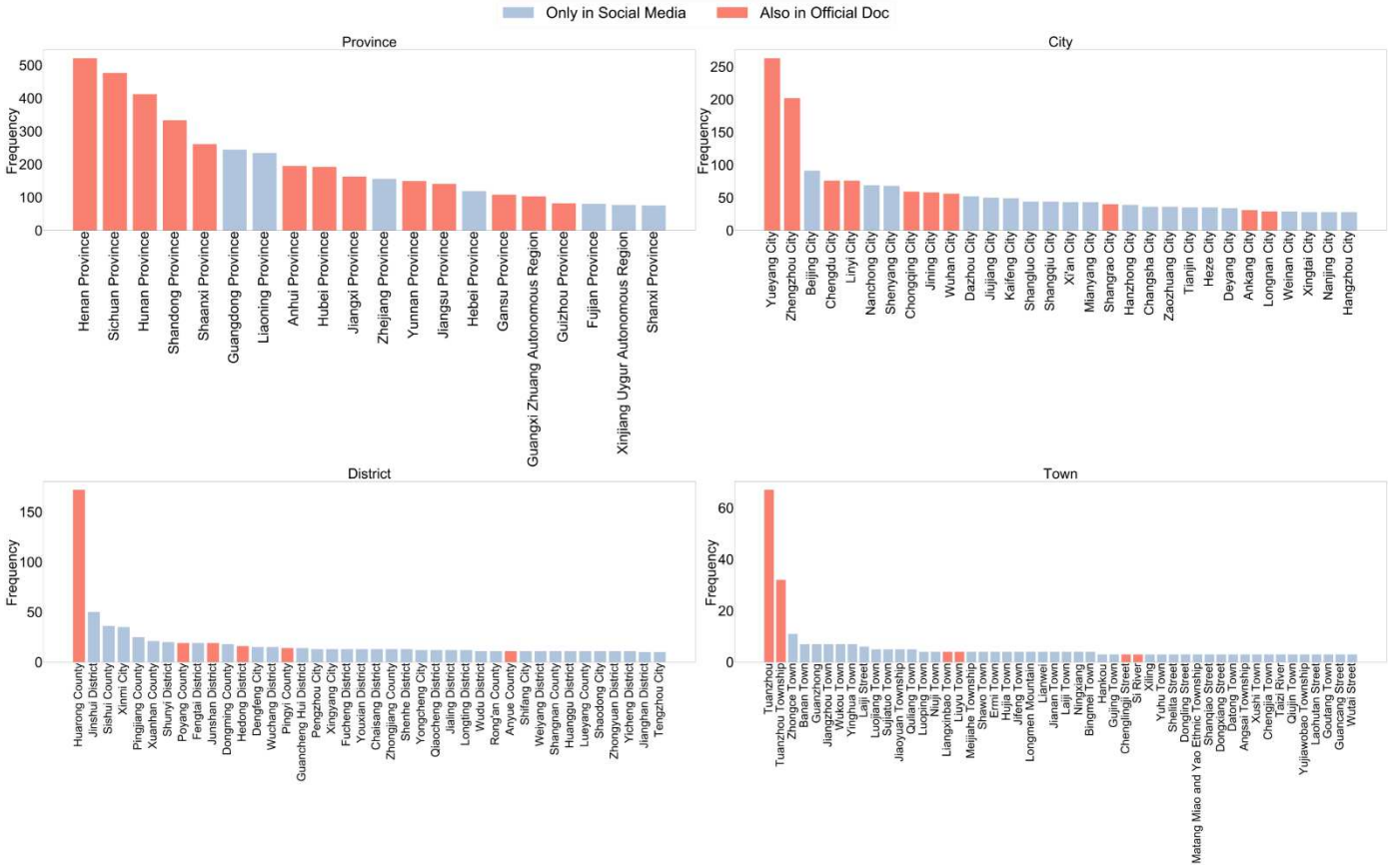
(July 5)


Only in Social Media
Also in Official Doc
Province
Frequency
Hunan Province
Shandong Province
Sichuan Province
Liaoning Province
Guangdong Province
Henan Province
Anhui Province
Jiangsu Province
Hubei Province
Shaanxi Province
Yunnan Province
Hebei Province
Zhejiang Province
Guangxi Zhuang Autonomous Region
Xinjiang Uygur Autonomous Region
Gansu Province
Jiangxi Province
Jilin Province
Guizhou Province
Heilongjiang Province
City
Yueyang City
Beijing City
Shenyang City
Dalian City
Chengdu City
Heze City
Chongqing City
Wuhan City
Qinhuangdao City
Mianyang City
Shanghai City
Nanjing City
Qingdao City
Linyi City
Hangzhou City
Baoji City
Guangyuan City
Lianyungang City
Changsha City
Jinan City
Nanning City
Zibo City
Longnan City
Shangrao City
Yiyang City
Yingkou City
Huaibei City
Changde City
Xi'an City
Weifang City
District
Huarong County
Pingjiang County
Faku County
Dongming County
Fengtai District
Junshan District
Pudong New Area
Poyang County
Shenhe District
Qinglong Manchu Autonomous County
Qiaocheng District
Zhenyuan County
Yueyanglou District
Yueyang County
Xihu District
Longkou City
Anyue County
Bayuquan District
Pingwu County
Ganjingzi District
Neihuang County
Ganyu District
Huangyan District
Duyun City
Yuanyang County
Wuming District
Hongjiang City
Xiqing District
Wangcang County
Funing District
Wafangdian City
Yiyuan County
Haicheng City
Qinnan District
Changsha County
Taoyuan District
Shuangliu District
Mancheng District
Huairou District
Changping District
Town
Tuanzhou
Tuanzhou Township
Cenchuan Town
Maotian Town
Chengguan Street
Chengjiang Town
Shaping Township
Chenyao Lake Town
Sahuten Town
Qianlilanghu Town
Linpu Town
Han Dongzhong Town
Qingtian Town
Banan Town
Huai River
Luyu Town
Gujing Town
Guanzhong
Laozhou Township
Wuxian Town
Paoya Township
Diqu Street
Qinba
Dongting
Jinghe Lu Na
Dengtang Town
Louwang Town
Wei Ziyu Town
Shengli Town
Liangzhu
Jiuhe
Xiongyue Town
Baijiagou Town
Zhaoqiao Township
Baiyun Mountain
Paizhouwan
Hongta Township
Yuanjia Town
Sanxingkou Township
Jiangbian
Jiayi Town
Miluo River
Shuanggou Town
Huangtu Township
Baoku Township
Guanglu Town
Chagan Town
Chengtun Town
Ximuzhen Town

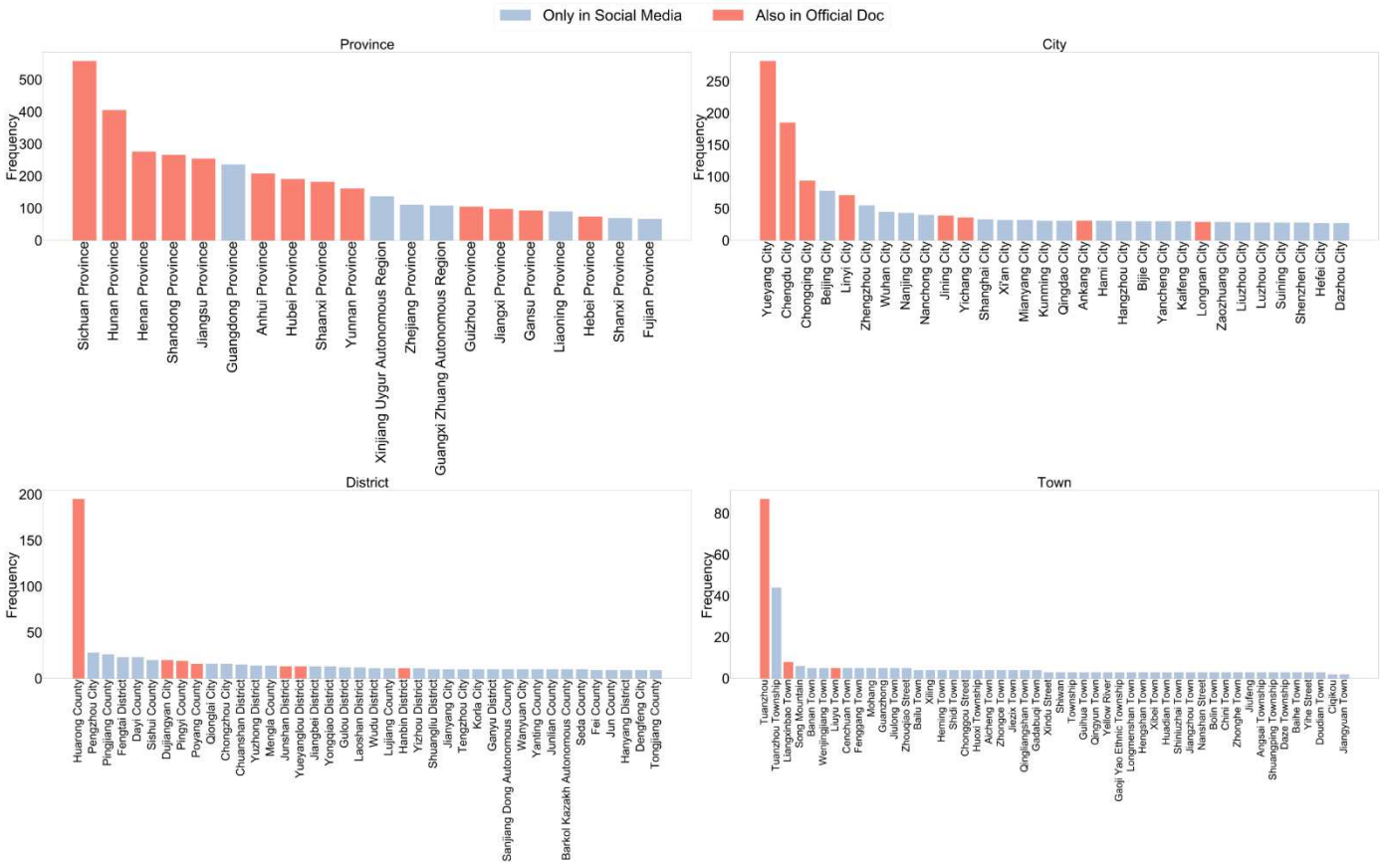
(July 6)


Only in Social Media
Also in Official Doc
Province
Frequency
Hunan Province
Sichuan Province
Shandong Province
Guangdong Province
Shaanxi Province
Henan Province
Hubei Province
Jiangsu Province
Hebei Province
Heilongjiang Province
Liaoning Province
Jiangxi Province
Yunnan Province
Zhejiang Province
Gansu Province
Anhui Province
Guangxi Zhuang Autonomous Region
Xinjiang Uygur Autonomous Region
Shanxi Province
Guizhou Province
City
Yueyang City
Linyi City
Chongqing City
Beijing City
Guangyuan City
Shanghai City
Xi'an City
Baoji City
Mianyang City
Longnan City
Bazhong City
Wuhan City
Guangzhou City
Jining City
Shangrao City
Chengdu City
Weinan City
Qiqihar City
Qingdao City
Dongguan City
Shijiazhuang City
Zhengzhou City
Nanjing City
Loudi City
Shangqiu City
Hanzhong City
Tianjin City
Meizhou City
Hangzhou City
Jiujiang City
District
Huarong County
Pingjiang County
Nanjiang County
Pingyi County
Poyang County
Lanshan District
Fengtai District
Junshan District
Changan District
Shuangfeng County
Miluo City
Nansha District
Zhaohua District
Anhua County
Qingxu County
Rong'an County
Lizhou District
Anyue County
Youxian District
Songjiang District
Wucheng District
Raoping County
Longgang District
Dongming County
Pudong New Area
Jiangbei District
Fengshun County
Longkou City
Dujiangyan City
Hedong District
Chaisang District
Qinnan District
Raohe County
Ganyu District
Atushen City
Yongjing County
Wen County
Putou District
Jiujiang City
Jinshan District
Town
Tuanzhou
Tuanzhou Township
Zhongtang Town
Banan Town
Liangxinbao Town
Liuyu Town
Lugiaoba Town
Jiangzhou Town
Cenchuan Town
Cenchuan
Guanzhong
Dahutownship
Maiyu Township
Li
Township
Qujiang
Nalizhen
Nanyuan
Changtai Town
Chengqu Street
Song Mountain
Jiufeng
Goutang Town
Hongchun Town
Gaohua Street
Jihua Street
Longzhen Town
Fenglijang Town
Langxia Town
Zhengjiayi Town
Zhexi Town
Houxi
Cuifen Town
Dongshan Town
Huai River
Guanzhuang Town
Shuoli Town
Longjiang Town
Hua Mountain
Chengguan Town
Gaangfu Town
Qinba
Dongting
Zhangcheng Town
Maotan Town
Zhuxin Township
Wuyicun Township
Xijiao Street
Feng River
Yanyuan Town

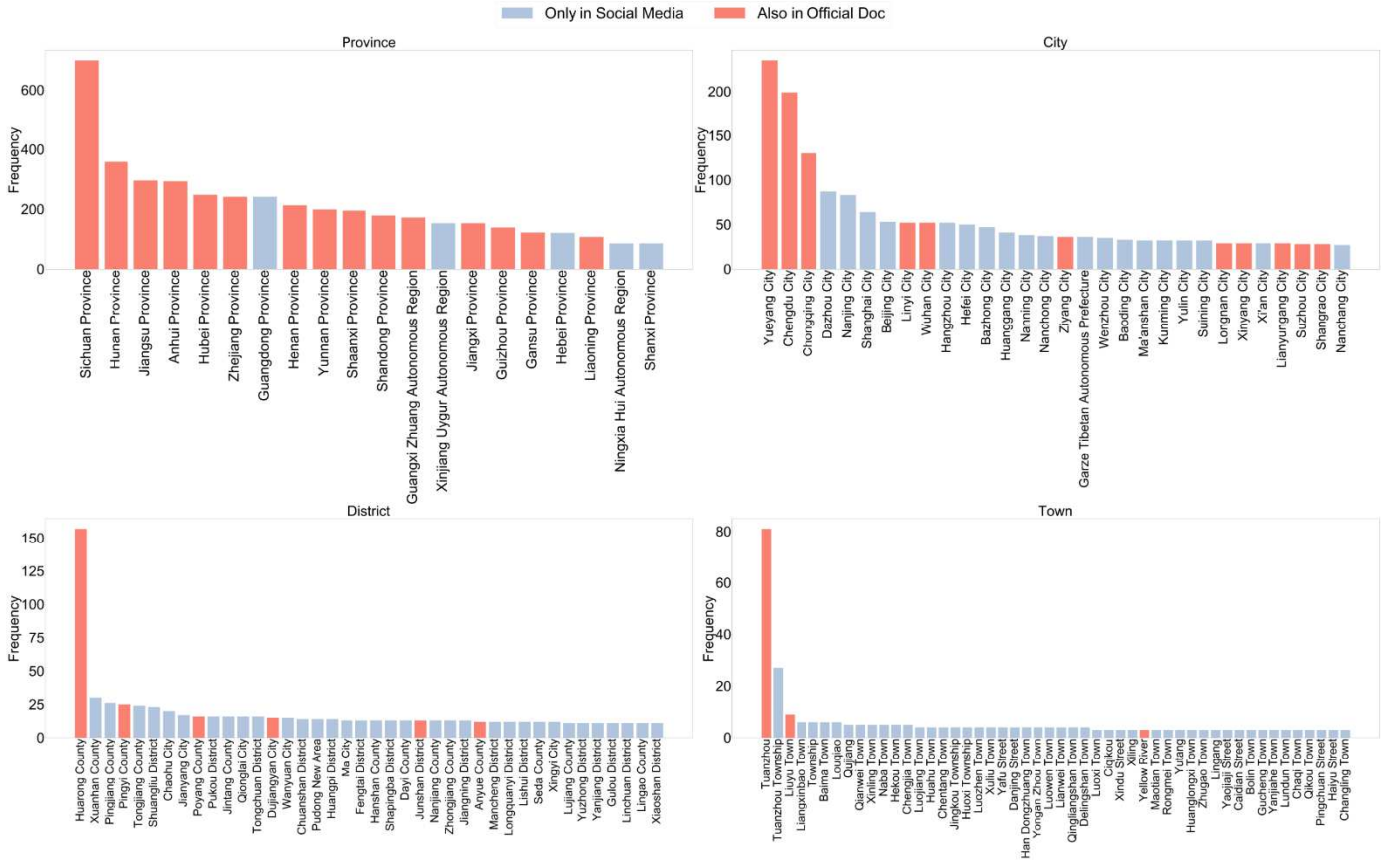
(July 7)


Only in Social Media
Also in Official Doc
Province
Frequency
Henan Province
Sichuan Province
Hunan Province
Shandong Province
Shaanxi Province
Guangdong Province
Liaoning Province
Anhui Province
Hubei Province
Jiangxi Province
Zhejiang Province
Yunnan Province
Jiangsu Province
Hebei Province
Gansu Province
Guangxi Zhuang Autonomous Region
Guizhou Province
Fujian Province
Xinjiang Uygur Autonomous Region
Shanxi Province
City
Yueyang City
Zhengzhou City
Beijing City
Chengdu City
Linyi City
Nanchong City
Shenyang City
Chongqing City
Jining City
Wuhan City
Dazhou City
Jiujiang City
Kaifeng City
Shangluo City
Shangqiu City
Xi'an City
Mianyang City
Shangrao City
Hanzhong City
Changsha City
Zaozhuang City
Tianjin City
Heze City
Deyang City
Ankang City
Longnan City
Weinan City
Xingtai City
Nanjing City
Hangzhou City
District
Huarong County
Jinshui District
Sishui County
Xinmi City
Pingjiang County
Xuanhan County
Shunyi District
Poyang County
Fengtai District
Junshan District
Dongming County
Hedong District
Dengfeng City
Wuchang District
Pingyi County
Guancheng Hui District
Pengzhou City
Xingyang City
Fucheng District
Youxian District
Chaisang District
Zhongjiang County
Shenhe District
Yongcheng City
Qiaocheng District
Jialing District
Longling District
Wudu District
Rong'an County
Anyue County
Shifang City
Weiyang District
Shangnan County
Huanggu District
Lueyang County
Shaodong City
Zhongyuan District
Yicheng District
Jianghan District
Tengzhou City
Town
Tuanzhou
Tuanzhou Township
Zhongce Town
Banan Town
Guanzhong
Jiangzhou Town
Wuchuan Town
Yinghua Town
Laiji Street
Luojiang Town
Sujiatuo Town
Jiaoyuan Township
Qujiang Town
Luojing Town
Niuji Town
Liangxinbao Town
Liuyu Town
Meijiahe Township
Shewo Town
Fenru Town
Hujia Town
Jifeng Town
Longmen Mountain
Lianwei
Jianan Town
Naiji Town
Nongzhan Town
Bingmei Town
Hankou
Gujing Town
Chengjingji Street
Si River
Xiling
Yuhu Town
Sheilla Street
Dongling Street
Matang Miao and Yao Ethnic Township
Shanqiao Street
Dongkang Street
Dachang Town
Angsai Township
Xushi Town
Taizi River
Chengjia Town
Qiujin Town
Yujiawobao Township
Lugang Street
Goutang Town
Guancang Street
Wutai Street

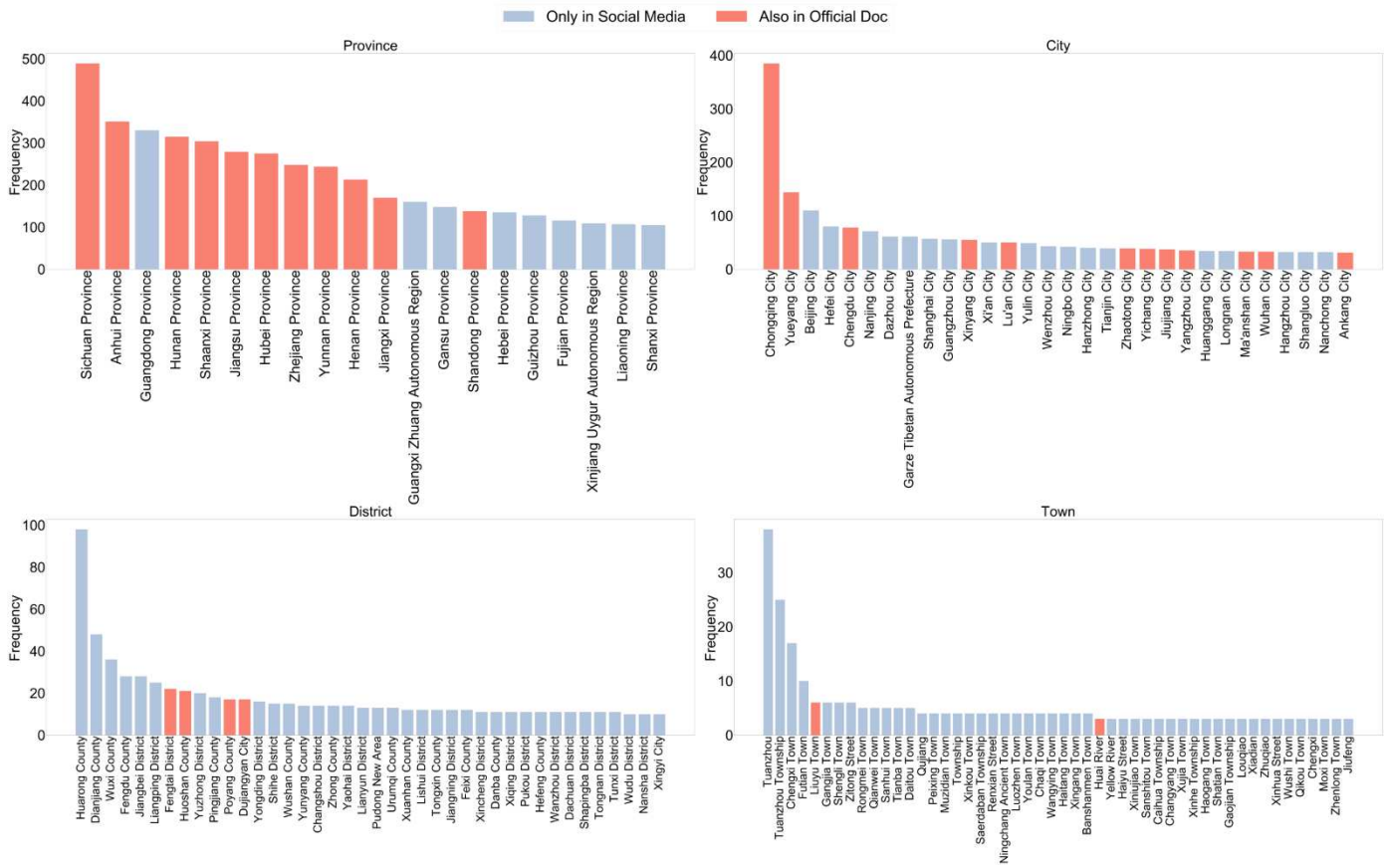
(July 8)



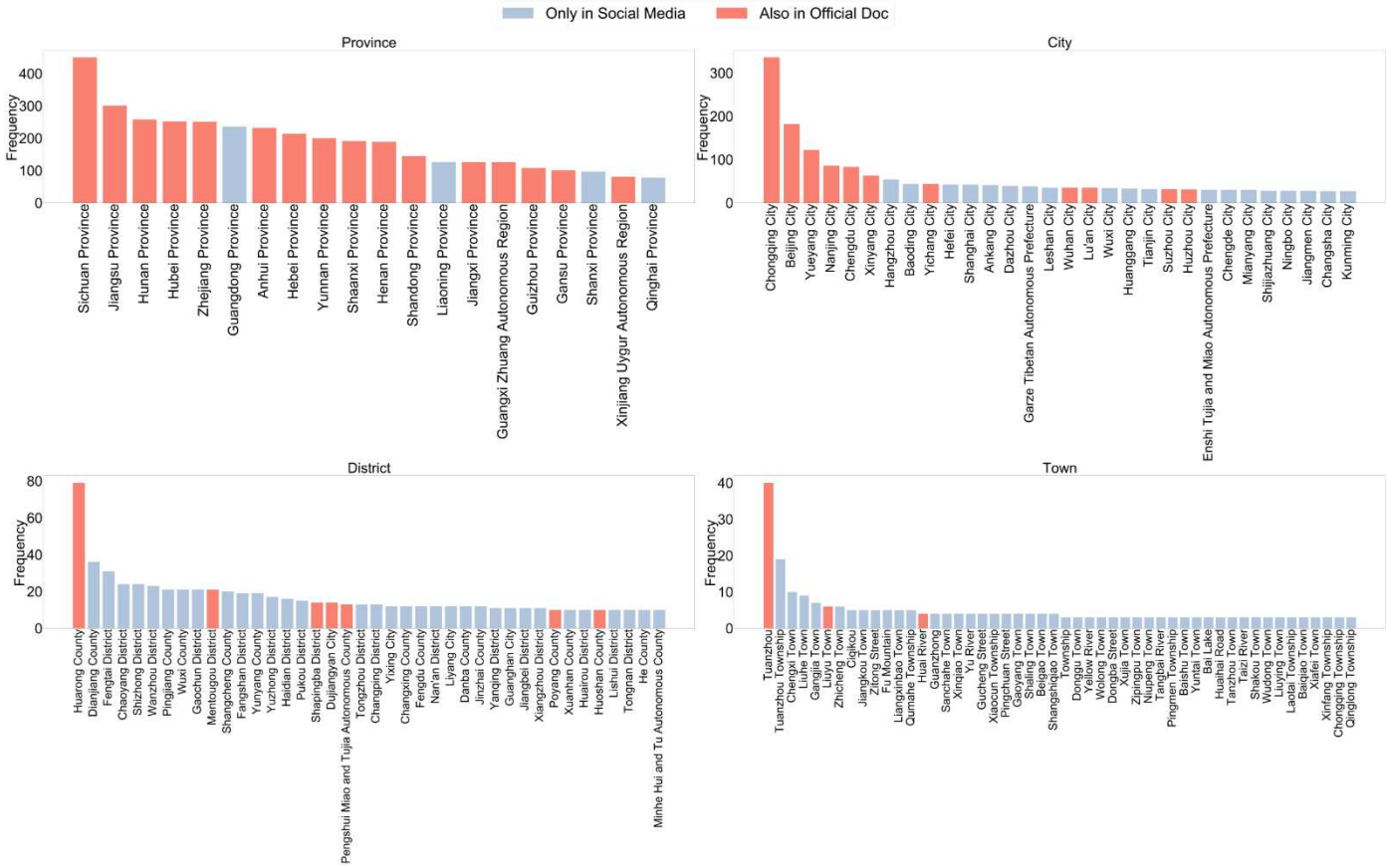
(July 9)



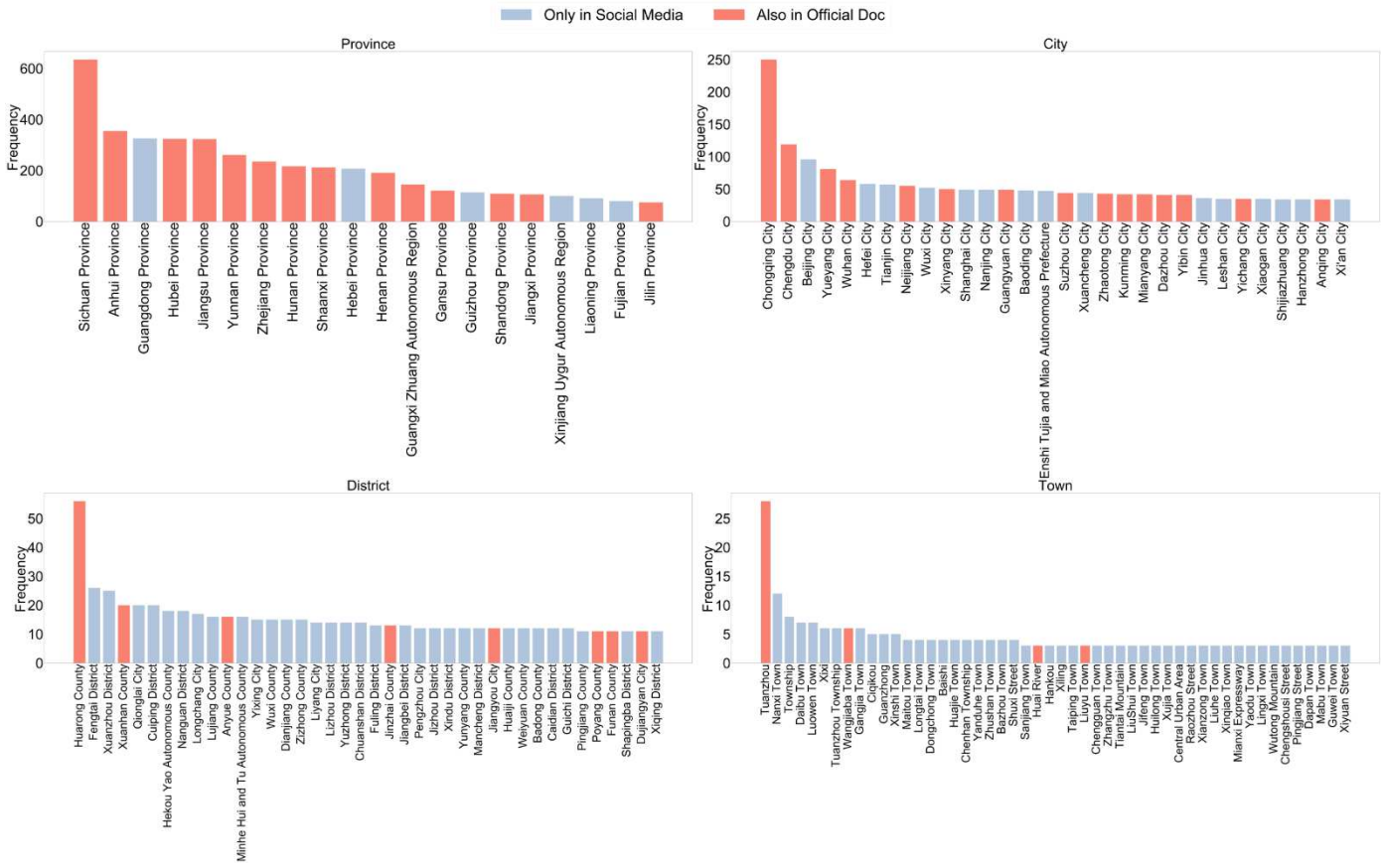
(July 10)



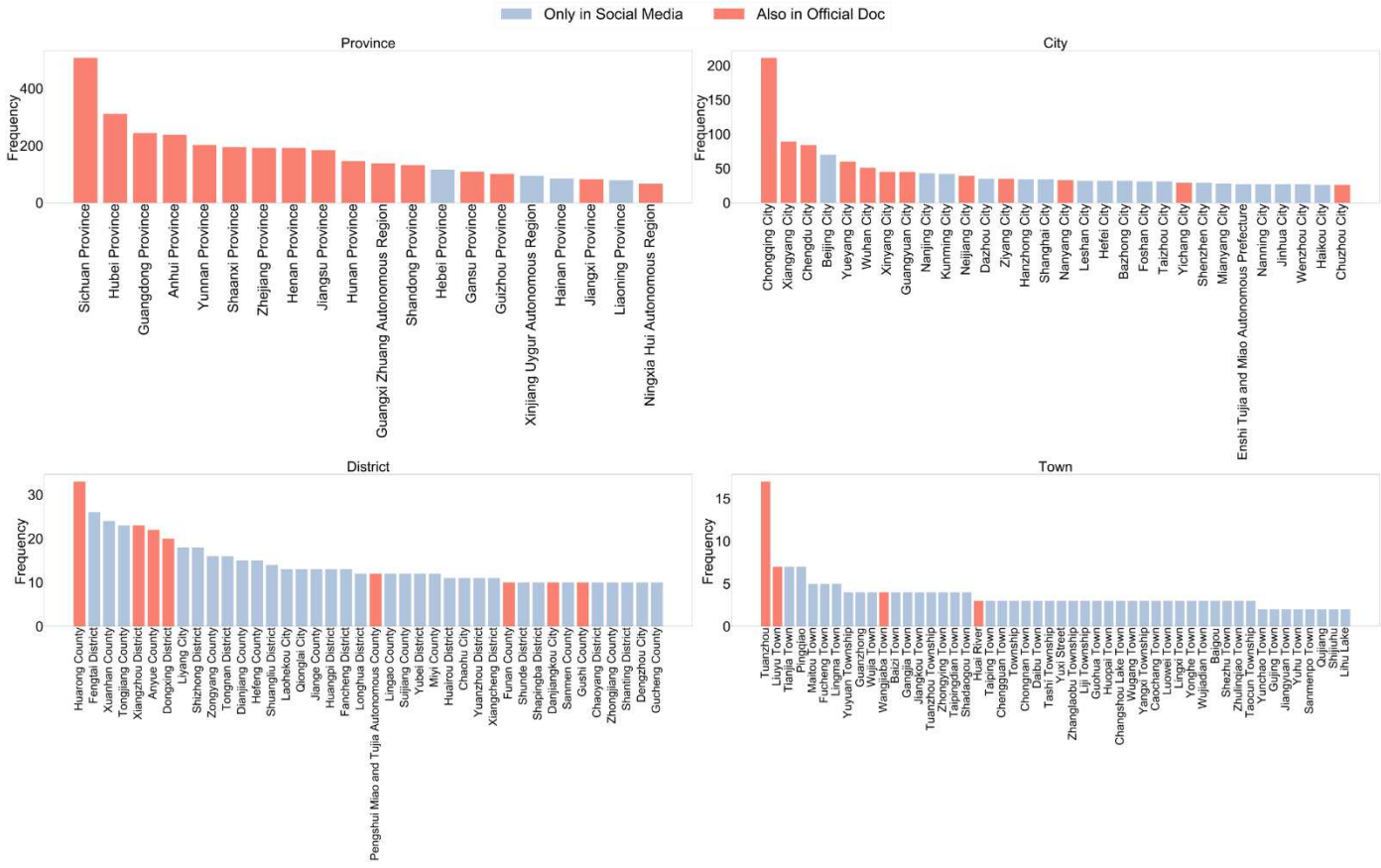
(July 11)



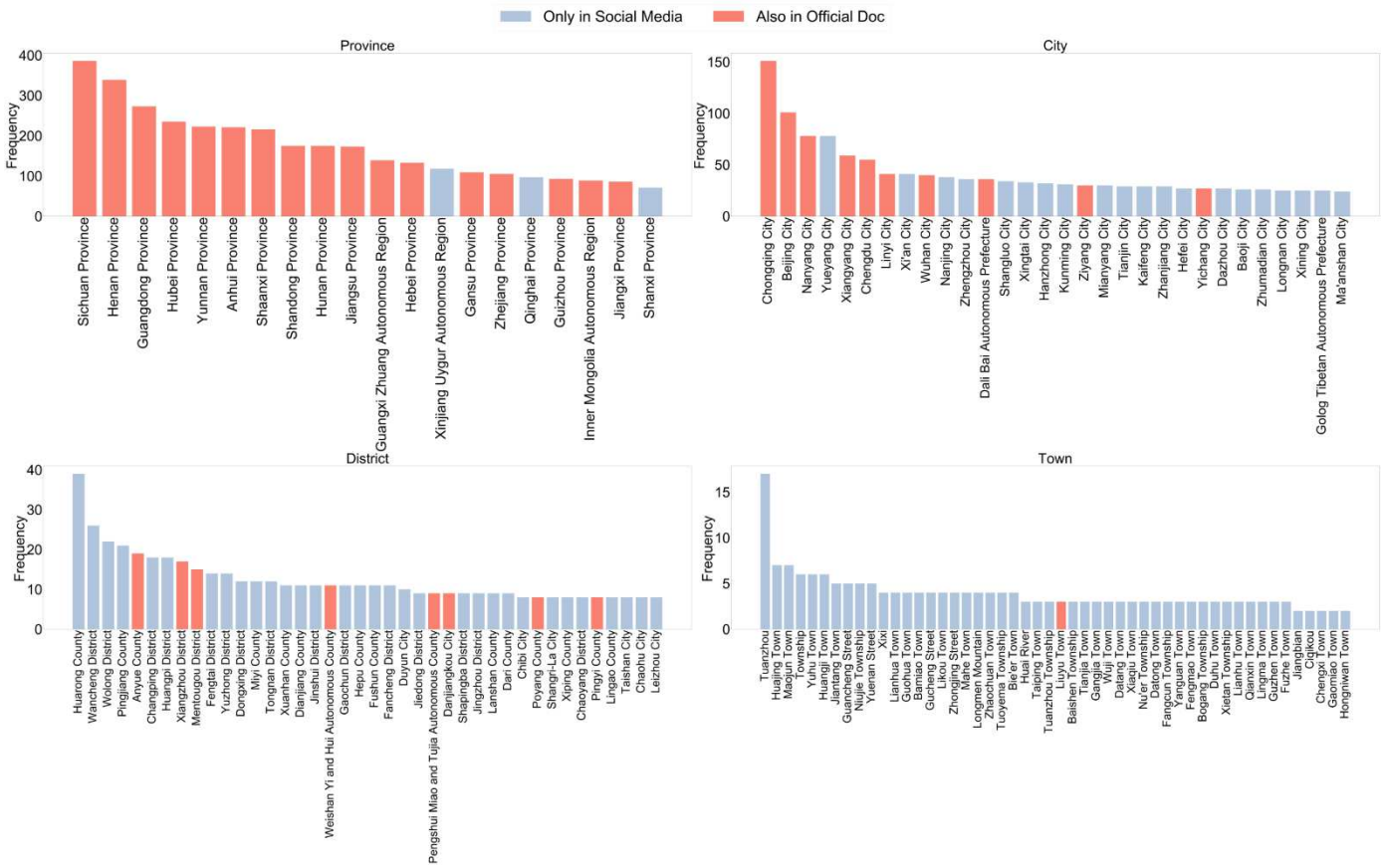
(July 12)



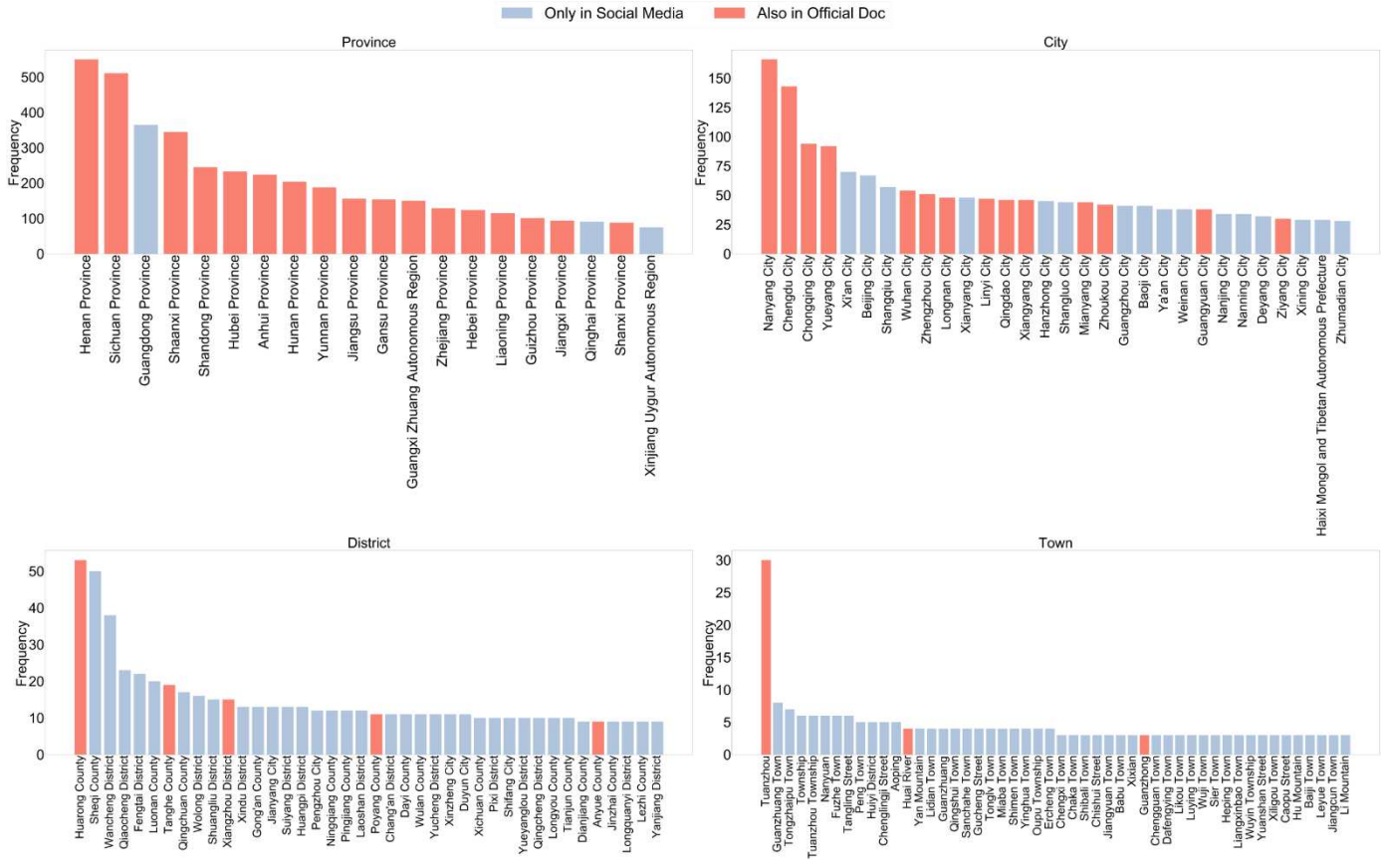
(July 13)



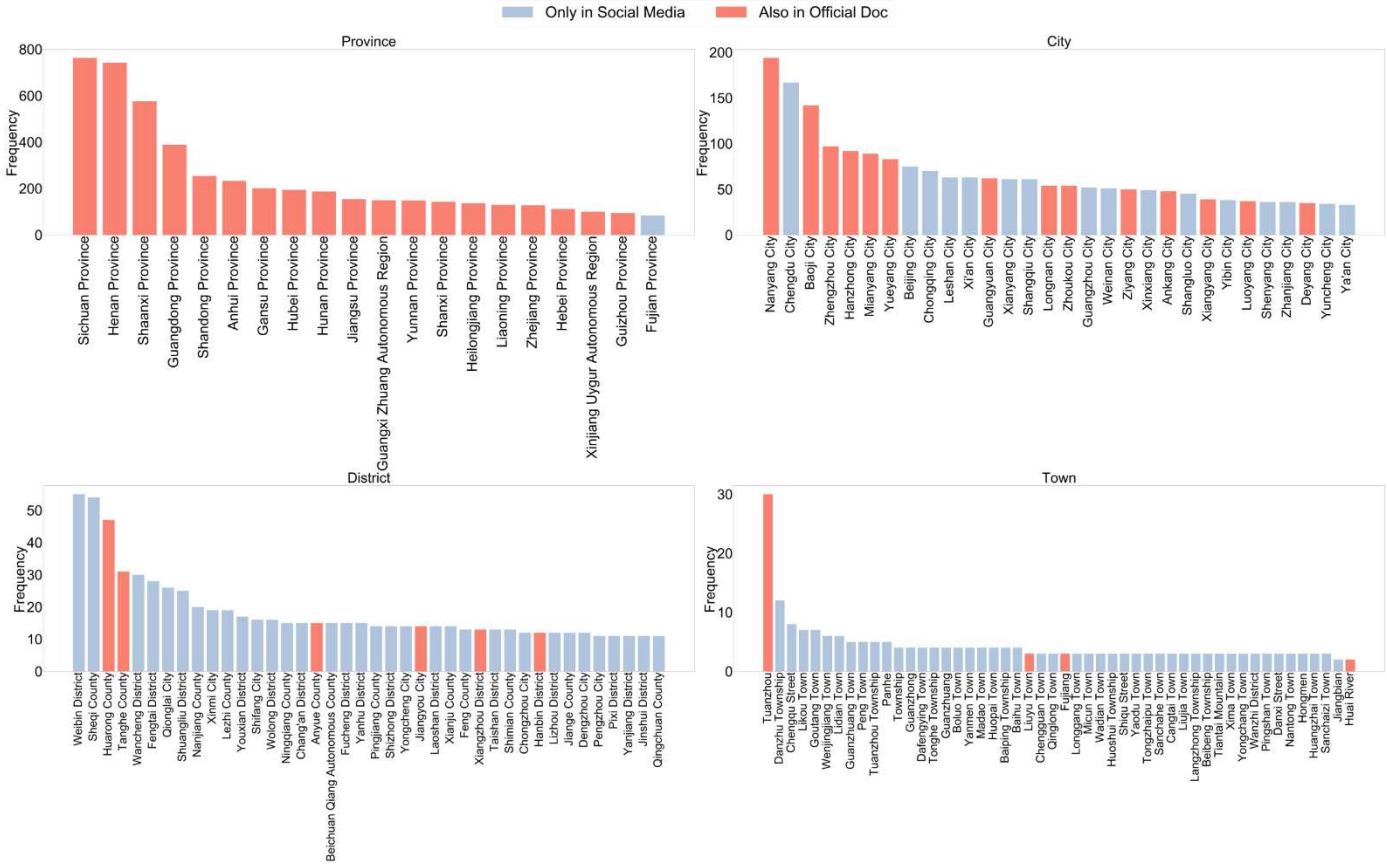
(July 14)



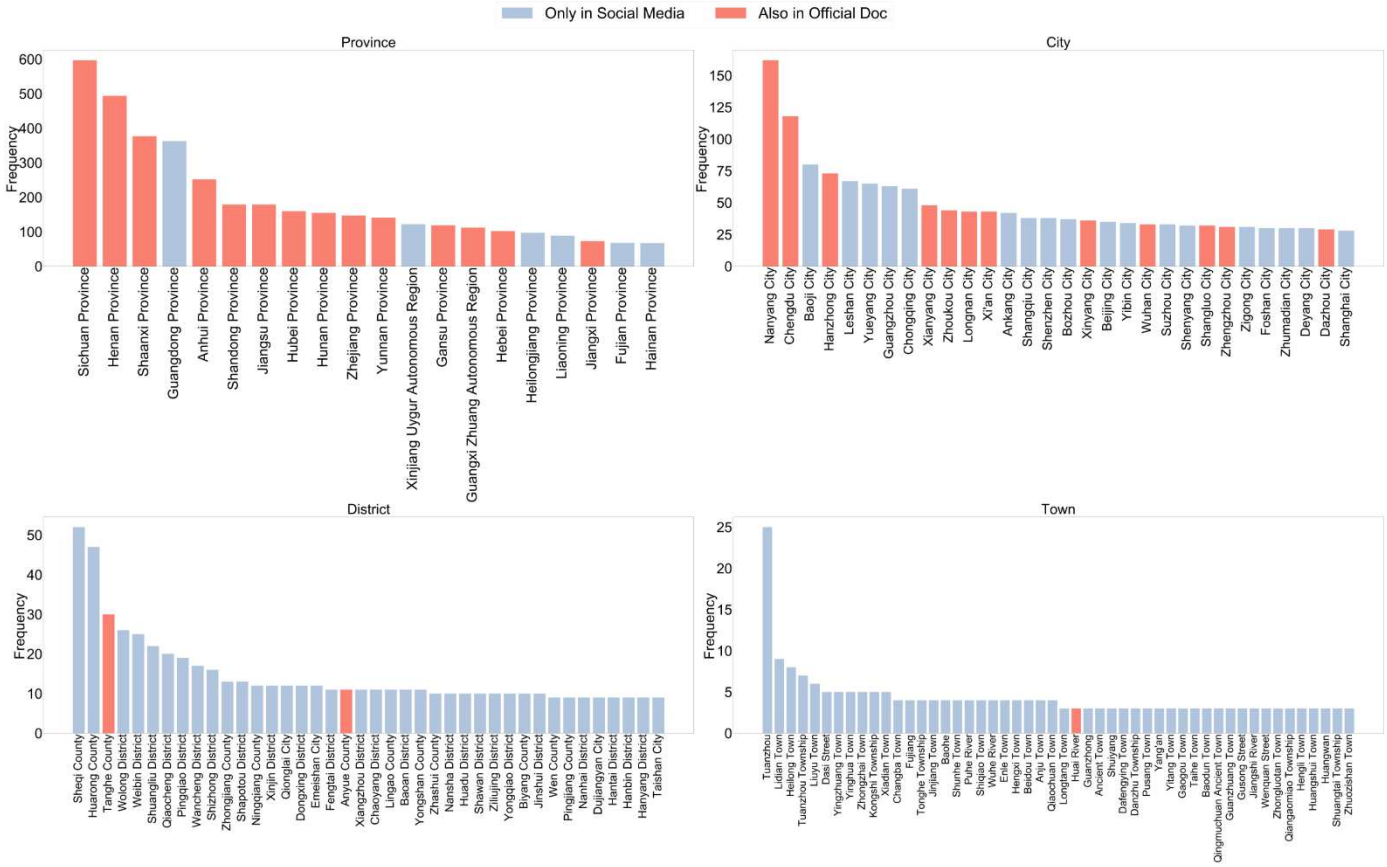
(July 15)



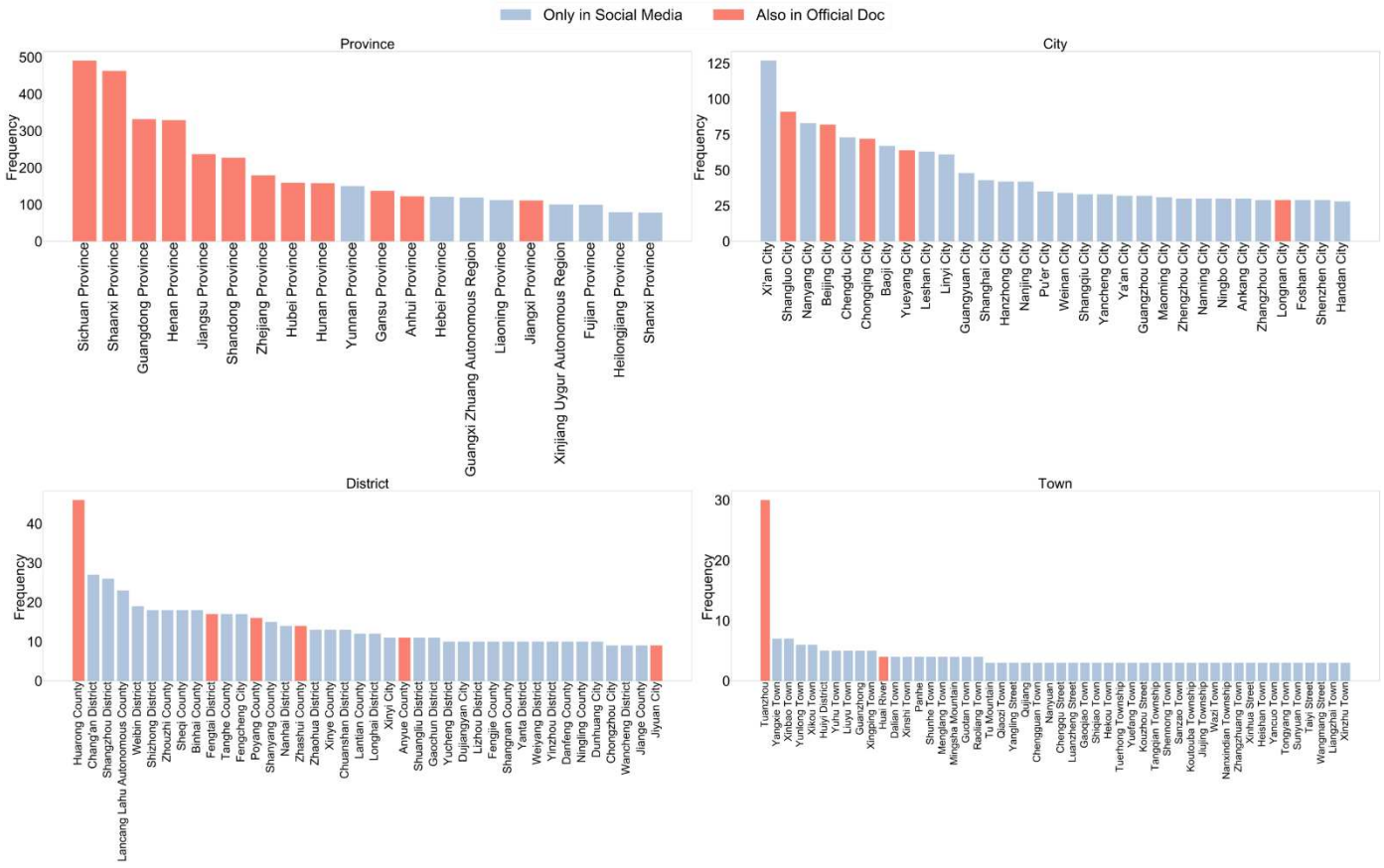
(July 16)



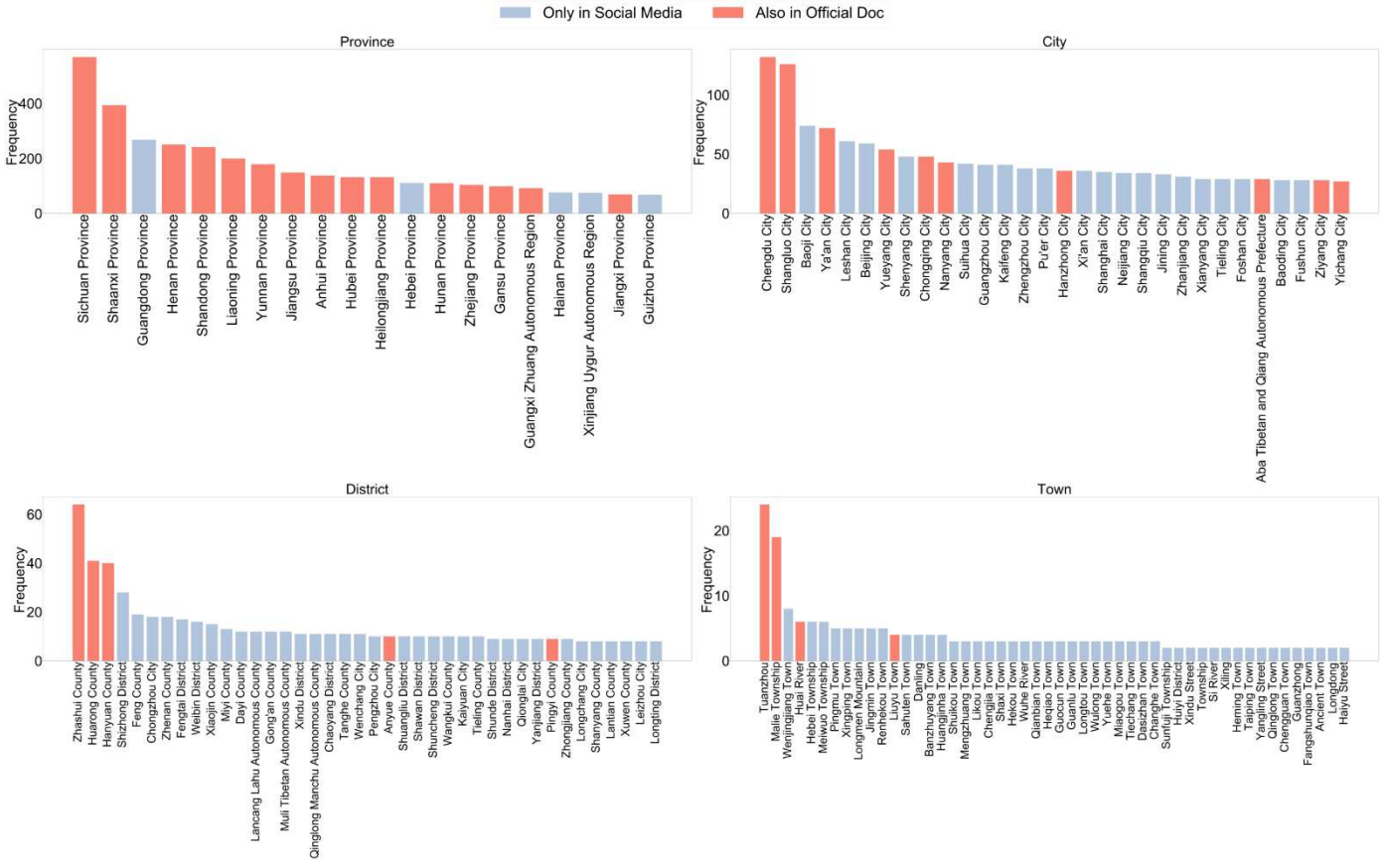
(July 17)



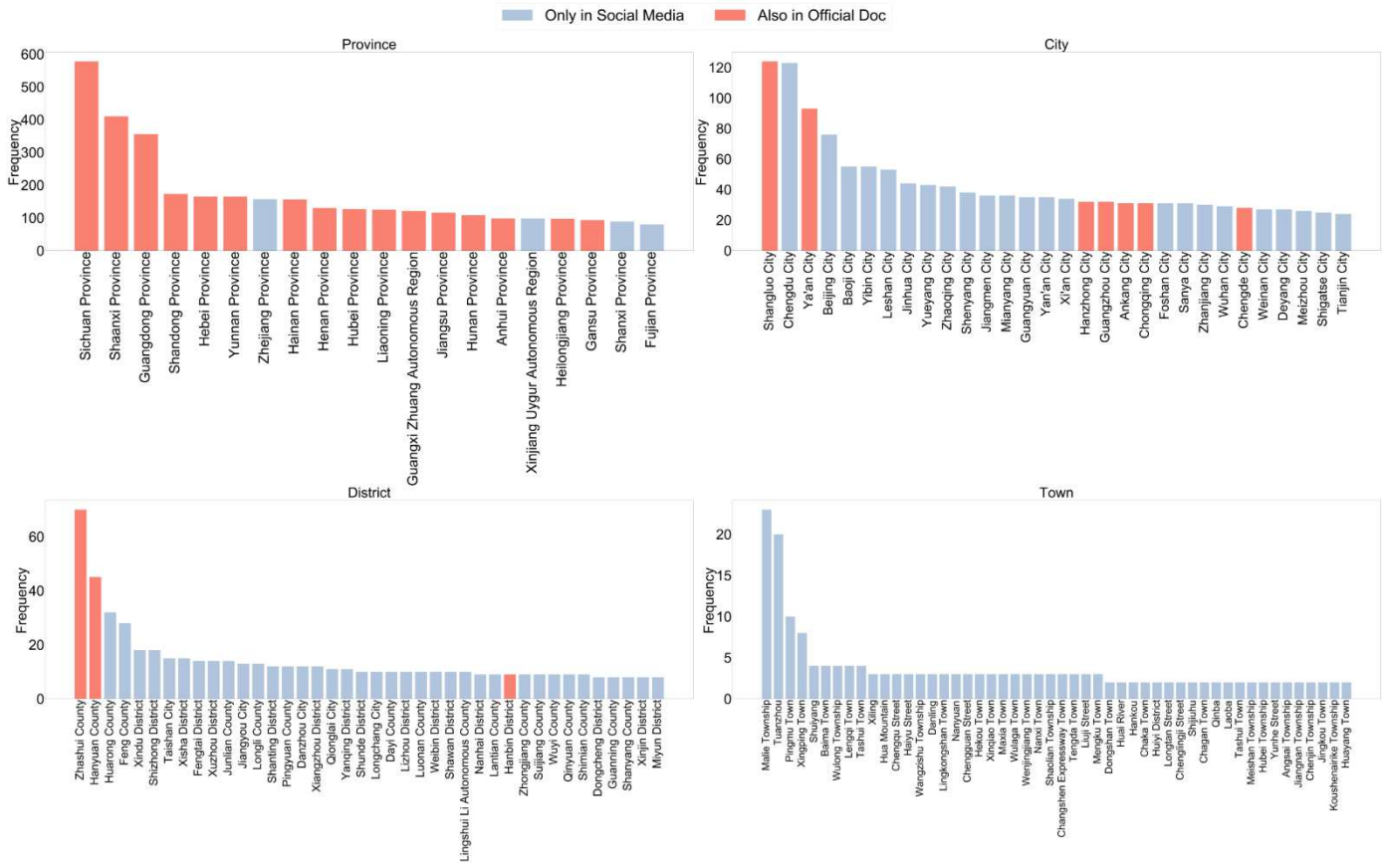
(July 18)



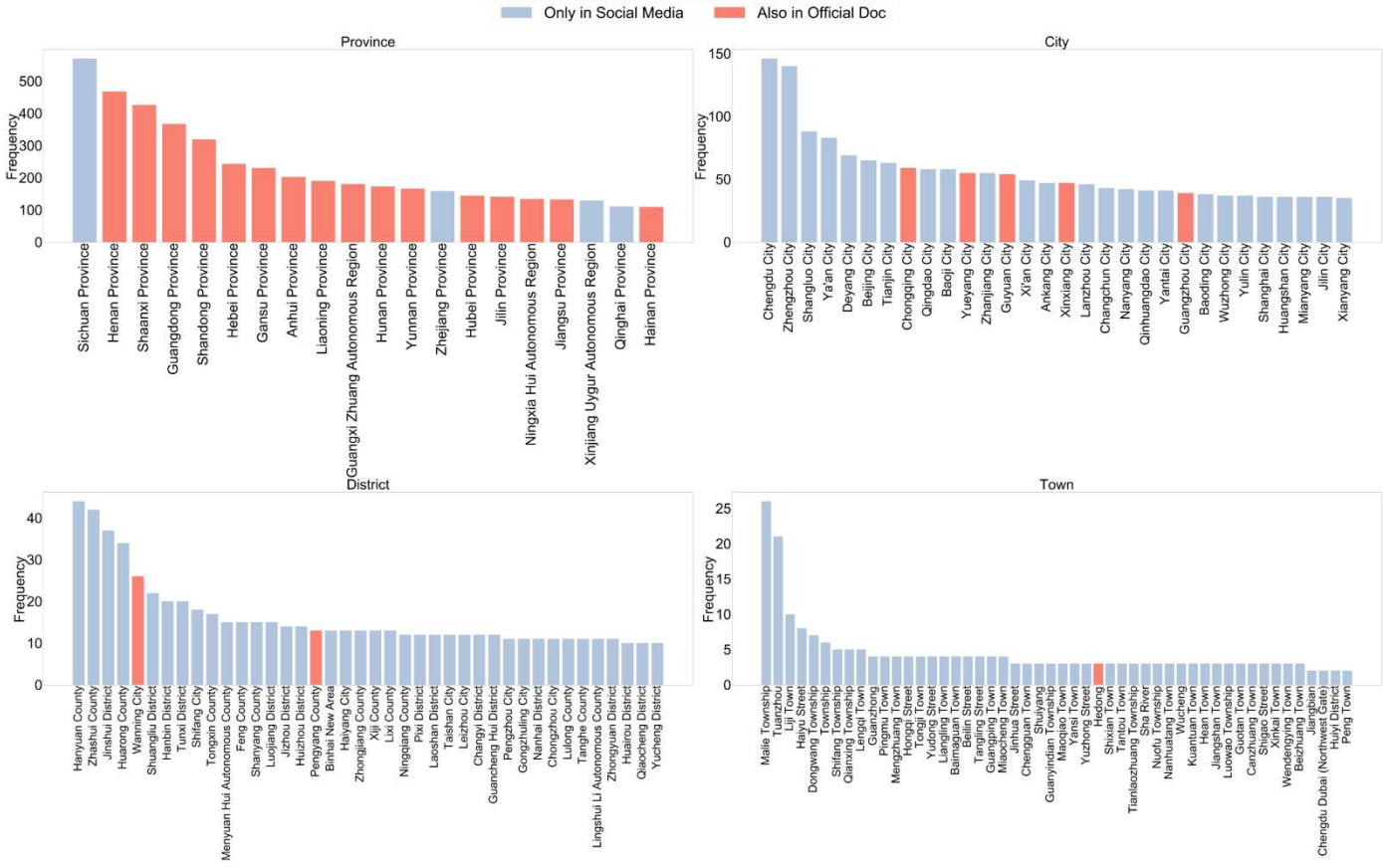
(July 19)



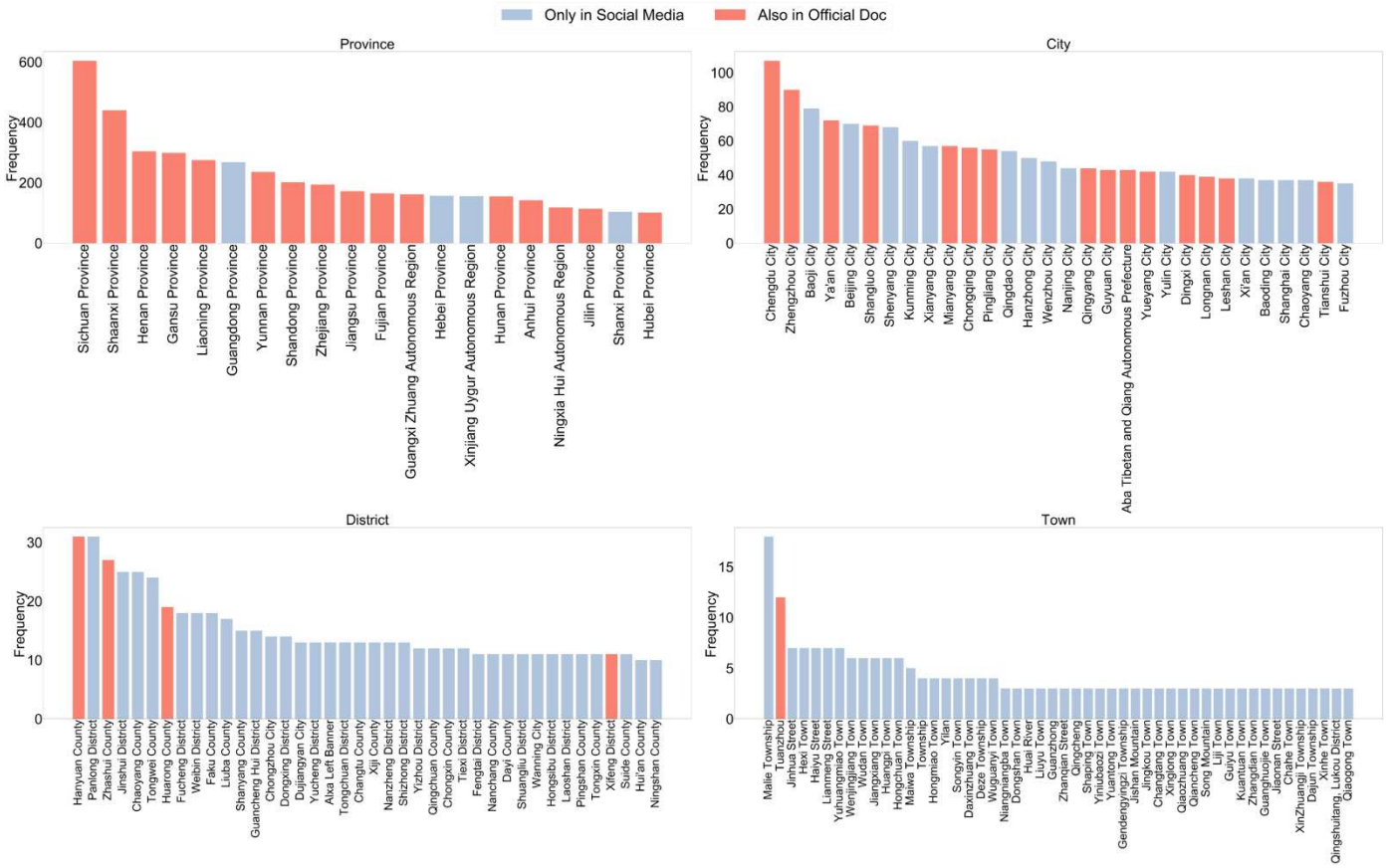
(July 20)



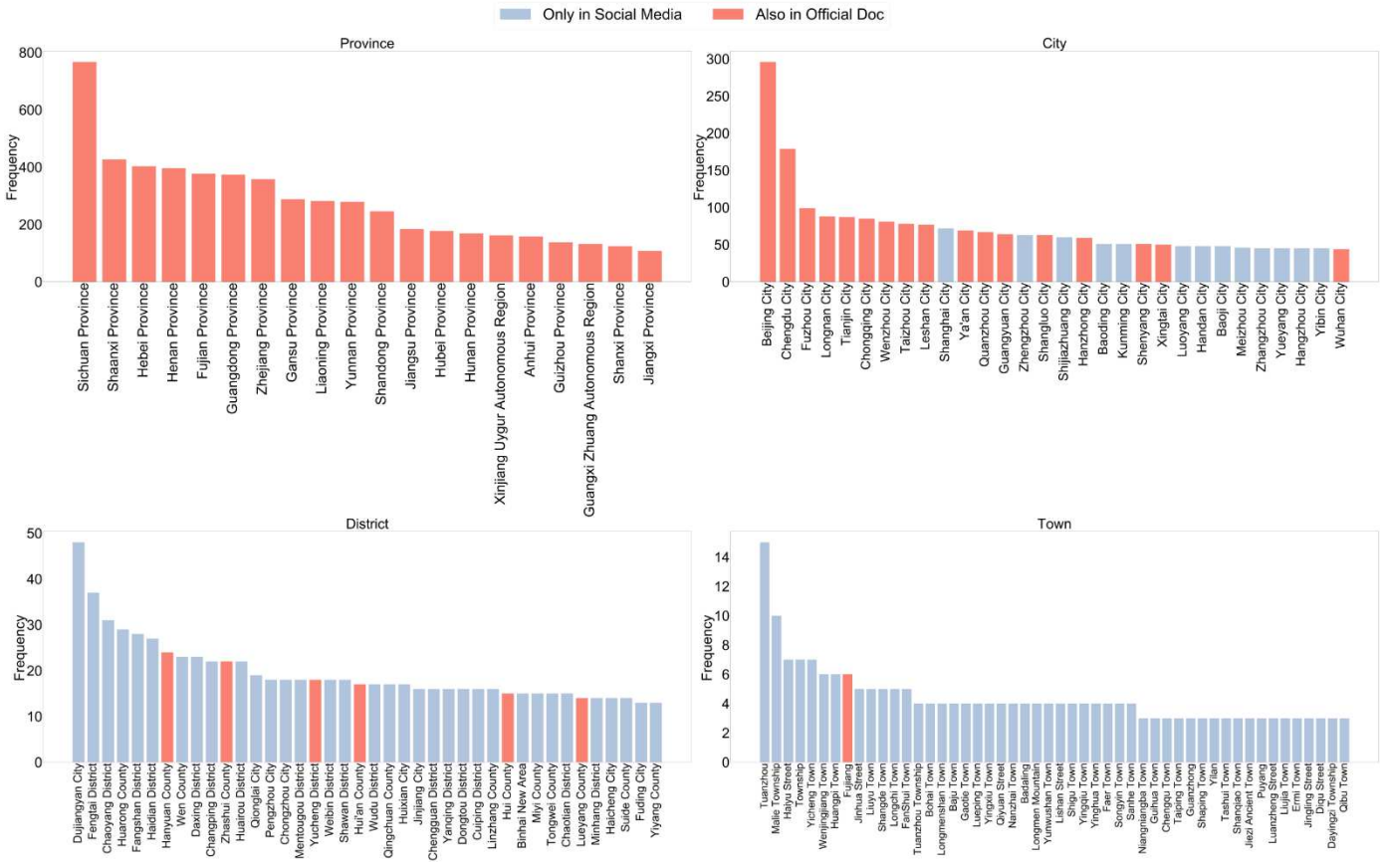
(July 21)



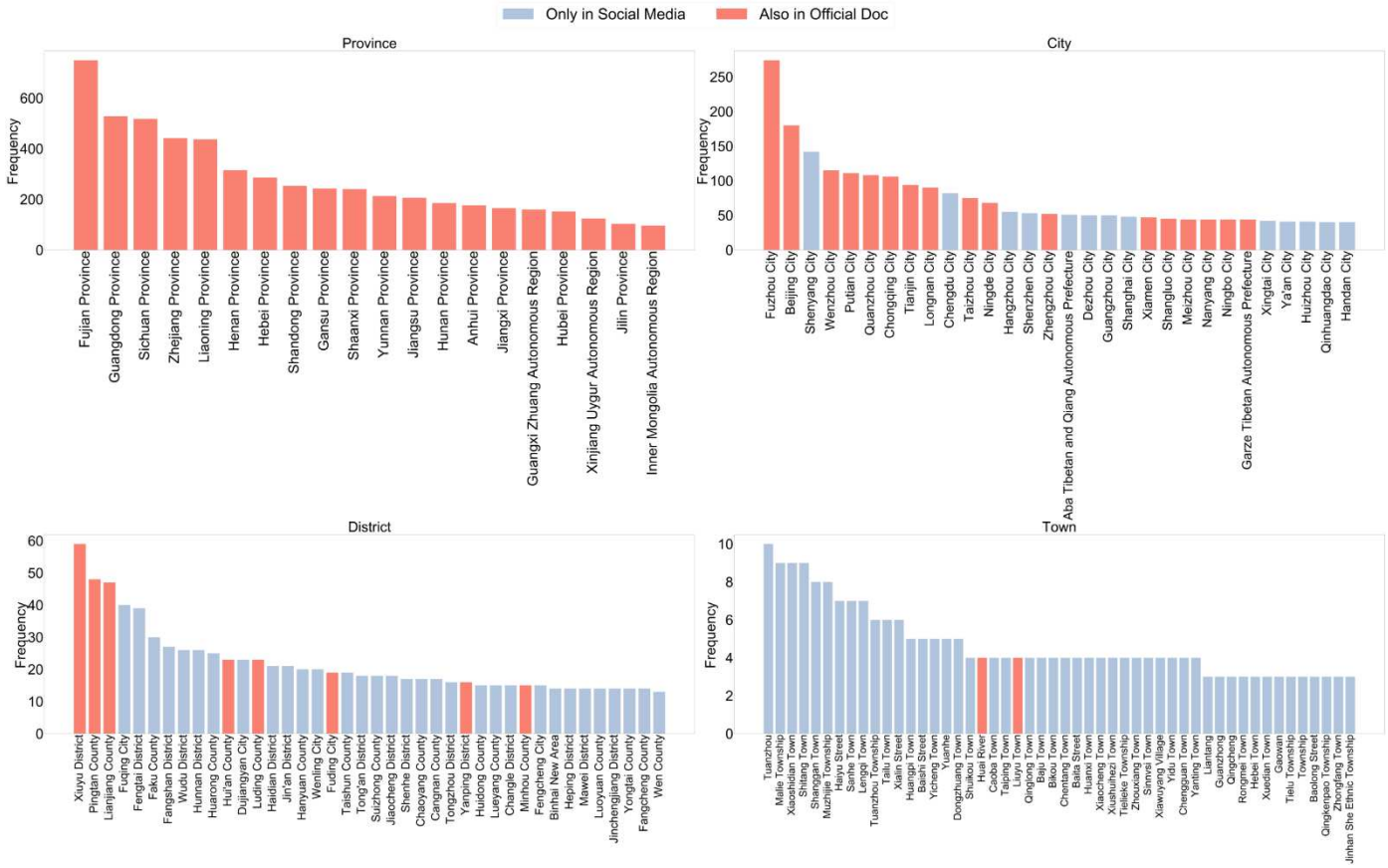
(July 22)



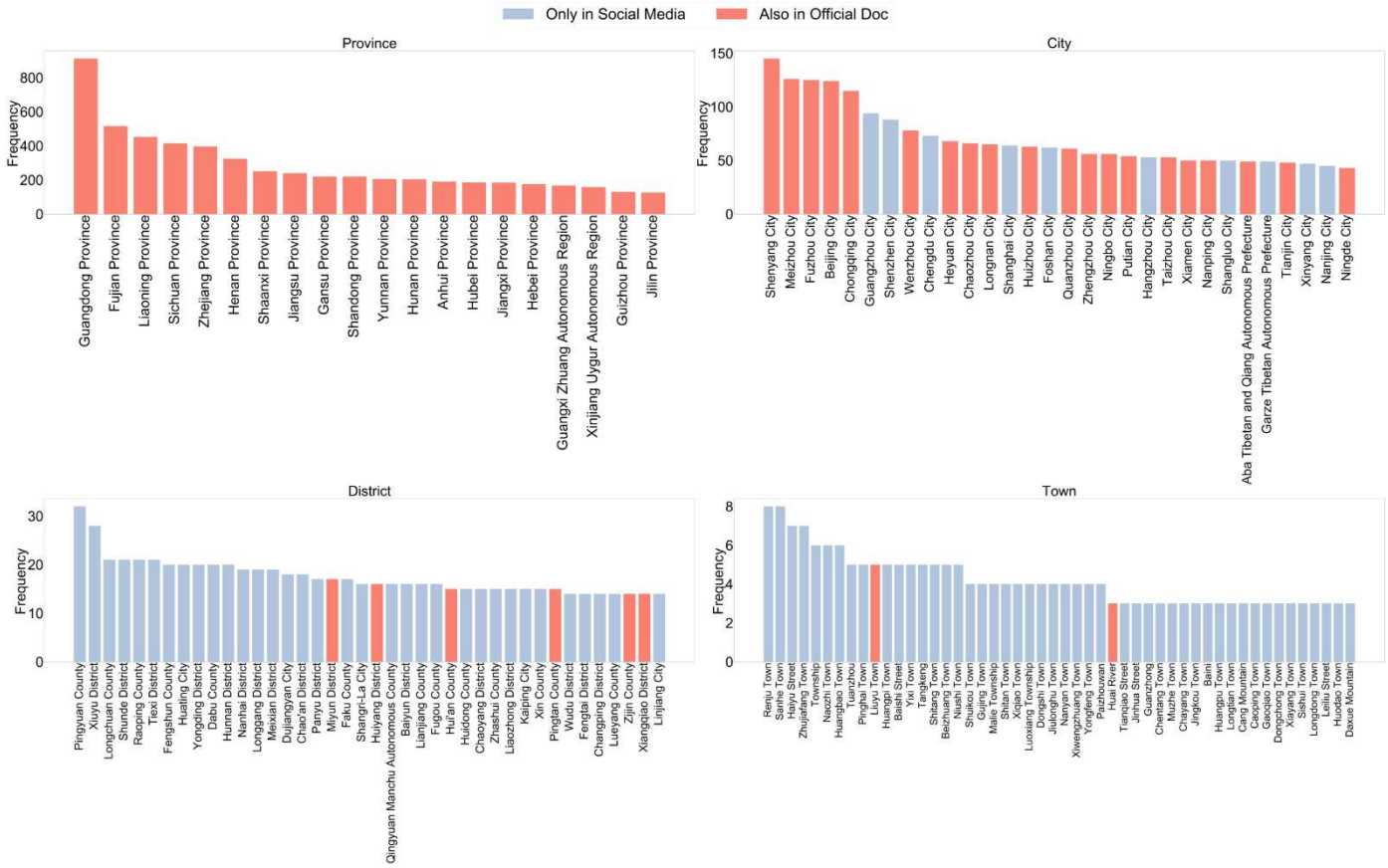
(July 23)



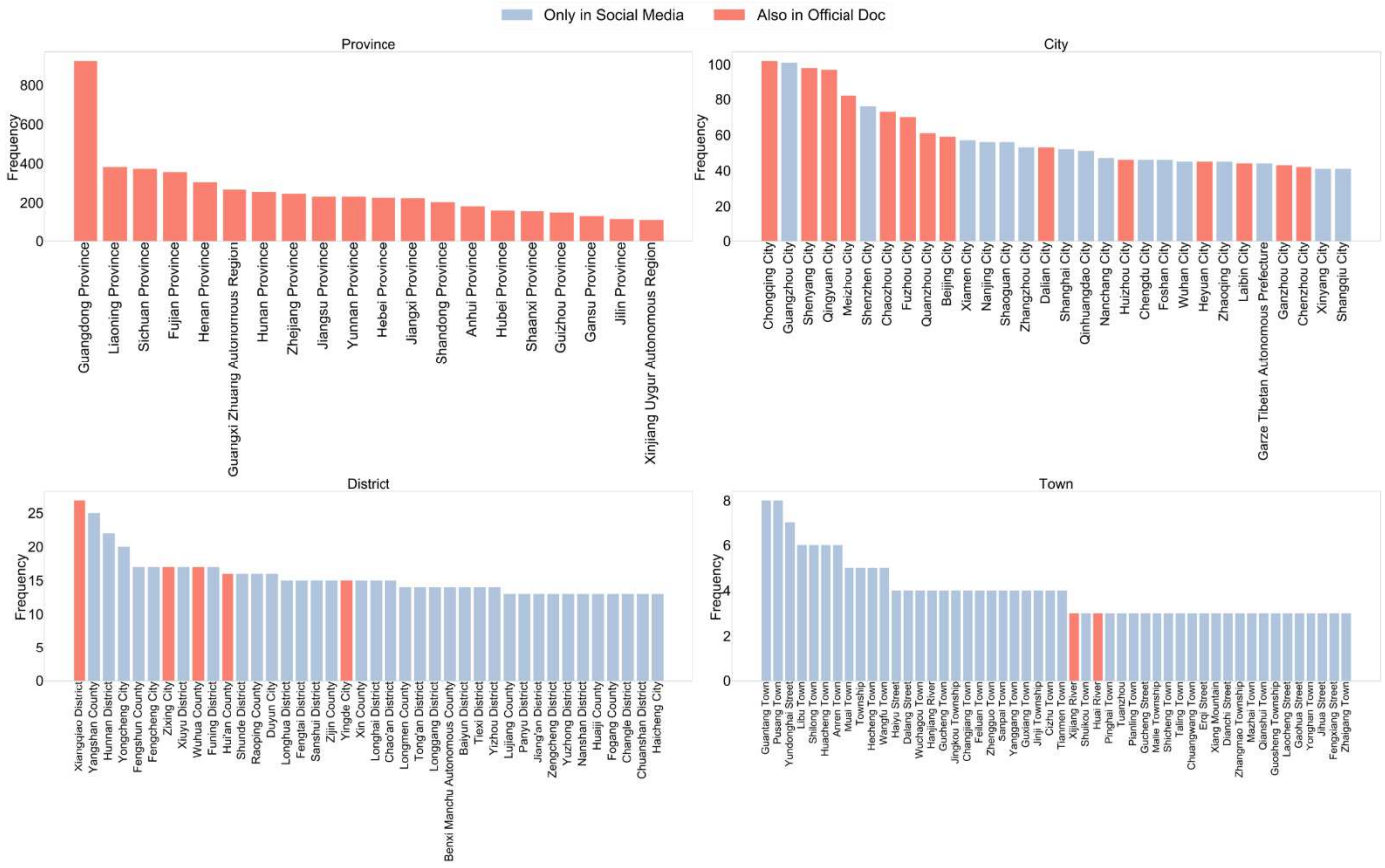
(July 24)



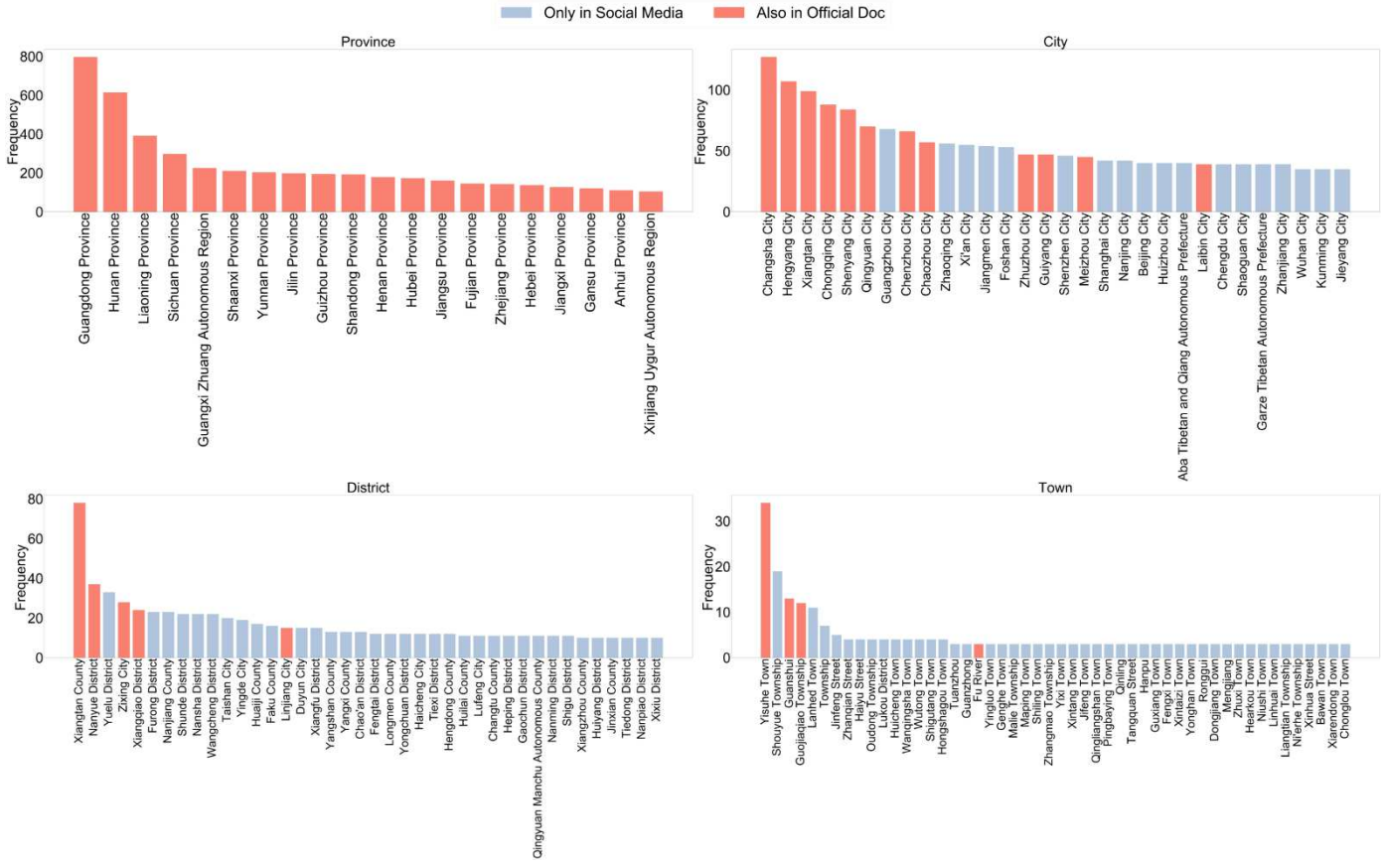
(July 25)



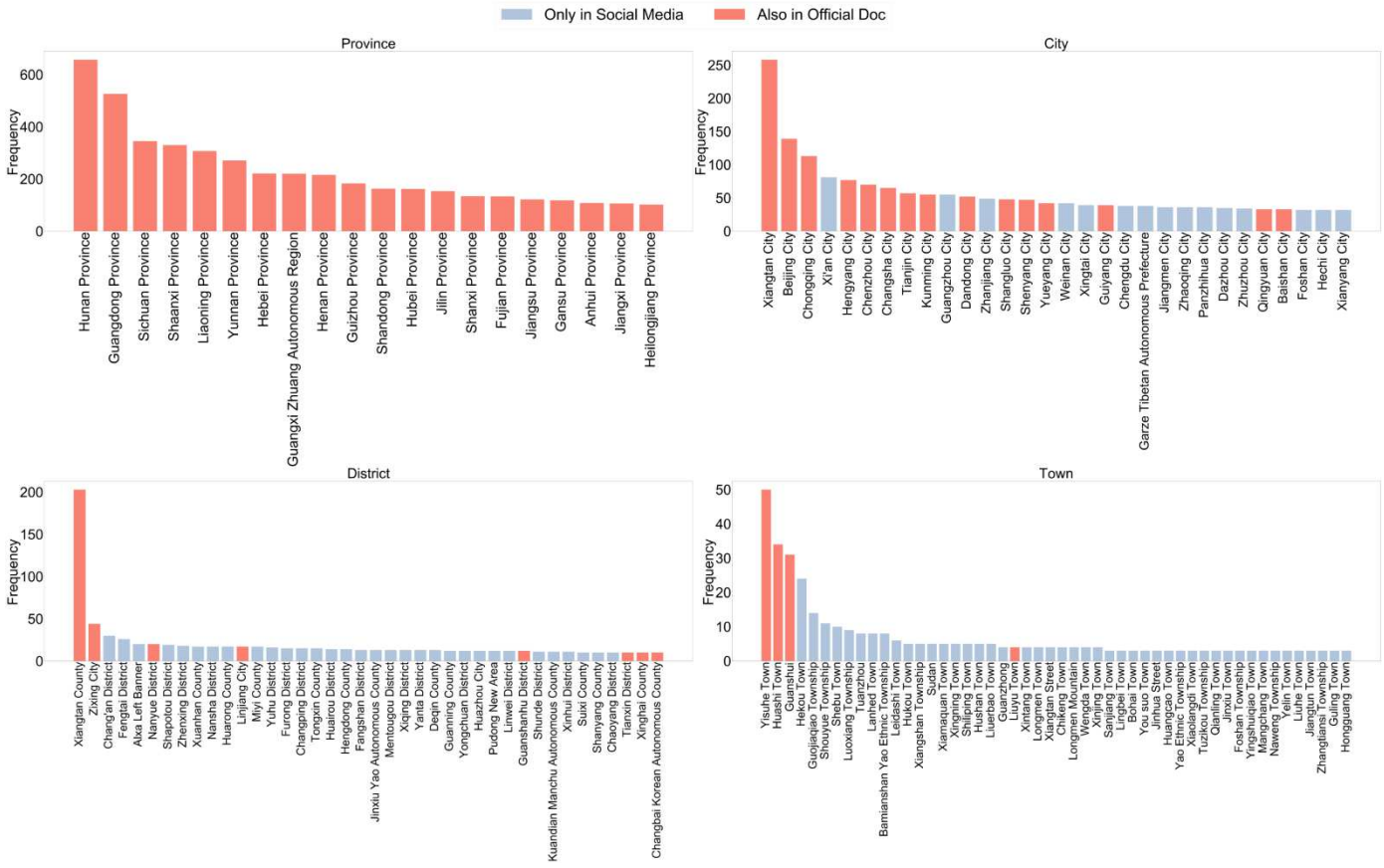
(July 26)



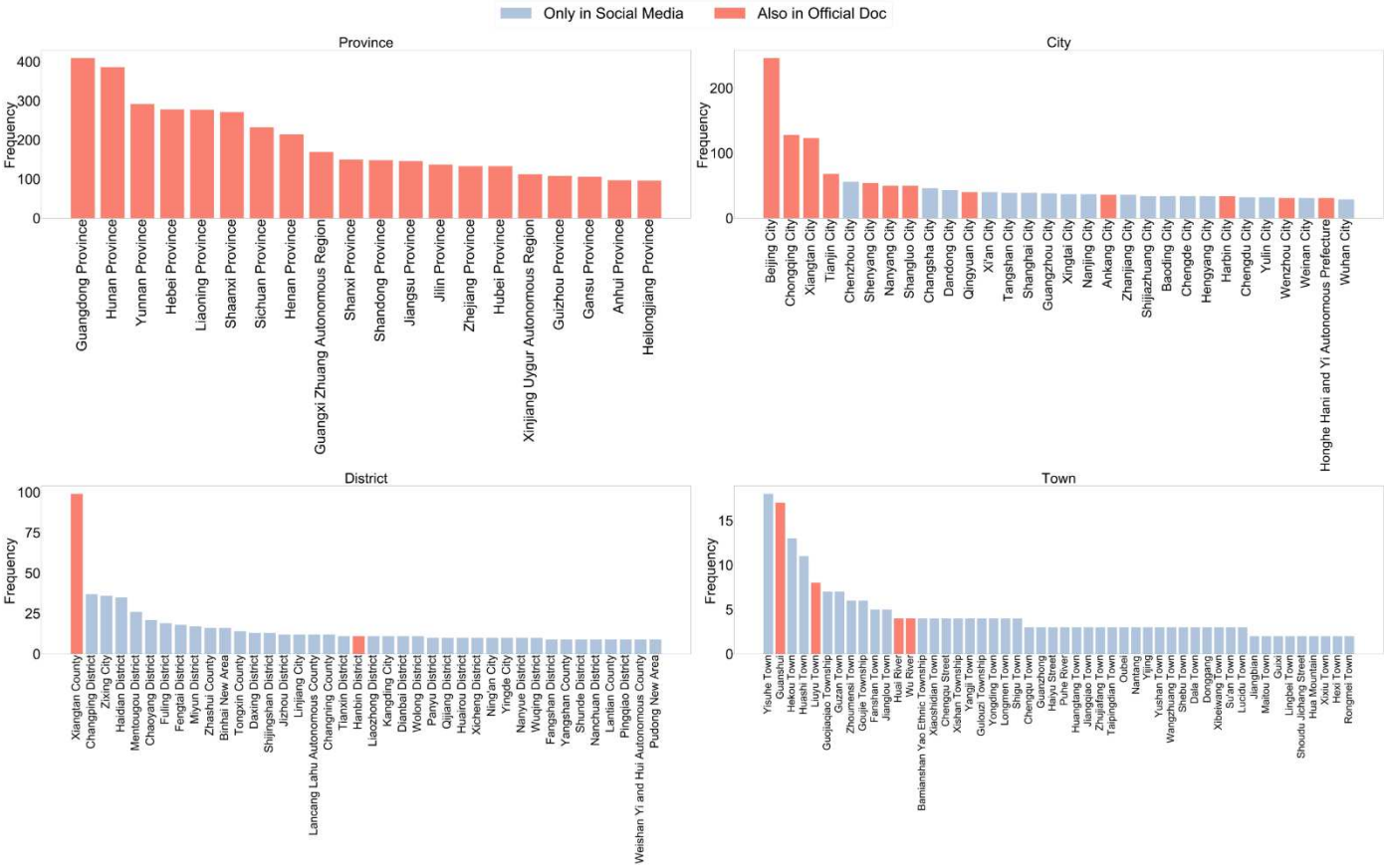
(July 27)



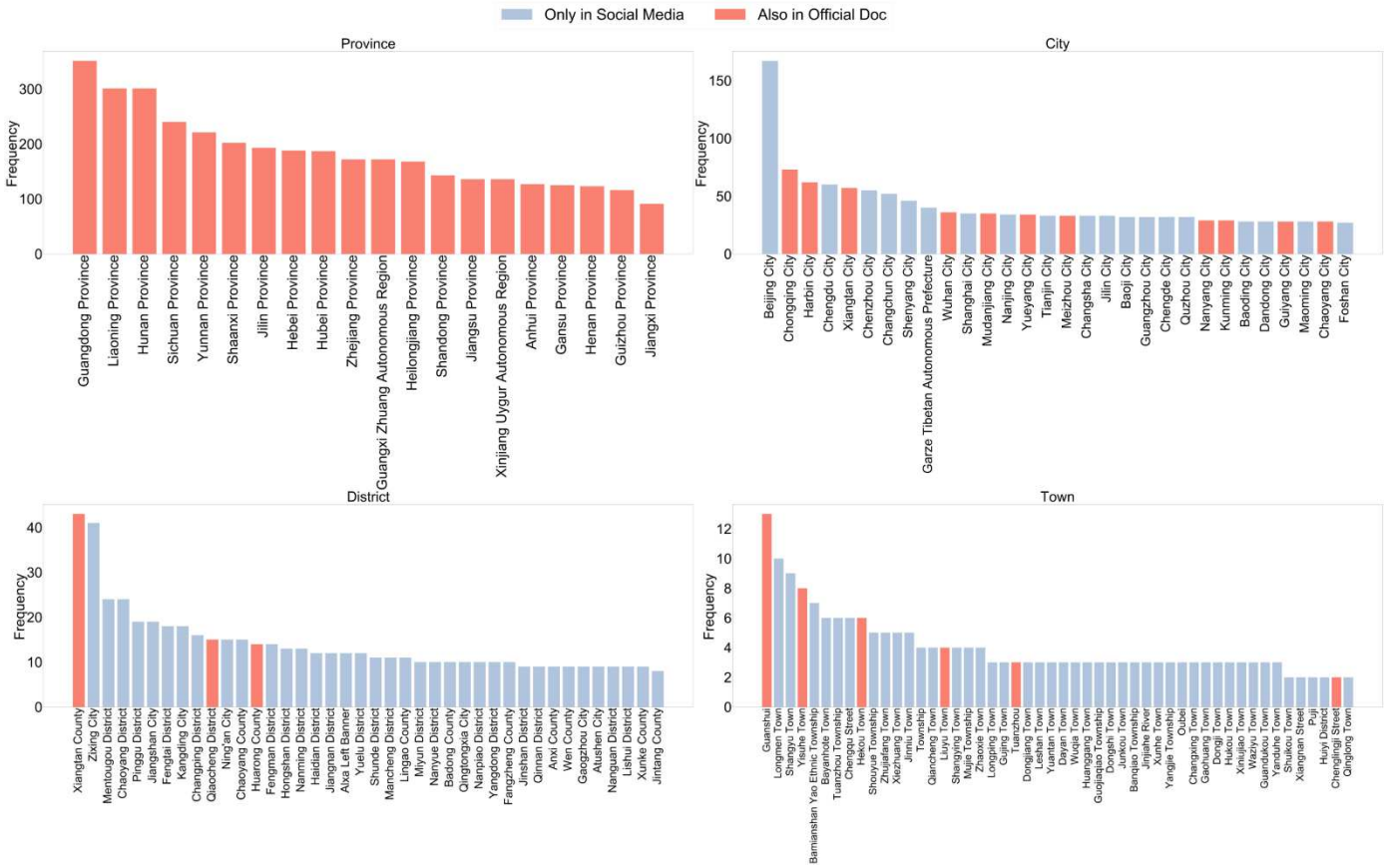
(July 28)



(July 29)



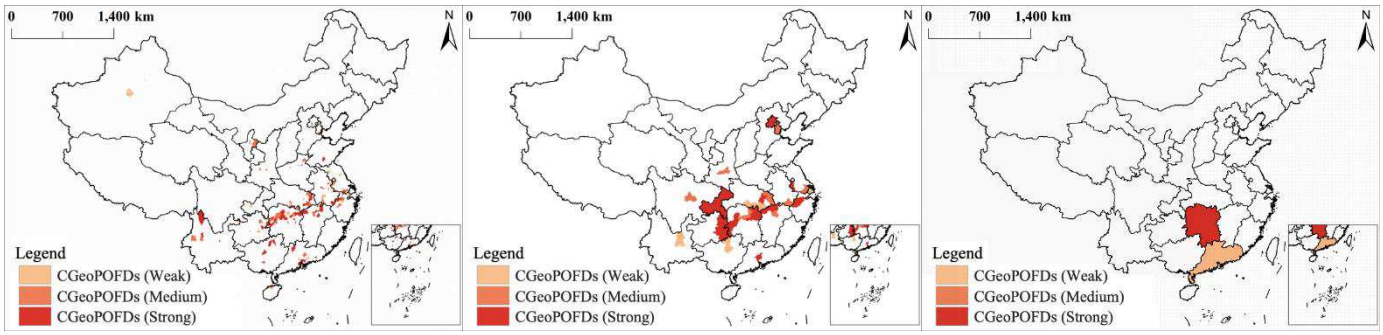
(July 30)



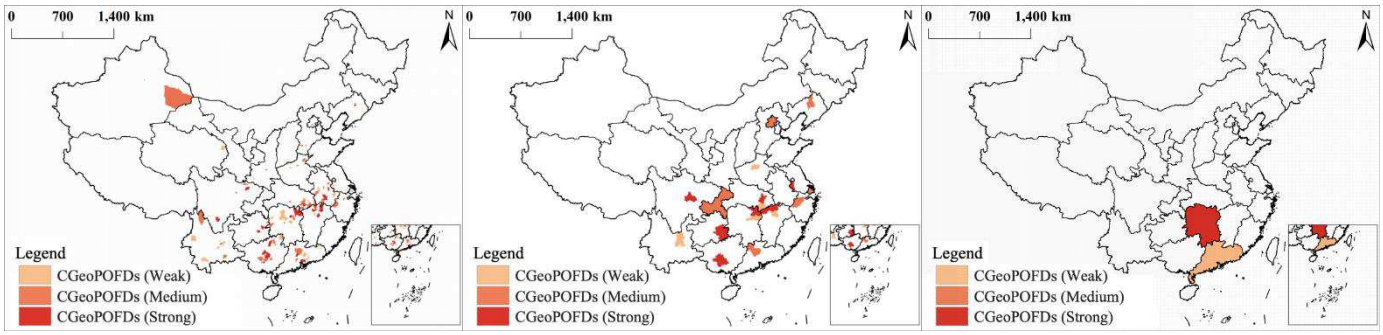
(July 31)

Fig11. Spatio-temporal joint verification results (each subgraph represents one day's data).

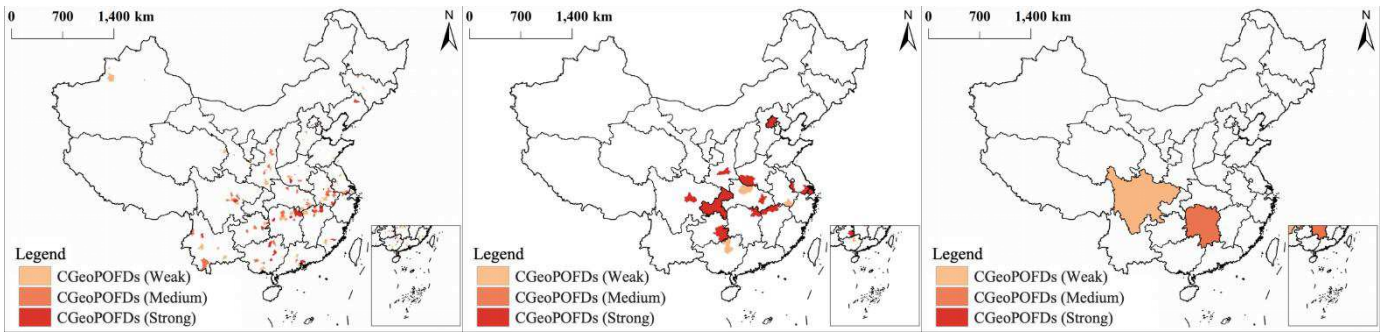
Appendix D. The Spatiotemporal Distribution of CGeoPOFDs.



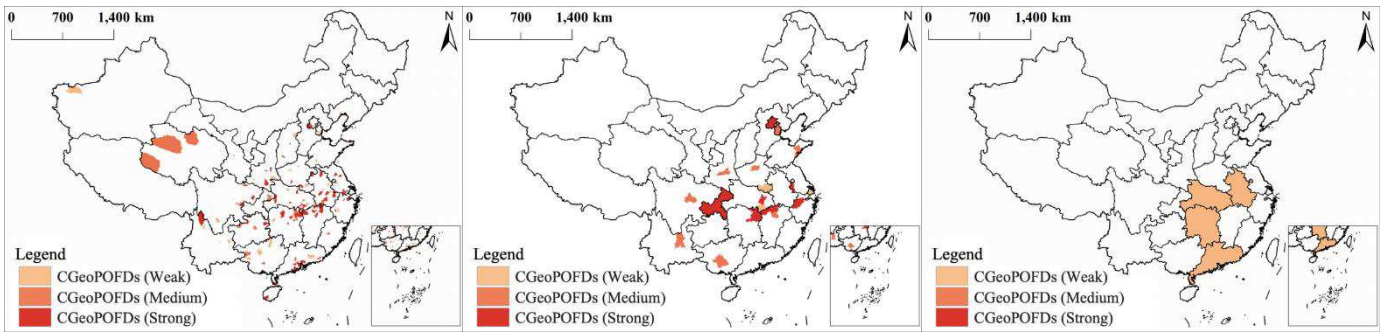
(July 1st - District Level) (July 1st - City Level) (July 1st - Provincial Level)



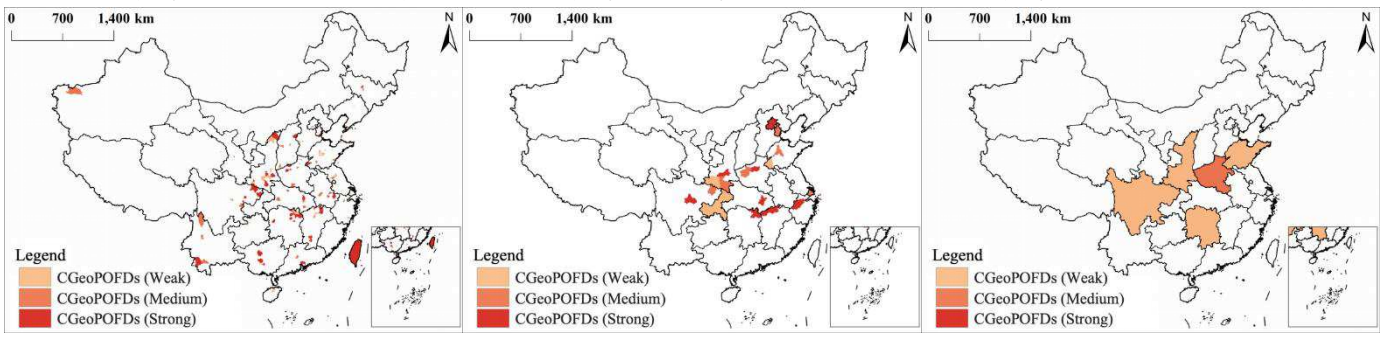
(July 2st - District Level) (July 2st - City Level) (July 2st - Provincial Level)



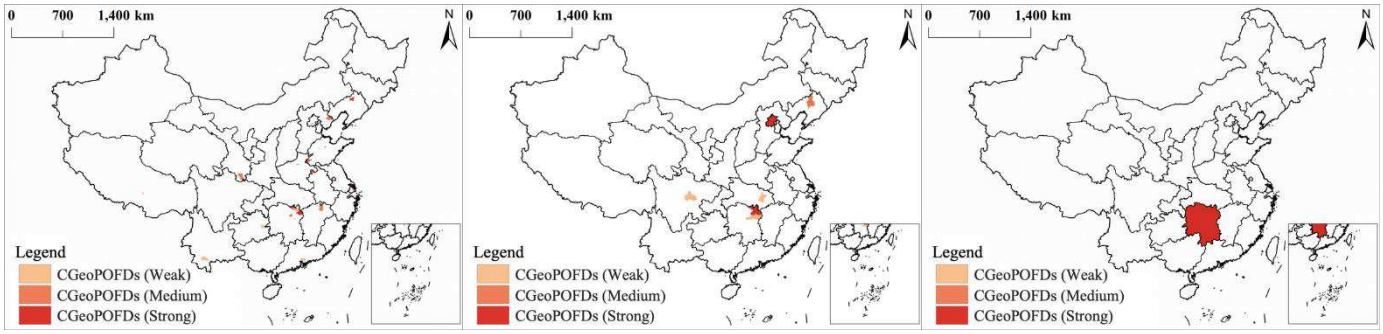
(July 3st - District Level) (July 3st - City Level) (July 3st - Provincial Level)



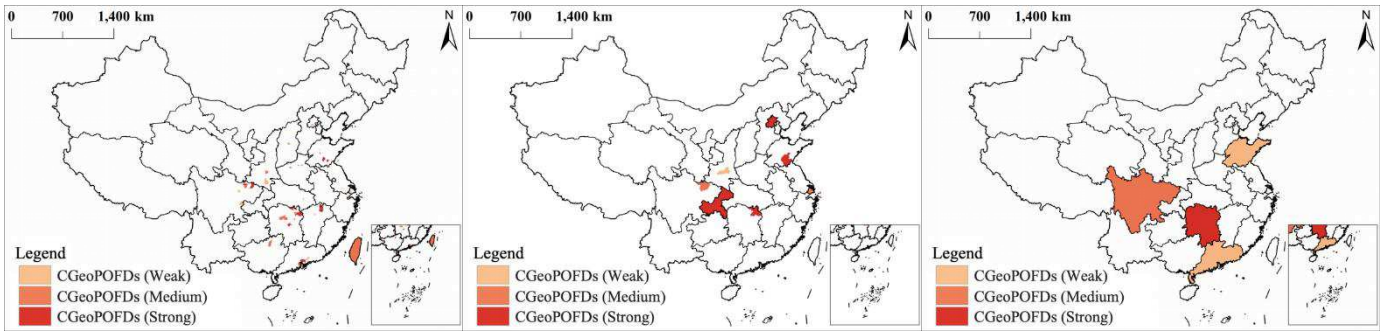
(July 4st - District Level) (July 4st - City Level) (July 4st - Provincial Level)



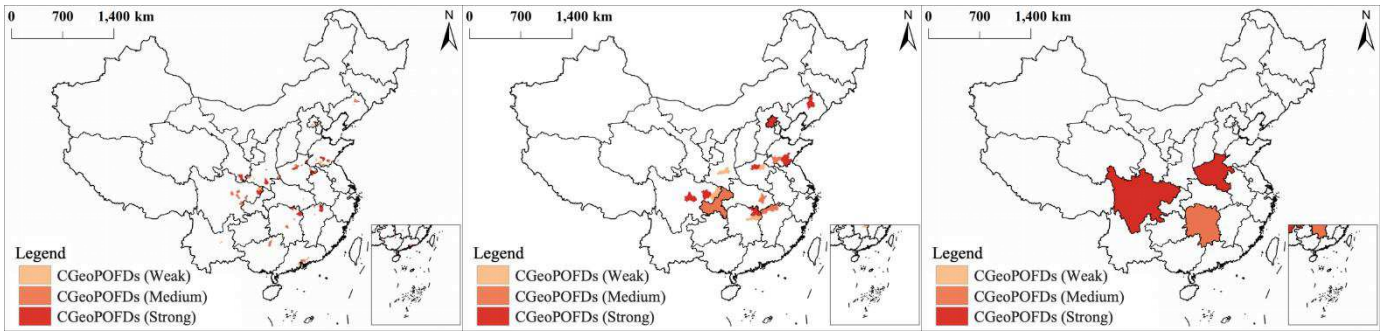
(July 5st - District Level) (July 5st - City Level) (July 5st - Provincial Level)



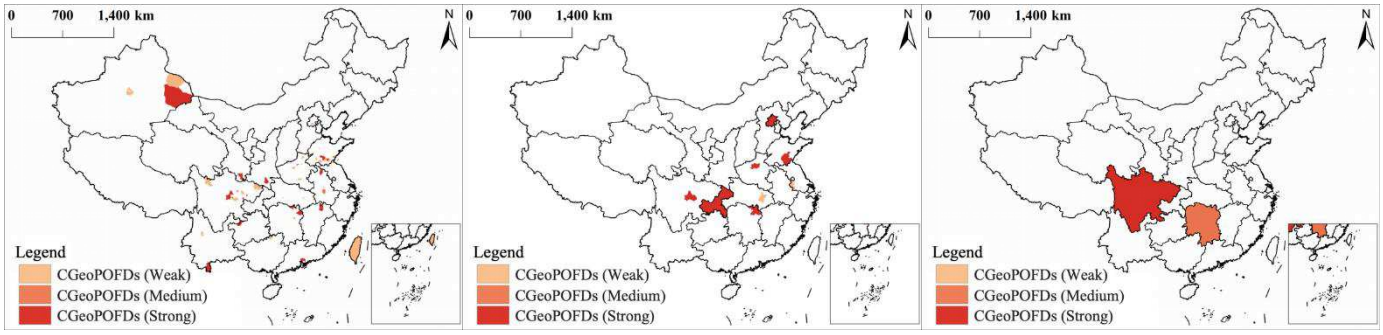
(July 6st - District Level) (July 6st - City Level) (July 6st - Provincial Level)



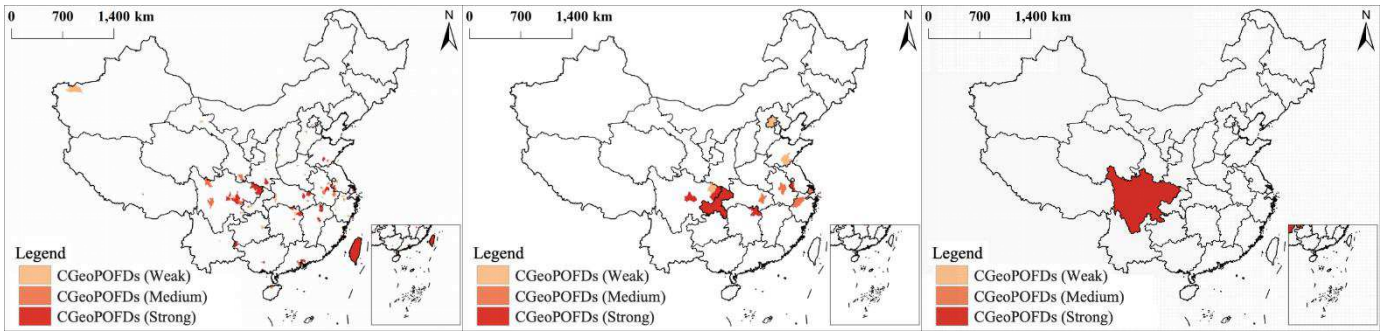
(July 7st - District Level) (July 7st - City Level) (July 7st - Provincial Level)



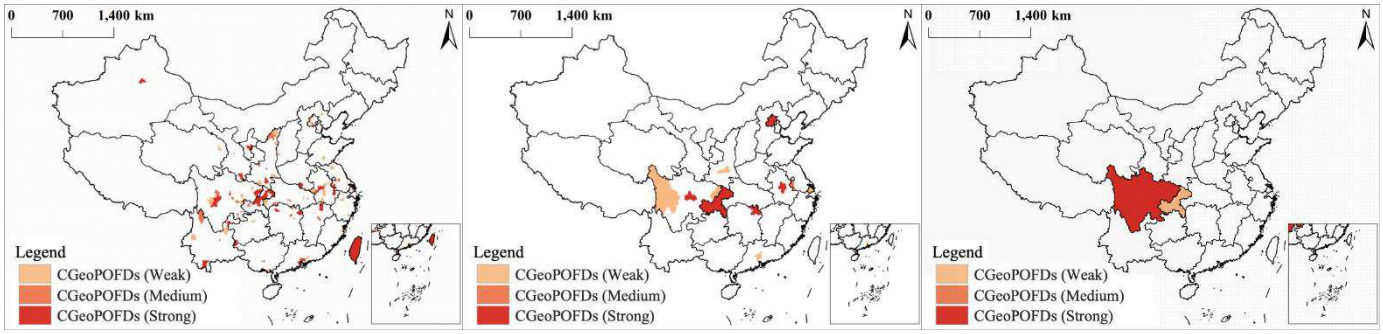
(July 8st - District Level) (July 8st - City Level) (July 8st - Provincial Level)



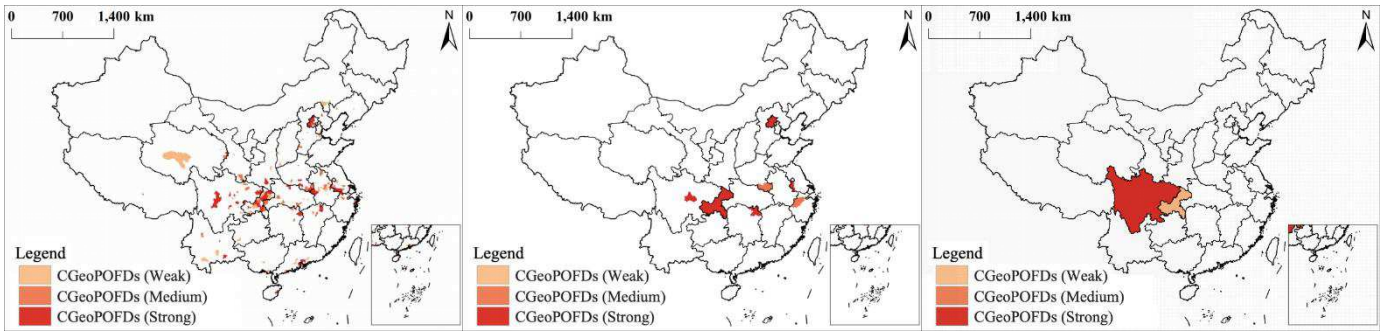
(July 9st - District Level) (July 9st - City Level) (July 9st - Provincial Level)



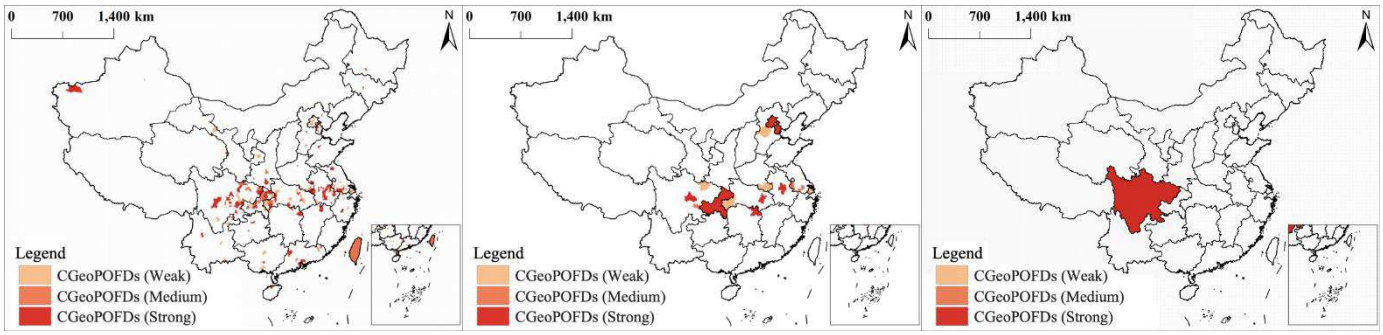
(July 10st - District Level) (July 10st - City Level) (July 10st - Provincial Level)



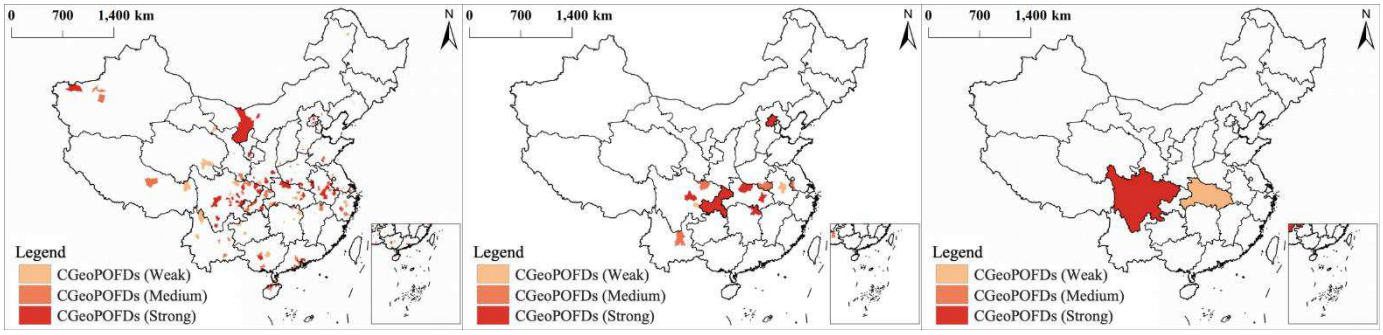
(July 11st - District Level) (July 11st - City Level) (July 11st - Provincial Level)



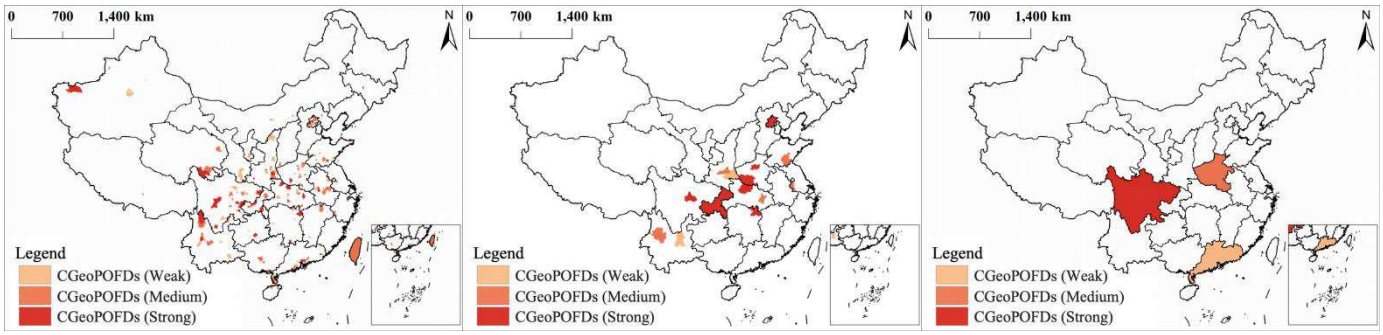
(July 12st - District Level) (July 12st - City Level) (July 12st - Provincial Level)



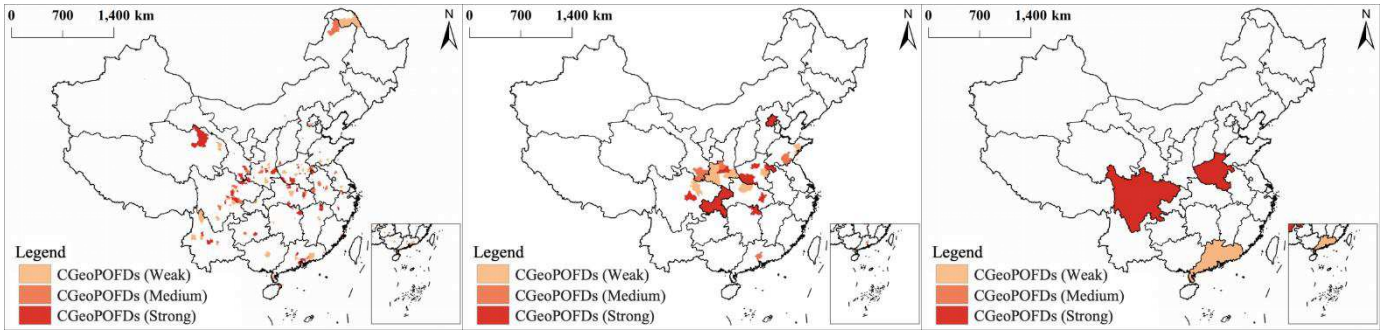
(July 13st - District Level) (July 13st - City Level) (July 13st - Provincial Level)



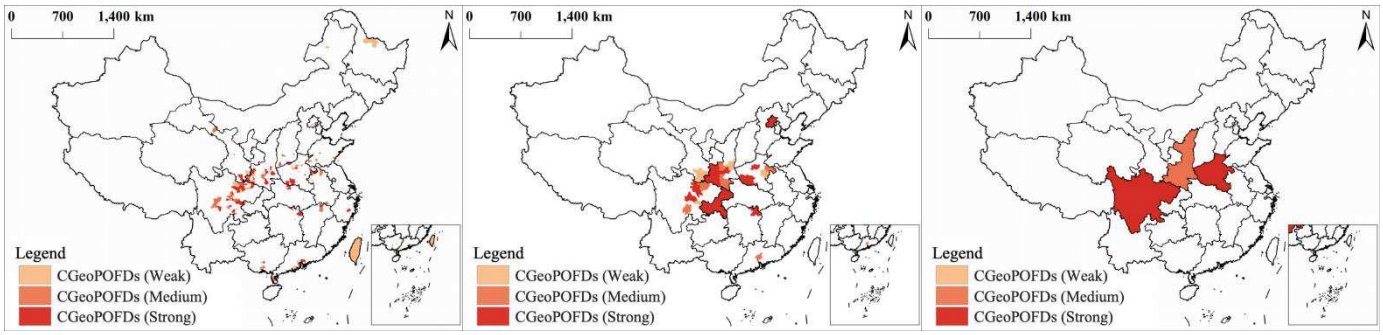
(July 14st - District Level) (July 14st - City Level) (July 14st - Provincial Level)



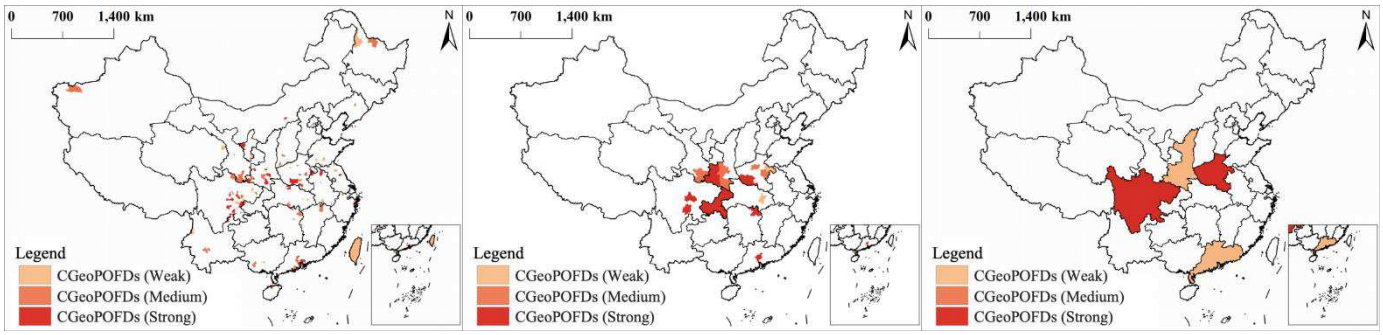
(July 15st - District Level) (July 15st - City Level) (July 15st - Provincial Level)



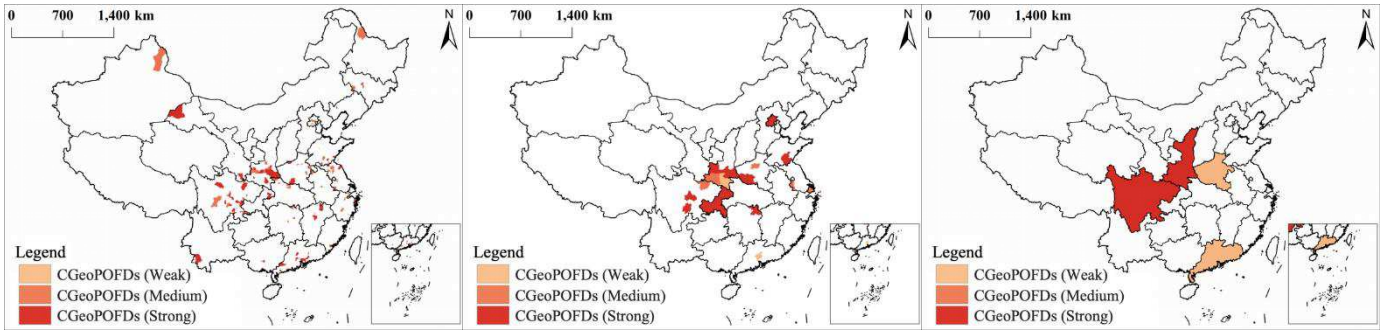
(July 16st - District Level) (July 16st - City Level) (July 16st - Provincial Level)



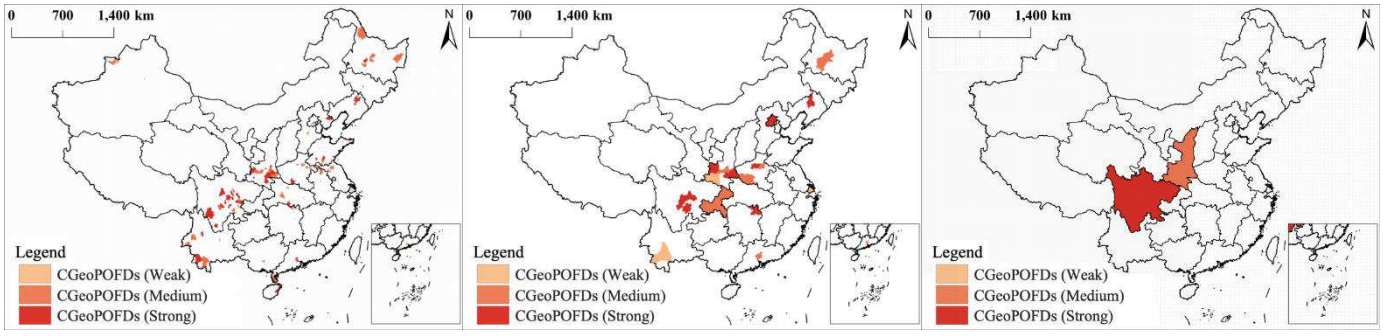
(July 17st - District Level) (July 17st - City Level) (July 17st - Provincial Level)



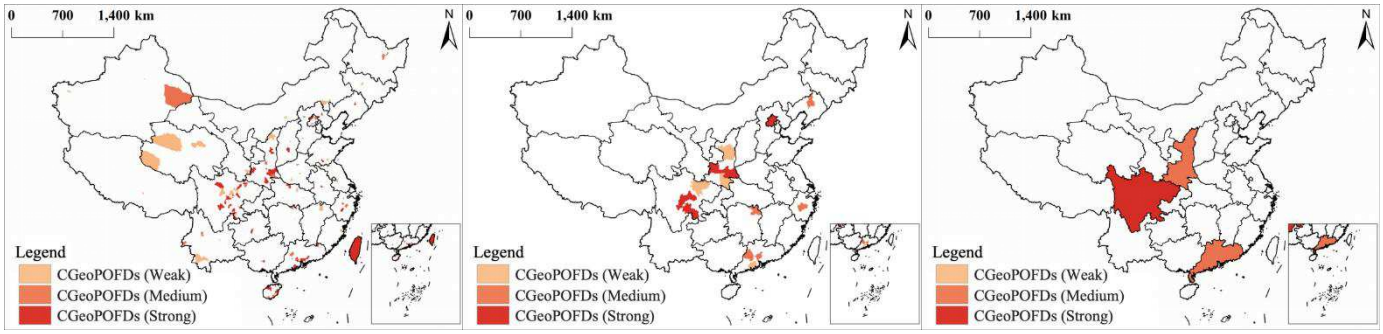
(July 18st - District Level) (July 18st - City Level) (July 18st - Provincial Level)



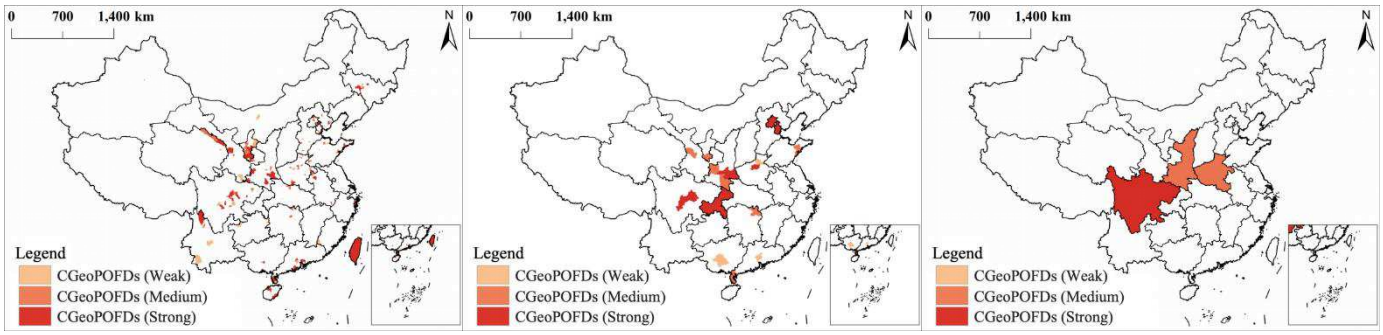
(July 19st - District Level) (July 19st - City Level) (July 19st - Provincial Level)



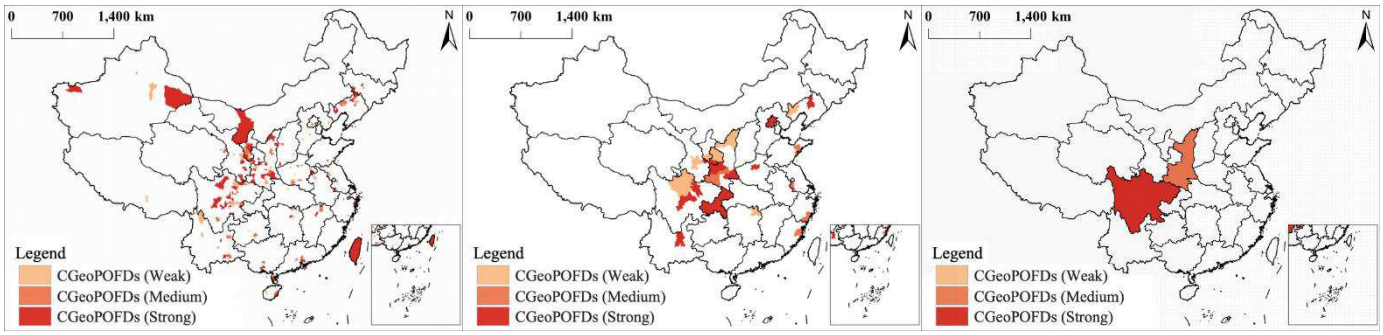
(July 20st - District Level) (July 20st - City Level) (July 20st - Provincial Level)



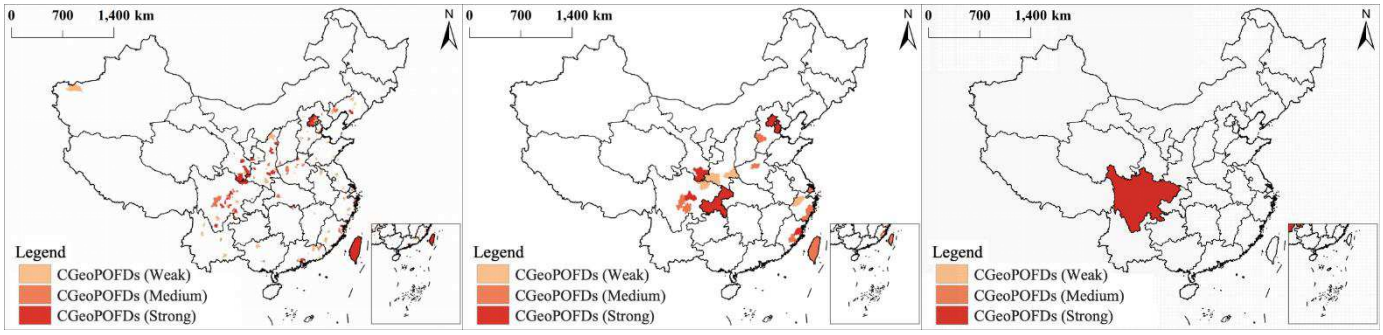
(July 21st - District Level) (July 21st - City Level) (July 21st - Provincial Level)



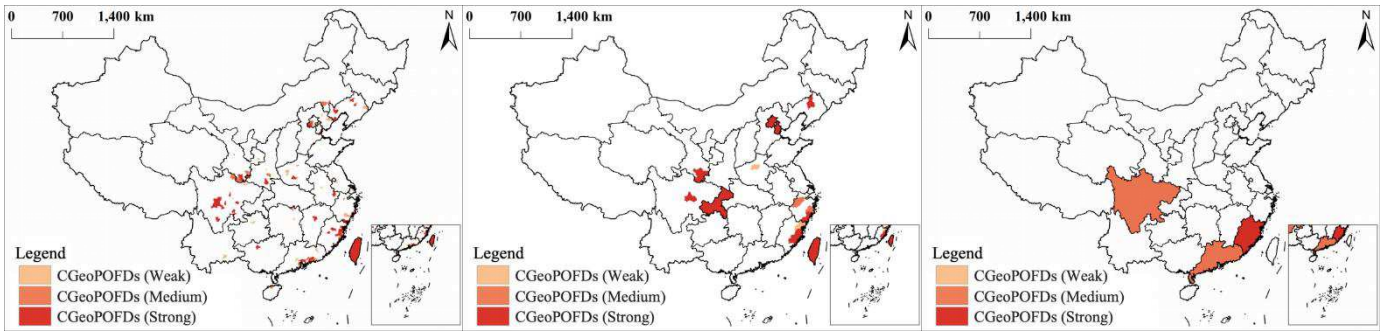
(July 22st - District Level) (July 22st - City Level) (July 22st - Provincial Level)



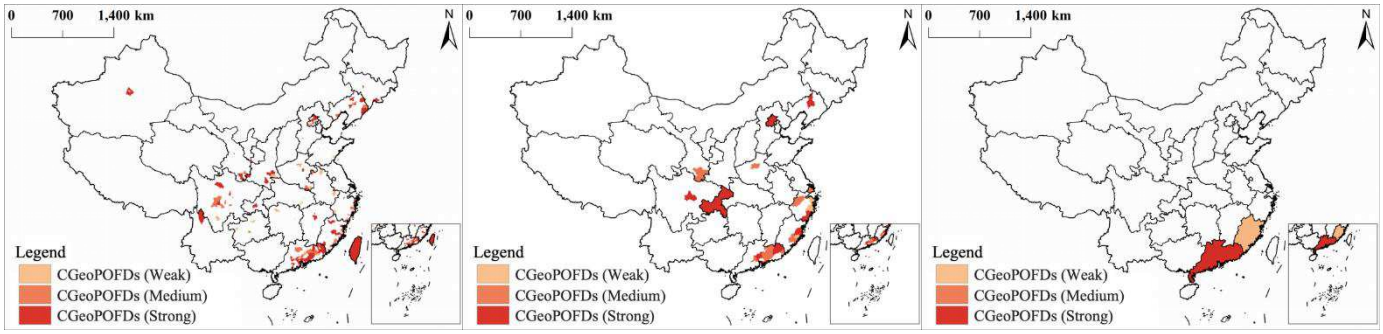
(July 23st - District Level) (July 23st - City Level) (July 23st - Provincial Level)



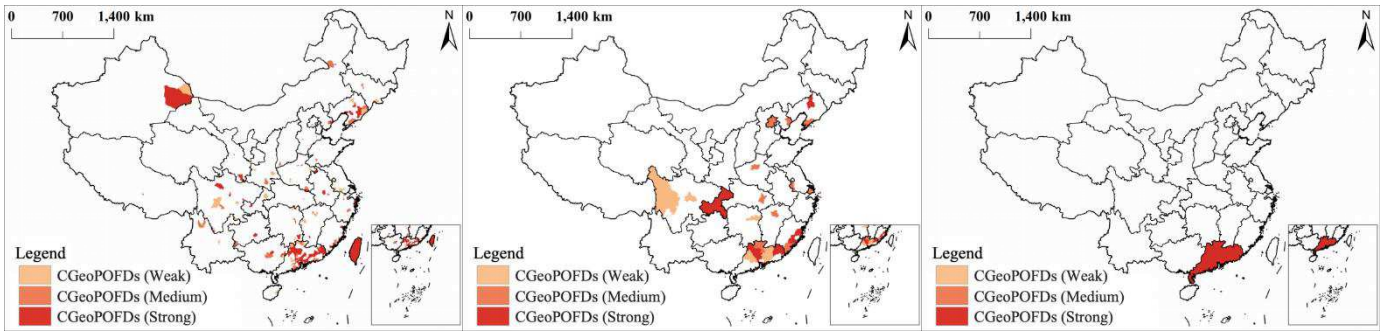
(July 24st - District Level) (July 24st - City Level) (July 24st - Provincial Level)



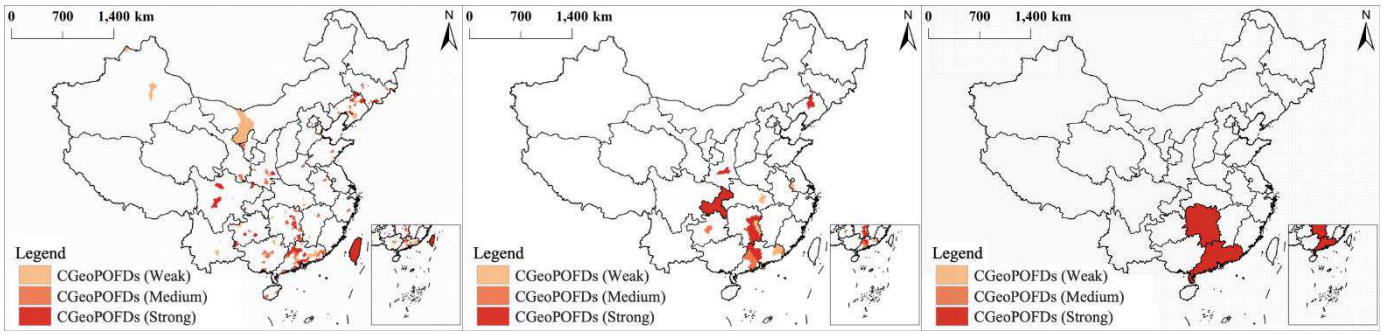
(July 25st - District Level) (July 25st - City Level) (July 25st - Provincial Level)



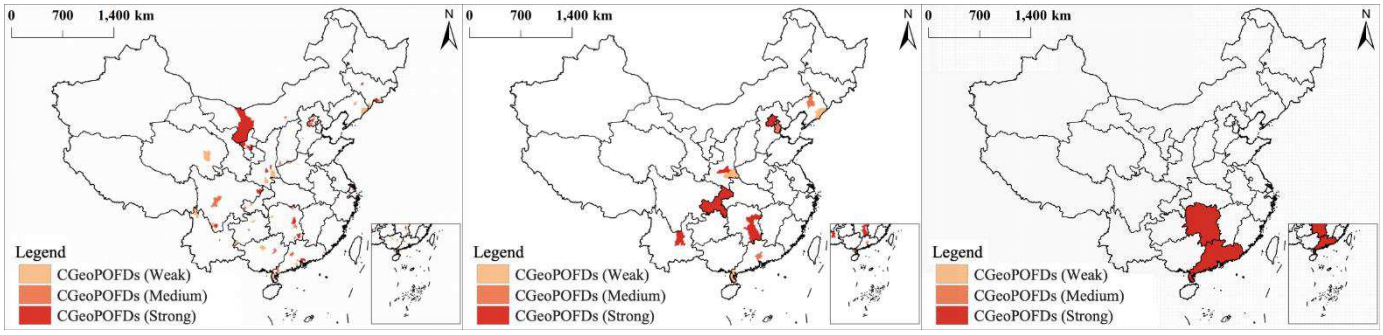
(July 26st - District Level) (July 26st - City Level) (July 26st - Provincial Level)



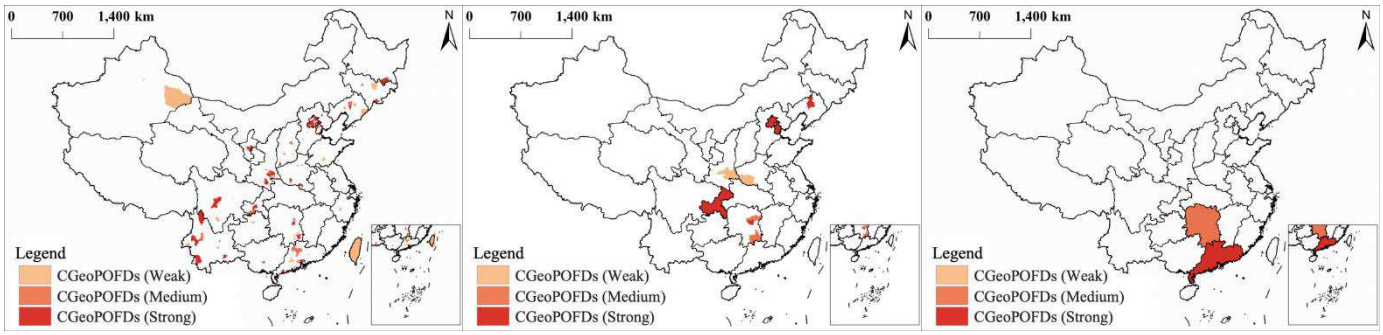
(July 27st - District Level) (July 27st - City Level) (July 27st - Provincial Level)



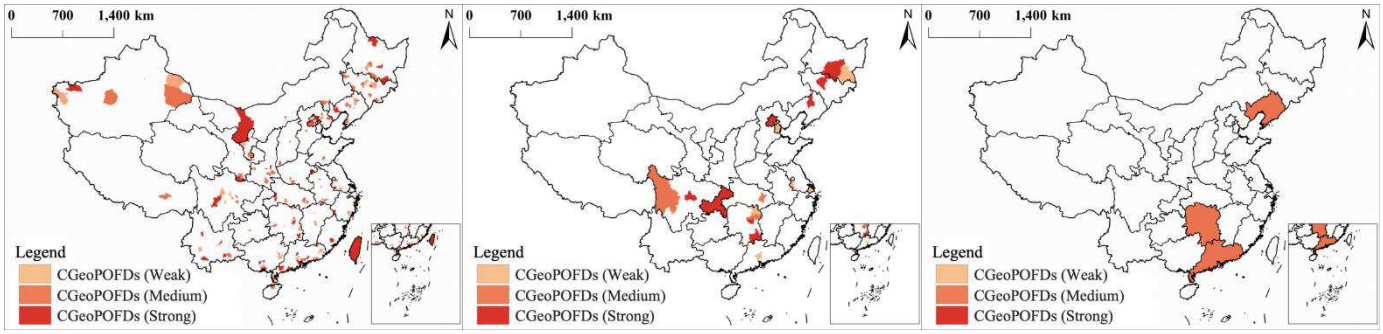
(July 28st - District Level) (July 28st - City Level) (July 28st - Provincial Level)



(July 29st - District Level) (July 29st - City Level) (July 29st - Provincial Level)



(July 30st - District Level) (July 30st - City Level) (July 30st - Provincial Level)



(July 31st - District Level) (July 31st - City Level) (July 31st - Provincial Level)

Fig12. Spatio-temporal analysis of the flood disaster geographic public opinion center.